NAVAL POSTGRADUATE SCHOOL
Monterey, California

THESIS

AN ANALYSIS OF SHORT TERM MESOSCALE FORECASTS IN THE LOS ANGELES BASIN USING SOUTHERN COAST OZONE STUDY 1997 DATA

by

Christopher J. Sterbis

September 2000

Thesis Advisor: Douglas K. Miller
Second Reader: Wendell A. Nuss

Approved for public release; distribution is unlimited.

REPORT DOCUMENTATION PAGE		Form Approved OMB No. 0704-0188

Public reporting burden for this collection of information is estimated to average 1 hour per response, including the time for reviewing instruction, searching existing data sources, gathering and maintaining the data needed, and completing and reviewing the collection of information. Send comments regarding this burden estimate or any other aspect of this collection of information, including suggestions for reducing this burden, to Washington headquarters Services, Directorate for Information Operations and Reports, 1215 Jefferson Davis Highway, Suite 1204, Arlington, VA 22202-4302, and to the Office of Management and Budget, Paperwork Reduction Project (0704-0188) Washington DC 20503.

1. AGENCY USE ONLY *(Leave blank)*	2. REPORT DATE	3. REPORT TYPE AND DATES COVERED
	September 2000	Master's Thesis

4. TITLE AND SUBTITLE: Title (Mix case letters)
An Analysis Of Short Term Mesoscale Forecasts In The Los Angeles Basin Using Southern Coast Ozone Study 1997 Data

5. FUNDING NUMBERS

6. AUTHOR(S)
Christopher J. Sterbis

7. PERFORMING ORGANIZATION NAME(S) AND ADDRESS(ES)
Naval Postgraduate School
Monterey, CA 93943-5000

8. PERFORMING ORGANIZATION REPORT NUMBER

9. SPONSORING / MONITORING AGENCY NAME(S) AND ADDRESS(ES)
N/A

10. SPONSORING / MONITORING AGENCY REPORT NUMBER

11. SUPPLEMENTARY NOTES *The views expressed in this thesis are those of the author and do not reflect the official policy or position of the Department of Defense or the U.S. Government.*

12a. DISTRIBUTION / AVAILABILITY STATEMENT
Approved for public release; distribution is unlimited

12b. DISTRIBUTION CODE

13. ABSTRACT

Mesoscale models are important, useful tools for analyzing and forecasting small-scale atmospheric phenomena. Ideally, finer grid-point resolution should make a model more likely to capture realistic small-scale structure. Because these models work to resolve phenomena that exist on very fine spatial- and time-scales, they are subject to high variability. Accurate initialization of mesoscale models is crucial to skillful short-term forecasting.

This study exercises four different initialization and model physics experiments of four nested MM5 forecast domains and examines their respective short-term (f03, f06, f09, f12) forecasts. The exceptionally rich meteorological data set taken from the Southern Coast Ozone Study of 1997 (SCOS97) provides the basis for our model verification.

We show that 3km and 9k resolutions produce better forecasts than the 27km resolution model, however, differences between the 3km and 9km resolution forecasts are essentially insignificant. We also show that different model initializations and physics schemes have an insignificant impact on improving the absolute accuracy of the numerical forecasts produced by a non-hydrostatic mesoscale model.

14. SUBJECT TERMS	15. NUMBER OF PAGES
Mesoscale modeling, Predictability, Model Verification	116
	16. PRICE CODE

17. SECURITY CLASSIFICATION OF REPORT	18. SECURITY CLASSIFICATION OF THIS PAGE	19. SECURITY CLASSIFICATION OF ABSTRACT	20. LIMITATION OF ABSTRACT
Unclassified	Unclassified	Unclassified	UL

NSN 7540-01-280-5500

Standard Form 298 (Rev. 2-89)
Prescribed by ANSI Std. 239-18

Approved for public release; distribution is unlimited

AN ANALYSIS OF SHORT TERM MESOSCALE FORECASTS IN THE LOS ANGELES BASIN USING SOUTHERN COAST OZONE STUDY 1997 DATA

Christopher J. Sterbis
Lieutenant, United States Navy
B.S., United States Naval Academy, 1993

Submitted in partial fulfillment of the
requirements for the degree of

MASTER OF SCIENCE IN METEOROLOGY AND PHYSICAL OCEANOGRAPHY

from the

NAVAL POSTGRADUATE SCHOOL
September 2000

Author: _____
Christopher J. Sterbis

Approved by: _____
Douglas K. Miller, Thesis Advisor

_____
Wendell A. Nuss, Second Reader

_____
Robert L. Haney, Chairman
Department of Meteorology

ABSTRACT

Mesoscale models are important, useful tools for analyzing and forecasting small-scale atmospheric phenomena. Ideally, finer grid-point resolution should make a model more likely to capture realistic small-scale structure. Because these models work to resolve phenomena that exist on very fine spatial- and time-scales, they are subject to high variability. Accurate initialization of mesoscale models is crucial to skillful short-term forecasting.

This study exercises four different initialization and model physics experiments of four nested MM5 forecast domains and examines their respective short-term (f03, f06, f09, f12) forecasts. The exceptionally rich meteorological data set taken from the Southern Coast Ozone Study of 1997 (SCOS97) provides the basis for our model verification.

We show that 3km and 9k resolutions produce better forecasts than the 27km resolution model, however, differences between the 3km and 9km resolution forecasts are essentially insignificant. We also show that different model initializations and physics schemes have an insignificant impact on improving the absolute accuracy of the numerical forecasts produced by a non-hydrostatic mesoscale model.

TABLE OF CONTENTS

ACKNOWLEDGEMENTS

I would like to thank Dr. Wendell Nuss for taking some of his valuable time to be my second reader. His expertise and experience have been a tremendous help.

LT Rick Mohammed was crucial in almost every computer-related aspect of this project. He taught me a lot and was always offered a hand when I got stuck.

Dr. Doug Miller dedicated countless hours sparking my interest, maintaining my focus, and challenging my abilities over the course of this endeavor. Being one of his thesis students has been extremely rewarding and was my distinct pleasure.

Most importantly, I thank my wife, Liz. Her great patience, understanding, and support made this and all of my professional accomplishments possible.

I. INTRODUCTION

A. WHY MESOSCALE MODELS ARE IMPORTANT

Scientists and weather forecasters are often interested in understanding small-scale phenomena within specific regional areas. In many cases, intended areas of study would be impossible without the employment of mesoscale models. Mesoscale models take accepted global-scale atmospheric models and, with more detailed physics and smaller grid spacing, provide details of smaller scale atmospheric phenomena smoothed over by the global-scale models. This ability to better resolve topography and look with finer spatial and temporal resolution makes a mesoscale model an invaluable tool in many places. For example, in areas of complex terrain, such as the Los Angeles Basin, accurate representation of wind flow requires a scale of 4-5 km, or less (Stauffer et al., 2000). This requirement far exceeds the resolution of any global scale. Without mesoscale models, better understanding of atmospheric structures within some areas of study would be impossible.

For the U. S. Navy, mesoscale models provide valuable and necessary information into Tactical Decision Aids (TDAs). Whereas atmospheric soundings can be input to a TDA to gain a real time analysis of the atmospheric environment, output from mesoscale models is used to gain insight of the atmosphere in the future. Mesoscale models are more likely to capture atmospheric details that a rawindsonde would show than a synoptic-scale model would. Assuming the mesoscale model has been initialized with accurate synoptic-scale structure, the mesoscale model

output gives the warfighter the opportunity to better exploit the environmental battlespace in the short-term future.

B. WHY FORECASTING AIR QUALITY IS IMPORTANT

The California Air Resources Board (CARB) was a cosponsoring agency of the South Coast Ozone Study of 1997 (SCOS97). One objective of CARB and its cosponsors in SCOS97 was to measure particulate levels over the Los Angeles Basin. Many local, regional, and national agencies are interested in the measurement of atmospheric particulates and the short-term prediction of the atmospheric pollutant contents. Locally, hospitals may be concerned with poor air quality days because it could mean increased numbers of patients with respiratory problems exacerbated by high ozone levels. Regional authorities would be interested in high ozone level predictions. With high ozone predictions in the short term, appropriate officials would issue carpool advisories or public notices of increased ozone level risk. By using a pollutant level prediction, high concentrations of ozone may be mitigated before they actually happen. National and international agencies, such as the North American Research Strategy for Tropospheric Ozone (NARSTO) have vested interest in ozone measurements and predictions. Forecasted areas of high ozone concentration would lead them to better place measurement instruments. The U.S. Navy also cosponsored the SCOS97 study. Tracking pollutants in the Los Angeles basin has direct correlations to tracking smoke, biological, or chemical parcels in a littoral battlespace.

Air quality models (AQMs) are necessary for these applications and externally driven meteorological models influence these AQMs. The Pennsylvania State University (PSU) /National Center for Atmospheric Research (NCAR) Mesoscale Model Version 5 (MM5) is recognized as a superior model for driving other AQMs and air quality applications (Pielke et al., 1991).

C. PREDICTABILITY THEORY

Atmospheric predictability is the ability of a numerical model to properly describe the atmosphere at a future time. All models, in an attempt to maximize predictability, strive for accuracy and skill. Accuracy is an objective measure of how well a particular model's forecast fits the observed sequence of events. Skill is a relative measure of forecast accuracy where one particular forecast is compared to another forecast (Nuss, 2000).

Figure 1-1 illustrates the hypothetical error of a numerical model forecast compared against a climatology-based or persistence-based forecast. A climatology-based forecast has constant error over time. A persistence-based forecast has less error initially until its error degrades to that of climatology at time t_2 and is worse than climatology beyond t_2. The numerical model forecast has relatively larger error in the very short term. This initial error is due to the lack of consistency between the initial model state and the dynamic allowances set in the model physics (Kuypers, 2000). Initial error is also due to unresolvable scales of motion the model cannot capture (Anthes and Baumhefner, 1984). After the model adjusts and achieves a stable agreement between the initial

observations and model physics (also called "spin up"), the process leading to the error peak (at t_1) decreases to a minimum. Here the model shows skill over both climatology and persistence. The initial errors grow over time, and at some point t_3, the model no longer shows skill over climatology.

Many factors affect atmospheric predictability, one of the most important being resolution. Mesoscale models with finer resolution grasp more spatial and topographic detail, and, using more sophisticated physics, can incorporate smaller scales of motion that a larger scale model could not resolve. When applied over a tightly defined geographic region, the mesoscale model can resolve motions caused by local forcing, necessary for mesoscale phenomena that a global or coarser model would not resolve. Over complex terrain, for example, a model needs a resolution of 4-5 km or less in order to properly resolve the flow (Stauffer et al., 2000).

For a given area of study, if weather is well observed, we expect less initial error with a finer resolution model. Finer resolution is more likely to capture smaller-scale phenomena, and a finer resolution model will maintain these phenomena longer through a forecast period. However, with more detailed physics and finer spatial separation, mesoscale models can have great variability over an area.

These phenomena of interest have shorter lifespans than those of synoptic-scale models, adding more complications to mesoscale forecasts. It is difficult to observe these phenomena on such fine spatial- and time-scales, let alone forecast them. Observations aloft are

even sparser than surface observation sites, making the ability to capture accurate vertical structure very challenging.

It is fair to compare one model's forecasts under different resolutions provided that a reasonable time scale is considered for all of the forecasts. Error growth, at any resolution, eventually contaminates all scales of motion (Anthes and Baumhefner, 1984). To minimize this, we consider only short-term forecasts (specifically 3hr, 6hr, 9hr, and 12hr) for this study.

D. MODEL VERIFICATION

Model verification is most often done one of two ways: comparing model forecasts against model-generated analyses or comparing model forecasts against observations. The former is most convenient because the forecast and analysis fields are on collocated model grids. The latter is more challenging because there are rarely enough observations over a particular area to create a picture as complete as the model-generated analysis. In areas of sparse observational data, the first guess forecast is the heaviest influence on the current analysis. The Cooperative Program for Meteorology, Education and Training (COMET) Numerical Weather Prediction Module discusses the details of each model verification method.

This case study compares synoptic patterns from NOGAPS (Navy Operational Global Atmospheric Prediction System) to MM5 to ensure MM5 has the correct "big picture" (not included) and compares model forecasts against observations to generate statistical results. The SCOS97 provides an exceptionally rich data field over the area of study.

E. HYPOTHESIS

Meteorologists generally accept that a static initialization, or cold start, of a mesoscale model produces poorer forecasts than a model with a dynamic initialization, or warm start. A cold start of a mesoscale model incorporates a global model (in this study NOGAPS 1°x1° horizontal resolution) and National Weather Service (NWS) observations for defining initial and lateral boundary conditions (LBCs). From these inputs, the mesoscale model derives its analysis and forecasts. A warm start uses the same, but also incorporates a previous mesoscale model forecast as its first guess. Conventional wisdom says the warm start is better because it maintains the mesoscale structure generated by the first guess that a global model cannot. Essentially, the cold start resets the mesoscale structure and must redevelop it at each initialization.

Also, a model with more complex physics and complex terrain resolution should perform better than a simpler model. Sophisticated physics and terrain resolution should allow a model to see and interpret finer mesoscale phenomena. It follows that the more sophisticated model physics, for an accurately defined initial state, should have less initial error. Therefore, a model run with sophisticated physics has less initial error propagating through its forecast cycle. Also, the model may trace a parcel more precisely over terrain through a forecast, lessening the model user's need to round off or interpret some values.

Another widely accepted theory is more observations fed into a model at analysis time will lead to better

forecasts. Again, more observations lead to a more complete picture of the atmosphere at analysis time. Any model analysis will have some initial error. However, decreasing initial error means less initial error will propagate, yielding better forecasts.

We hypothesize these principles are not always true. Because the phenomena a mesoscale model attempts to follow are short lived in both time and space, there will always be error in any analysis or forecast. A warm start may propagate an error in a model's forecast further than would a cold start. More sophisticated physics may not provide any significant benefit to a forecast if the initial error is too great or if the model physics use assumptions not valid for the scale of interest. Lastly, more observations may not add any significant insight to the initial state of the atmosphere the model is trying to resolve because they might not be located in a position relevant to defining important small-scale structural details.

F. OBJECTIVES

In this study, we examine four one-way nested domains of MM5, namely MM5 81km, 27km, 9km, and 3km. We examine the ability of each domain to capture the flow over the area of study and examine the error statistics of each model compared against observations. We will run a control experiment model run for each domain using a warm start and sophisticated planetary boundary layer (PBL) scheme. Our first experiment will be to run a cold start for each domain, maintaining the same complex PBL scheme. Our second experiment will look at running a warm start using simpler physics (a less complex PBL scheme). Lastly, we

will run the same control experiment and inject extra observations from the SCOS97 study into the model initialization that were not part of the original control case.

We will show that, for our case, the accepted conventional wisdom mentioned earlier is not necessarily correct.

A description of the model used in this study will be given in Section II. Background information related to the SCOS97 study and related observations will be given in Section III. Section IV will discuss weather over the area of study for 4-7 August 1997. Our methodology and results will be discussed in Section V and Section VI. Lastly, Section VII will offer our conclusions and ideas for further study.

II. MODEL DESCRIPTION

The PSU/ NCAR MM5 Version 3.3 is used for this study. MM5 is a one or two-way continuous, multi-nested, non-hydrostatic, terrain-following, sigma coordinate, primitive equation model. For this study, MM5 was run on a one-way continuous, quadruply-nested configuration with horizontal grid spacings of 81km, 27km, 9km and 3km. The 81km domain is centered at 34.2N 119.38W with 41 points in the E-W direction and 45 points in the N-S direction. The 27km domain has dimensions 43 x 43. The 9km domain has dimensions 73 x 73 and the 3km has dimensions 97 x 97. Figure 2-1 shows the horizontal extent of each domain.

NOGAPS with 1° x 1° resolution is used for both the initial and boundary conditions. Warner and his coauthors describe limitations and concerns about lateral boundary conditions applied to local area models (Warner et al., 1997).

Two-dimensional multiquadric interpolation (2DMQ) (Nuss and Titley, 1994) is used to blend first guess grid fields and observations to MM5 grid fields. There are several key points to mention about the 2DMQ method. First, as the name implies, the method is two-dimensional. Each isobaric level is solved independently of any other. For example, wind direction at 850mb is solved for independently of wind direction at 925mb.

A second point to note is this method is univariate, meaning each parameter in the model is solved for independently of another. For another example, wind speed is solved independently of temperature.

One compelling argument for using the MM5 is the ability to test the sensitivity of model forecasts to different physical parameterization schemes. We choose to compare the more sophisticated physics in the Gayno-Seaman PBL scheme (Gayno et al., 1994) to the simpler physics of the Blackadar PBL scheme (Blackadar, 1979). We use a five-layer soil model parameterization scheme and no convective parameterization scheme for our MM5 runs.

All domains incorporated a vertical resolution of 30 vertical levels. A total of 12 levels are located between the 850mb level and the surface.

Topographic resolution for each domain is incorporated from the U.S. Geological Survey. The 81km and 27km domains derive their topography and land use from 19km terrain and land use resolution. The 9km domain derives its topography and land use from 9km terrain and land use resolution, and the 3km domain derives its topography and land use from 1km terrain and land use resolution.

III. BACKGROUND

A. ABOUT THE SCOS97 STUDY

SCOS97 incorporated a very large base of meteorological observations spread over an 80,000 square mile area within the Los Angeles basin. The massive amount of data was collected over a period from 16JUN1997 to 15OCT1997 from 259 different observation sites.

This paper focuses on the period from 04-07 August. These dates envelop a measured high ozone event, with surface ozone measurements peaking near 2200Z on August 5th (Boucouvala, 2000).

B. DESCRIPTION OF OBSERVATION STATIONS

Figure 3-1 depicts the general topography of the Los Angeles basin. The basin is bordered on the west and south by the Pacific Ocean. The Santa Monica and San Gabriel Mountains border the northern area of the LA basin and the San Bernadino and San Jacinto mountains mark the eastern boundary. The Santa Ana Mountains are southeast of Los Angeles and also affect area weather. Figure 3-2 shows the boundaries of our area of verification and also shows how each of the 37 chosen observation stations fits with the local terrain. Table 3-1 provides the location specifications of each station.

Surface sites provided hourly observations. Five rawindsonde sites made observations every six hours (00Z, 06Z, 12Z, 18Z). Continuous profiler data (mean values only) came from nine sites. All observations were quality checked by CARB, and all observations of uncertain quality were excluded from our study.

All observations were noted at heights in meters above ground level (AGL). These values were used as the "control" for the model measurements. Since MM5 is a sigma coordinate model, all model values were interpolated vertically to the same level as the observations for comparison purposes, with the exception of the surface observation comparison. Surface comparison was done using the model forecast parameters at the lowest sigma level, located at about 22m AGL.

Infrequent gaps in the observation data exist for various reasons. The most likely reason for these gaps is due to the quality control scrub by CARB. We should also note the gaps in observational data at non-synoptic times. At the synoptic times, we are afforded the additional data from the rawindsonde measurements.

IV. METHODS

A. HOW WE SEGMENTED OUR DATA

Table 3-1 and Figure 3-2 describe the stations from which our observational data came. We divided our atmospheric area of interest into six layers, specifically described in Table 4-1. Over the area of study and within each layer, we summed all appropriate data points to derive an average for a particular time. For any particular time, there will be six values for a given parameter, one value for each of the six layers.

The same principles were applied to model forecast results, and the MM5 data was interpolated to the exact AGL location as the upper air observation data. The interpolated values come from model grid point values within the verification area. The 81km domain has three grid points over this area, while the 27km, 9km, and 3km domains have 36, 322, and 2912 grid points, respectively.

This study is concerned with short-term forecasts, namely MM5's 3hr, 6hr, 9hr, and 12hr forecasts. These are the only forecasts plotted over time. To further clarify, examine Figure 4-1. At 05/03Z and 05/15Z, five values for mean temperature in the surface layer are plotted, namely the observed mean temperature and the mean temperature 3hr forecasts for all four domains. At 05/06 and 05/18Z, the mean observed temperature is plotted along with the 6hr forecasts of the four MM5 domains. Likewise, 05/09Z and 05/21Z plot 9hr forecasts, and 05/12Z and 06/00Z plot 12hr forecasts.

From the observational data, we compute mean and standard deviation fields for wind speed, wind direction,

temperature, and virtual temperature and derive the same information from the model forecasts. In addition, we calculated a root mean square difference and bias for each model domain. We used the same definitions of error and bias as the U. S. Navy's Fleet Numerical Meteorology and Oceanography Center (FNMOC). Error is the difference of model forecast minus observation. Bias is model's tendency to over or under-forecast a parameter. FNMOC's Monthly Models Report has a section of routine statistical measures that describes these in greater detail.

A parallel study (Mohammed, 2000) uses the same data set to study the WOCSS (Winds Over Critical Streamline Surfaces) model. Some data related to his study is also seen in this study's results.

B. WARM START VS. COLD START

Our control experiment (noted CTRL), the normal MM5 set up to which we compare our other experiments, is a warm start. It is initialized using a previous 12hr MM5 forecast blended with NWS surface and rawinsonde observations. The MM5 12hr pre-forecast is generated using a cold start initialized with NOGAPS analyses and available NWS observations. This CTRL run employs the sophisticated Gayno-Seaman PBL scheme (Gayno et al., 1994).

The first study is a comparison to a cold start of MM5 (noted COLD). In COLD, MM5 is initialized using only NOGAPS analyses and NWS observations. COLD also employs the Gayno-Seaman PBL scheme.

C. VARYING PBL SCHEMES

The second experiment (noted TEST1) looks at changing the PBL scheme used in MM5. For this study, we ran MM5 using the Blackadar PBL scheme (Blackadar, 1979). The Blackadar PBL scheme is a lower order closure model than the Gayno-Seaman PBL scheme. All other aspects of the model set-up in TEST1 match those in CTRL.

D. INJECTING ADDITIONAL OBSERVATION DATA

The final experiment (noted TEST2) examines the effect of injecting additional observations into MM5's initialization. The NWS observations are the normal input expected to initialize MM5 on a regular, consistent basis. Our study takes additional observations from the SCOS97 data set and inputs them into MM5's initialization. These observations were not part of the input to CTRL and are independent from those used in model verification.

E. DATA PROCESSING

Weather chart analysis was done using GARP Version 5.4. FORTRAN programs were used to compute some observation and model statistics and to bin the data into appropriate files. Microsoft Excel computed additional statistics and was used for plotting statistical results.

THIS PAGE INTENTIONALLY LEFT BLANK

V. WEATHER DISCUSSION

A. CLIMATOLOGICAL DISCUSSION OF THE LOS ANGELES BASIN

The Los Angeles basin has a climate dominated by two distinct seasonal rainfall patterns, a rainy winter season and a dry summer season. The modified Köppen classification system categorizes this climate as *Mediterranean* (Bruno, 2000). This study is embedded in the heart of the dry summer season. During this season, southern California is dominated synoptically by the Eastern Pacific High. Warmer, dryer air aloft subsides over cooler, moister air at the surface to create a *marine layer*, the predominant weather feature during the Los Angeles summer. Under this high pressure, synoptic winds are generally light and variable. Mostly clear skies over inland areas and often times cloudy skies over coastal areas lead to a substantial surface temperature gradient. This temperature front induces the prevailing summertime sea/land breeze regime over the Los Angeles basin.

Figure 5-1 depicts a typical diurnal sea breeze regime (Ahrens, 1991). Uneven heating rates between land and water induce a mesoscale circulation, producing onshore winds during the day (sea breeze) and offshore winds during the night (land breeze). An important consequence of the sea breeze is the sea breeze front, the onshore push of cooler marine air over land. Ahrens provides more details of the sea/land breeze regime in his text.

The rainy winter season (NOV-APR) is influenced by the migratory track of the Polar Front Jet. Cool air aloft and storms in the mid-latitude cyclone track break down any substantial marine layer. This marine layer is a concern

because it tends to trap and hold smog. It logically follows that more bad air quality days exist in the summer months than in the winter months. The National Weather Service publication NWS WR-261 is an excellent data source for providing much greater detail on the climatology of Los Angeles.

B. SYNOPTIC SITUATION

For the period between 040000ZAUG1997 and 080000ZAUG1997, large scale synoptic conditions are generally unchanging. For readability, all ddhhmmZMONYEAR times shall be abbreviated. For example, 051200ZAUG1997 shall be noted as 05/12Z.

Building heights at 300mb over the western U.S. keeps the long wave trough and the Polar Front Jet far from any areas that may affect southern California. In fact, NOGAPS analyses show no 300mb winds greater than 15-20kts over southern California during this period (not shown).

At 04/00Z, a 5580m cut-off low sits west of Vancouver Island and a strong ridge sits over the western U.S. at 500mb (Figure 5-2). The low fills slightly over the next 36 hours (Figures 5-3 through 5-5) while heights rise over southern California and the western U.S. At 06/00Z, an approaching low over the Aleutian Chain influences the Vancouver low (Figure 5-6) while the western U.S. ridge reaches its maximum heights. The long wave trough deepens south of the Aleutian chain through 08/00Z while the ridge over California flattens and slightly weakens (Figures 5-7 through 5-10). Weak and constant vorticity values over southern California during this period show little, if any, vertical motion exists at this level.

The 925mb series of geopotential height and temperature plots shows a general warming trend throughout the period of interest. 04/00Z shows a closed 27C isotherm over southern California (Figure 5-11), and the chart following 12 hours later (Figure 5-12) shows that pool of warm air 3C cooler and closer the California/Mexico border. The charts on August 5th show not only a broader span of warmer temperatures over California, but also closed isotherms 3C greater over southern California on both the 00Z and 12Z analysis. 05/00Z shows another 3C change over California near Point Conception, as well as a 3C change over the California/Arizona border, increasing to closed isotherms of 33C and 36C respectively (Figure 5-13). The 12Z analysis on August 5th (Figure 5-14) shows a 3C warm up over southern California bight region from the previous 24 hour 12Z time frame. Temperatures at 00Z on August 6th (Figure 5-15) remain fairly constant compared with the previous day, while 12Z temperatures (Figure 5-16) over the bight region cool slightly from the previous evening, evidenced by the lack of a closed 30C closed isotherm. Temperatures over the bight region cool by a few degrees on the 07/00Z analysis (Figure 5-17), while the warm temperatures over the California/ Arizona border change very little from the previous day, hinting toward the end of the warming trend. Temperatures at 07/12Z (Figure 5-18) similar to those from the previous day further support the conclusion of the warming trend. Temperatures continue to cool at 08/00Z (Figure 5-19), with the warmest pocket of warm air shifting eastward into Arizona, drawing the thermal tongue eastward and allowing temperatures over the

bight region to cool another 2-3C from the previous 24 hour period.

The surface plot of mean sea level pressure shows the diurnal shift of the inverted thermal trough over California. Figures 5-20 through 5-28 show the series of surface pressure analyses. Intense heating during the day draws the thermal trough further east from the coast, evidenced by the 00Z plots. At night (12Z plots), the trough is slightly less pronounced and further toward the Pacific coast. Surface pressure change over southern California is minimal during the period. However, the eastern Pacific surface high pressure center west of central California along 130W longitude builds from 1024mb on 05/00Z to 1026mb on 06/00Z. This time corresponds to the peak of the upper level ridge as well as the lowest surface pressure over California/ Arizona/ Mexico border. The result is an increased pressure gradient over the central California coast for a brief time between 00Z and 12Z on August 6th (Figures 5-24 and 5-25). The surface high continues to build through the rest of the period, but shifts northward and westward as it does so, producing little impact on any pressure gradient over central or southern California after 06/12Z.

C. MESOSCALE SITUATION

For the mesoscale meteorological situation, attention is focused on the period from 04/12Z to 07/00Z.

We make some assumptions and define thresholds for winds over the area of study. We assume strong onshore flow (sea breeze) to be a primarily west-southwesterly wind, from 220° to 290°, and offshore flow (land breeze) to

be a primarily north-northeasterly wind, from 020° to 100°. More importantly, we define a speed of 3 ms^{-1} or less to be an insignificant enough wind speed to determine a verifiable wind direction. That is, 3 ms^{-1} winds are considered, for this study, light and variable.

The plots of domain-averaged mean observed temperatures across the timeline show a distinct difference in between the lower layers and the upper layers (Figure 5-29). The surface layer demonstrates a clear diurnal cycle, warmer temperatures at the 18 and 00Z time frames and cooler temperatures at 06Z and 12Z. Layers two and three also show a diurnal temperature wave, and though these two layers are generally in phase, they lag the surface plot. Further aloft, the recognizable diurnal temperature wave becomes a bit more complex.

All layers seem to verify the general warming trend seen on the synoptic charts. Over the area of study, the general warming trend begins on August 4th and continues until early morning of August 6th. All layers show a warmer temperature at 05/12Z than the time 24 hours previous. The same is true when looking at the warm part of the diurnal cycle. Five of the six layers at 06/00Z are warmer than the 05/00Z plot.

After 06/12Z, the warming pattern of the 48 hours earlier starts to disappear. At 12Z on August 6th, the surface layer and layer four have continued to warm up compared to the previous evening, but the other four layers have returned to their previous low or have cooled.

Looking at wind speeds for the time period (Figure 5-30), surface wind speeds peak at approximately 21Z of each day and slow to a minimum at night between 09Z and 12Z.

Peak upper layer winds show a more complex variation from diurnal change. Speeds on August 4th and 5th are relatively weak, rarely getting above 5 ms^{-1} in any layer at any time.

For August 4th, the peak time of the sea breeze occurs between 21Z and 00Z. Looking at the 05/00Z time frame, winds are strongly onshore from the surface up through layer four. Layers five and six show light and variable winds. Recalling Figure 5-1, we conclude that our six layers fail to capture the entire sea breeze solenoid, as no strong evidence of return flow exists (Figure 5-31).

At 05/12Z, winds are light and variable throughout all six layers. Like the night before, no evidence exists of any organized land breeze.

Wind speeds increase again as temperatures rise, and the sea breeze again dominates the surface layer by 05/21Z. At 06/00Z, wind speeds in the upper layers follow the surface and strengthen, but they are greater than the winds from the previous afternoon. In fact, layers three through six increase by more than 2ms^{-1} from their wind speed on the 05/00Z chart. Conversely, mean speeds in the surface layer and layer two decrease.

Comparing the 06/00Z observations against those from 24 hours previous reveals a definitive change in the strength of the solenoid. Peak temperatures at 06/00Z would drive a stronger sea breeze in the surface layer, not a weaker one. Upper layers would also tend to reflect a mean direction similar to the sea breeze of the day before. Instead, upper layer winds have gained a more northerly component at 06/00Z (Figure 5-31). A decrease in wind direction standard deviation over layers three through six (not shown) indicates the wind is more consistently from

one direction over the area of study. It is the brief synoptic change interfering with Los Angeles mesoscale regime that alters the state of the solenoid early on August 6th. This interruption is very brief. Surface winds are light and variable again by 06/12Z, and upper level winds are decreasing as well. As for the previous night, no strong demonstration of a nighttime land breeze exists in any layer.

By 07/00Z, temperatures at the surface begin to increase slightly. The surface layer sea breeze strength increases, and winds throughout all six layers demonstrate onshore flow.

Another important feature to trace in the mesoscale regime is the sea breeze front. The push of the sea breeze advects cooler marine air inland, lifting the inversion base. We trace the sea breeze front from hourly profiler observations, specifically examining profiles taken at 00Z and 12Z.

Profiler stations not located in close proximity to the coast (all but PHE and LAX) show surface-based inversions at night (12Z) and various changes in the inversion base height during the day (00Z). A 00Z station profiler showing an elevated inversion base as well as surface temperatures similar to those at 12Z tells us the sea breeze front has reached that station, perhaps even pushing further inland. Refer to Figure 3-2 to see the location of each profiler site.

At 04/12Z, only PHE and LAS have inversion bases above the surface, showing they are the only stations embedded in marine air. At 05/00Z, the sea breeze front has reached USC, SMI, LAX, and TTN, evidenced by a rise in inversion

base height and/or a drop in surface temperature. The front retreats toward the coast again at night, with only LAX showing any signs of marine air at 05/12Z. At 06/00Z, the front has again moved inland as far as EMT, SMI, USC, and TTN. 06/12Z profilers show the front has again retreated back to the coast, with only PHE showing evidence of marine air. A key station in these profilers is VNS. In this entire time frame, VNS shows neither an elevated inversion nor a drop in surface temperature. We conclude the sea breeze front never penetrates as far inland as VNS.

In summary, the sea breeze solenoid is the dominant mesoscale feature over Los Angeles for the period, with the exception of the brief synoptic influence shortly after 06/00Z.

VI. RESULTS

A. PARAMETER AVERAGE TIME SERIES

The surface layer presents the greatest variability of the six layers, not only between each domain, but also between each experiment. Figures 6-1 through 6-3 show the time series plots for domain-averaged mean wind speed, mean wind direction, and mean temperature in the surface layer for CTRL. The same is done for each parameter in COLD (Figures 6-4, 6-5, 6-6), TEST1 (Figures 6-7, 6-8, 6-9), and TEST2 (Figures 6-10,6-11, 6-12). Mean observations are also plotted in each figure and are a good comparison marker.

Looking at the wind speed time series, observations show a clear diurnal cycle with one peak speed at the hot part of the day. No domain in any of the four experiments grasps a similar pattern. Each domain in each experiment shows over-forecasted speeds in the cold part of the day.

Wind direction also has a distinct diurnal wave in the observations. Very low wind speeds (less than 1.5 ms^{-1}) at night make a definitive wind direction difficult to ascertain. During the daytime, however, it is clear that a sea breeze exists. Each model experiment shows a diurnal pattern, although there are some significant differences. Each experiment shows the different domains forecasting nighttime winds with an offshore component greater than the observations. In each experiment, the 3km and 9km forecasted directions are more similar to the observations and have a more damped wind direction wave than 27km or 81km.

The temperature time series present some interesting results. As the observations show, there is a strong diurnal temperature wave that experiences a gradual warming over the period, supporting the trend seen in the NOGAPS charts. In each experiment, all domains grasp this diurnal pattern, although each domain in each experiment lags the observations to some extent. By lag, we mean the tendency for the models to forecast a minimum temperature approximately three hours later than the observed minimum is seen. All domains do an adequate job in forecasting the warm part of the day, but all experiments fail to cool the surface temperature enough at night. At these cool times (06Z, 09Z, 12Z), COLD shows forecasted temperatures 1-4C closer to the observed temperature than CTRL, TEST1, and TEST2 in each domain.

B. STUDY PERIOD STATISTICS

Tables 6-1a, 6-1b, and 6-1c show a further simplified representation of CTRL's forecasts in Figures 6-1, 6-2, and 6-3. The mean and standard deviation for wind speed, wind direction, and temperature for each domain's forecast have been averaged over the entire timeline. The same was done for the observed values. In addition, we calculated error (RMSD) and bias for each forecast. With over 500 forecast points to calculate each error or bias, we know even minor differences between domains are significant. Similar calculations have been done for COLD (Tables 6-2a, 6-2b, 6-2c), TEST1 (Tables 6-3a, 6-3b, 6-3c), and TEST2 (6-4a, 6-4b, 6-4c).

Recall the 81km domain had only three grid points over the verification area, meaning that all 500 points for the

81km domain were interpolated from many fewer grid points than the other domains. It is unlikely that such coarse resolution would capture any significant mesoscale structure we are interested in. If this domain appears to perform better than other domains, we conclude it is getting better error statistics for the wrong reasons.

Beginning with CTRL, forecasted wind speed gains significant improvement at 9km over 27km, and slight improvement at 3km over 9km. Forecasted mean, error (RMSD), and bias all improve with finer resolution, however, all domains have error greater than the standard deviation of observed wind speeds, indicating the forecasts show poor forecast skill (Kuypers, 2000).

The 3km wind direction is the closest to the observed mean direction. Each domain shows similar error, all of which are greater than the standard deviation of the observations.

The 27km, 9km, and 3km domains have a mean temperature more than 3C greater than the observed mean. Again, all domains have error greater than the observation's standard deviation.

In COLD's statistics, mean wind speeds for 27km and 9km domains are closer to the observed mean than in CTRL. Error and bias have also improved for these domains. The 3km wind speed statistics are nearly identical for COLD and CTRL.

Mean wind direction for COLD in each domain has changed more than 20° closer to the observed mean direction. Direction error in each domain is also less than CTRL, yet none are less than the observed direction standard deviation.

Mean temperature forecasts have also dropped nearly 3C for each domain. This measure, as well as error and bias, are much better than CTRL. Each domain's temperature forecast error exceeds observational standard deviation.

In TEST1, the simpler PBL scheme, results for each domain's wind speed and direction are slightly poorer than CTRL. Within TEST1, 3km and 9km domains show better speed and direction statistics than 27km.

TEST1 temperature statistics show slight improvement over CTRL, most noticeably in each domain's bias. Again, 3km and 9km prove better than 27km.

Lastly, TEST2's forecasts present numbers very similar to the statistics of CTRL. Adding extra observational data into MM5's initialization did little to change any values seen in the statistical result tables.

C. VERTICAL PROFILES

Figure 6-13 depicts the 9km domain-averaged vertical structure for each experiment at 04/12Z. Mean values for each parameter were derived at each layer (as done in the previous section) and plotted at the mid-level of each layer. This was done for each synoptic time through 07/00Z (Figures 6-14 though 6-18), and the same was done for the 3km domain (Figures 6-19 through 6-23).

As seen in the earlier times series plots, all domain forecasts in each experiment had difficulty in the cool part of the day (12Z). Looking at these times over the period of study shows very interesting results, such as the strong similarity between the 3km and 9km domains in each experiment.

Focusing near the surface on the 9km 04/12Z profile (Figure 6-13), each experiment forecasts temperatures much warmer than actually seen in the observations. The next two nights (Figures 6-15 and 6-17) show mean observation temperatures increasing, once again illustrating the warming trend. Note the model forecasts do not significantly change. The model forecasts are getting closer to the truth, but it is because the truth is moving toward the model solution. Each night, in both the 9km domain and 3km domain, the COLD profile comes closest to the observed vertical temperature structure.

Nighttime observations show a temperature inversion existing up into the third layer, while both domain forecasts only show the inversion existing up into layer two. COLD's profiles in both domains at 05/12Z and 06/12Z are the only profiles that show a PBL height within 500m of the observed PBL height.

Vertical wind speed structure at night shows the same forecast problem. For the 9km domain, each experiment shows wind speeds which are over-forecast at night. The 04/12Z profile of COLD's wind speed is the only exception.

Another feature of the profiles is how CTRL, TEST1, and TEST2 all show coast-parallel winds in layers three through six. Observations show winds with an onshore component at these heights AGL. COLD's wind direction profile stands out from the others.

Considering the water temperature of the Pacific Ocean to be essentially constant at 04/12Z, 05/12Z, and 06/12Z, the forecast from each domain and experiment shows a much stronger coastal temperature gradient than the observed

temperatures suggest. This implies a stronger thermal wind in the forecasts than in reality.

There are also some common problems with the 00Z (hot) profiles (Figures 6-14, 6-16, 6-18, 6-20, 6-22, 6-24). Observations show an elevated inversion layer at 05/00Z and 06/00Z, evidence of cooler marine air advancing inland. The forecasts in each experiment in each domain fail to recognize this feature.

Model forecasts show winds strongly backing between layers two and four to a definitively offshore direction in layers five and six. These layers are also where model wind speed peaks for each experiment except COLD.

Observations for 05/00Z and 06/00Z show peak speed in lower layers and backing much less with height. This is a typical signature expected for a strong sea breeze regime, very different from the signature presented by any of the forecasts.

Lastly, the 3km profiles are very close to the 9km profiles, similar to the nighttime comparisons. Neither domain shows a greater propensity than the other to match the observed profiles.

VII. DISCUSSION AND RECOMMENDATIONS

A. COMMON WEAKNESSES

Tables 6-1 through 6-4 present an important consideration for this study: no model domain, in any experiment, forecasts with distinguishable skill. No forecast wind speed, wind direction, or temperature error is less than the standard deviation of the observations. To show skill, numerical model error should at least be less than the standard deviation of the observations (Kuypers, 2000).

Another weakness seen throughout the study is the difficulty that each domain forecast has in approaching the cold part of the diurnal cycle. Forecasts tend to show higher winds at night, a result of the inaccurate lower layer thermal structure. Stronger winds would produce a deeper mixed layer and less pronounced nighttime inversion. Accurately depicting and tracing the evolution of the marine boundary layer is a critical element of pollutant forecasting (Ulrickson and Mass, 1990).

B. HORIZONTAL TEMPERATURE STRUCTURE

Figures 7-1, 7-2, and 7-3 show the nighttime CTRL near-surface horizontal temperature structure 12 hour forecasts over the entire 3km domain. Note the large areas of excessively warm forecasted temperatures shoreward of the basin's surrounding mountains, in some places more than 10C greater than the observed temperatures.

Figures 7-4 through 7-6 show the 22m AGL forecasted winds for the same times. Note on these figures the areas of downslope flow near the surface collocated with the warm

pockets seen in Figures 7-1 through 7-3. Subsidence associated with downslope flow acts to enhance the pre-existing coastal temperature gradient. This subsidence causes warming, due to adiabatic compression, which occurs in the warm air over land.

The strong coastal surface temperature gradient produces a strong thermal wind. Lower layer geostrophic wind plus thermal wind equals upper layer geostrophic wind. This large thermal wind is what drives the stronger upper wind speeds in CTRL than what was actually observed (Figure 6-15). The thermal wind is also what makes the model flow direction aloft coast parallel compared to onshore flow in the observations. The same can be said for forecasts in TEST1 and TEST2. COLD shows the least difference from observed temperatures in the lower layers. COLD, therefore, would have a less pronounced coastal temperature gradient, resulting in a weaker thermal wind. We hypothesize that this is why COLD's vertical speed structure more closely matches observations at 12Z.

Figures 7-7a, 7-7b, and 7-7c show the 3km domain 12 hour vertical profile forecasts for profiler site VNS. Tables 7-1 and 7-2 give the actual temperature and wind measurements taken from the VNS profiler at these same times, as well as some key lower-level model forecast wind values on Table 7-2. Note on Table 7-1 the slight increase in temperatures over the 48 hour period, again showing the general warming trend mentioned earlier. Table 7-2 shows the large disagreement between observed and forecasted winds at VNS. Downslope forecasted wind speeds near the surface are 2-3 times greater in the model than the observed downslope winds at VNS.

The model forecasted Skew-T plots do a fair job in capturing the shape of the temperature lapse when compared against the profiler temperature observations shown in Table 7-1. The forecasts show a profile indicative of subsidence at the surface, and the observations substantiate this with inversions between 473m and 683m AGL during the three 12Z times.

Figures 7-8, through 7-10 show a N-S vertical cross section through the VNS profiler site, from north of the site down south to the coast (section depicted on Figures 7-4 through 7-6). These figures again depict the 3km domain 12 hour forecasted temperatures and windspeeds.

At 04/12Z (Figure 7-8), the 31C isotherm sits aloft over VNS. The layer of temperatures greater than 31C over VNS increases each successive night (Figures 7-9 and 7-10). There is also a slight change in the 700mb wind forecasts over the three 12Z times. Higher heights further inland and lower heights offshore shift their orientation with the respect to the coast. The winds at 700mb back from slightly offshore at 04/12Z (Figure 7-11) to coast-parallel at 05/12Z (Figure 7-12) to slightly onshore at 06/12Z (Figure 7-13), reflecting a changing synoptic-scale pressure gradient orientation relative to the coastline.

The warm low-level temperatures near the coast at 04/12Z (Figure 7-8) contribute to decreased surface pressure near the coast by effectively reducing the mass of the surface-to-700mb layer. This results in an increased pressure gradient along the coast. The increased gradient results in increased downslope winds toward the coast. This leads to speed convergence near the coast, and increased upward vertical motion due to continuity. The

increased downslope flow also produces more warming over areas near the coast due to adiabatic compression. This warmer air will contribute to decreased surface pressure near the coast, and the self-induced feedback loop will continue.

The motion arrows in Figure 7-8 depict circulation vectors in the cross section. The 12 hour forecast valid at 04/12Z shows near surface windspeeds in excess of 3 ms^{-1} near VNS, far greater than indicated by the observations in Table 7-2. Figures 7-9 and 7-10 show 12 hour forecasts valid at 05/12Z and 06/12Z. At 05/12Z, the increased near-surface convergence produces greater upward vertical motion and is collocated with a low-level jet (LLJ). When the convergence decreases, as in Figure 7-10, the LLJ also decreases. The peak downslope winds, observed and forecasted at 05/12Z, correspond with maximum near-surface convergence and maximum strength of the LLJ.

The maximum strength of the LLJ occurs when the thermal gradient is parallel to the synoptic geopotential gradient. Thus the synoptic fields (Figure 7-12) and mesoscale pressure fields are working constructively, resulting in greater wind speeds in the lower levels (Table 7-2).

A preliminary look at long-term forecasts (15-24hr) shows similar subsidence problems for 24 hour forecasts valid at 12Z.

C. FINER RESOLUTION FORECASTS

An important consideration in any model is the significance of forecast resolution and resolution's influence on a forecast. Finer resolution models need

finer scale observations in order to exploit the forecast strengths built into the model.

For this study period, there is a definite gain in using the 3km or 9km domain vice the 27km domain. From Tables 6-1 through 6-12, no 27km forecast statistics are better than both the 3km and 9km forecasts. However, it is difficult to find any recognizable gain using a 3km domain forecast vice a 9km domain. The statistical results suggest little difference between the 9km and 3km forecasts. In each experiment, the 3km and 9km domain vertical structure plots are nearly identical.

D. MODEL PHYSICS

Each experiment is a change, to some degree, of the model physics. Although there was no experiment that forecasted particularly well, COLD presented the "least bad" experiment. For COLD to outperform CTRL, the pre-forecast had to inject more error into the model initialization. This error presents a cascading effect. The forecast has error, is used in the next time step's initialization, and the model has great difficulty in correcting itself. Theory says COLD loses any mesoscale structure continuity from model run to model run, but this study shows it also minimizes perpetuating mesoscale error.

The less complex PBL scheme in TEST1 was outperformed by the more sophisticated physics of CTRL. This study substantiates the theory that more complex physics schemes, when based on correct observations and valid assumptions, better resolve and forecast mesoscale structure.

Adding observations did little to improve forecast results. Inserting extra surface observations into the

model initialization should give a more complete *surface* picture to the model. However, it does little to change the *vertical* structure in the initialization process. The low-level vertical structure is the key to accurate PBL analyses and forecasts.

E. RECOMMENDATIONS

This study presents interesting results, but poses many more questions worthy of study. Some recommendations for future studies:

1. Try running MM5 using different soil models.

Will a different soil parameterization scheme result in better surface temperature forecasts valid at 12Z? Will it affect the coastal temperature gradient?

2. Try initializing MM5 with profiler observations.

Will adding upper air observations give more accurate initial vertical structure? Will better vertical structure at analysis time produce better forecasts?

3. Increase the number of vertical levels in the model boundary layer.

Will greater boundary layer definition improve the performance of different PBL schemes and MM5?

4. Apply these experiments at a different time of year.

Do we have model problems that are linked to a specific synoptic-scale pattern? Are there similar model problems under different seasonal or synoptic conditions?

5. **Employ a different initialization scheme (3DMQ, 3DVAR, 4DVAR).**

Does analyzing fields three-dimensionally better capture and maintain realistic mesoscale structure?

THIS PAGE INTENTIONALLY LEFT BLANK

APPENDIX A. TABLES

Station ID	Latitude	Longitude	Elevation (m)
Surface Ob Stations			
ACTN	34.45 N	118.20 W	793
ANAH	33.82 N	117.91 W	45
BRBK	34.18 N	118.32 W	168
CALB	34.15 N	118.61 W	320
ELDO	33.80 N	118.09 W	5
ELRO	34.26 N	119.13 W	34
EMMA	34.29 N	119.33 W	3
HAWH	33.93 N	118.37 W	21
IRVI	33.69 N	117.72 W	125
LANM	34.07 N	118.24 W	87
MBLD	34.24 N	117.65 W	1219
MILL	34.38 N	118.07 W	1070
NLGB	33.82 N	118.19 W	6
OJAI	34.45 N	119.27 W	231
PICO	34.01 N	118.06 W	75
PIRU	34.38 N	118.79 W	195
ROSE	34.54 N	119.18 W	1016
STAM	34.04 N	118.48 W	104
SVAL	34.28 N	118.68 W	310
SVLM	34.29 N	118.80 W	366
TOMP	34.21 N	118.87 W	232
SCLA	34.39 N	118.53 W	375
TUST	33.70 N	117.82 W	5
Rawinsondes			
EDW	34.90 N	117.92 W	723
PMG	34.11 N	119.20 W	2
POM	34.07 N	117.75 W	274
TUS	33.70 N	117.83 W	17
UCL	34.06 N	118.45 W	149
Profilers			
EMT	34.09 N	118.03 W	95
LAS	33.79 N	118.05 W	7
LAX	33.94 N	118.44 W	47
PDE	34.61 N	118.09 W	777
PHE	34.16 N	119.22 W	2
SMI	34.28 N	118.79 W	279
TTN	33.71 N	117.84 W	16
USC	34.02 N	118.28 W	67
VNS	34.22 N	118.49 W	241

Table 3-1. Observation stations.

	Surface Layer	Layer Two	Layer Three	Layer Four	Layer Five	Layer Six
Top	<30m AGL	<500m AGL	<1000m AGL	<1500m AGL	<2000m AGL	2500m AGL
Bottom	Surface	30m AGL	500m AGL	1000m AGL	1500m AGL	2000m AGL

Table 4-1. Division of atmospheric layers.

CTRL Case
Warm Start
Gayno-Seaman PBL Scheme
No SCOS97 Obs

Wind speed	Mean	StdDev	RMSD	Bias	Lag/Lead
Obs	2.028	0.991	--	--	--
81km	3.488	0.484	3.100	1.460	vrb
27km	4.042	1.755	3.377	2.015	vrb
9km	3.692	1.935	2.939	1.663	vrb
3km	3.649	2.044	2.784	1.621	vrb
WOCSS	2.361	1.520	2.171	0.333	vrb

Wind direction	Mean	StdDev	RMSD	Bias	Lag/Lead
Obs	194.865	73.535	--	--	--
81km	156.702	20.442	89.480	-7.739	lag
27km	143.946	50.630	92.655	-4.085	lag
9km	161.254	82.668	89.413	1.198	lag
3km	173.099	96.806	93.531	4.908	lag
WOCSS	170.563	79.879	88.920	-0.885	lag

Temp	Mean	StdDev	RMSD	Bias	Lag/Lead
Obs	27.101	3.499	--	--	--
81km	29.299	0.855	5.163	2.198	lag
27km	30.440	1.331	5.808	3.340	lag
9km	30.573	2.038	5.727	3.472	lag
3km	30.327	2.698	5.730	3.228	lag
WOCSS	--	--	--	--	--

Tables 6-1a, 6-1b, and 6-1c. CTRL case statistics.

COLD Case
Cold Start
Gayno-Seaman PBL Scheme
No SCOS97 Obs

Wind speed	Mean	StdDev	RMSD	Bias	Lag/Lead
Obs	2.028	0.991	--	--	--
81km	3.419	0.576	2.570	1.390	lag
27km	3.584	1.428	2.829	1.557	lag
9km	3.679	1.538	2.663	1.652	lag
3km	3.660	1.793	2.757	1.631	vrb
WOCSS	2.409	1.314	2.049	0.381	lag

Wind direction	Mean	StdDev	RMSD	Bias	Lag/Lead
Obs	194.865	73.535	--	--	--
81km	206.566	35.580	80.094	2.030	lag
27km	175.714	52.660	78.164	-4.736	lag
9km	192.460	59.982	78.243	-2.357	vrb
3km	196.540	67.183	78.930	3.845	vrb
WOCSS	197.640	56.768	78.551	3.718	vrb

Temp	Mean	StdDev	RMSD	Bias	Lag/Lead
Obs	27.101	3.499	--	--	--
81km	26.899	1.201	4.435	-0.201	lead
27km	27.133	1.404	4.328	0.033	lag
9km	27.324	2.061	4.088	0.222	lead
3km	27.598	2.573	4.040	0.499	vrb
WOCSS	--	--	--	--	--

Tables 6-2a, 6-2b, and 6-2c. COLD case statistics.

TEST1 Case
Warm Start
Blackadar PBL Scheme
No SCOS97 Obs

Wind speed	Mean	StdDev	RMSD	Bias	Lag/Lead
Obs	2.028	0.991	--	--	--
81km	4.054	0.660	3.421	2.028	lag
27km	4.324	1.857	3.669	2.296	lead
9km	3.935	2.153	3.146	1.907	lead
3km	3.971	2.206	3.077	1.943	lead
WOCSS	2.547	1.644	2.217	0.519	lead

Wind direction	Mean	StdDev	RMSD	Bias	Lag/Lead
Obs	194.865	73.535	--	--	--
81km	132.239	21.145	105.005	-12.164	lag
27km	130.726	51.881	102.643	-9.613	lag
9km	158.924	87.010	94.185	1.468	lag
3km	166.963	98.089	97.470	9.350	lag
WOCSS	169.478	73.535	93.418	-3.585	lag

Temp	Mean	StdDev	RMSD	Bias	Lag/Lead
Obs	27.101	3.499	--	--	--
81km	29.120	0.797	5.174	2.020	lag
27km	30.116	1.250	5.701	3.016	lag
9km	30.062	1.959	5.493	2.960	lag
3km	29.843	3.499	5.547	2.744	lag
WOCSS	--	--	--	--	--

Tables 6-3a, 6-3b, and 6-3c. TEST1 case statistics.

TEST2 Case
Warm Start
Gayno-Seaman PBL Scheme
Added SCOS97 Obs

Wind speed	Mean	StdDev	RMSD	Bias	Lag/Lead
Obs	2.028	0.991	--	--	--
81km	3.853	0.467	3.260	1.827	lead
27km	4.206	1.752	3.624	2.178	lead
9km	3.890	1.890	3.060	1.863	lead
3km	3.880	2.033	2.969	1.853	lead
WOCSS	2.453	1.494	2.247	0.425	vrb

Wind direction	Mean	StdDev	RMSD	Bias	Lag/Lead
Obs	194.865	73.535	--	--	--
81km	148.081	18.284	92.137	-14.380	lag
27km	138.215	46.691	92.734	-5.408	lag
9km	156.163	76.443	88.611	-0.078	lag
3km	172.410	93.119	91.483	0.977	lag
WOCSS	167.350	74.665	89.137	0.477	lag

Temp	Mean	StdDev	RMSD	Bias	Lag/Lead
Obs	27.101	3.499	--	--	--
81km	28.571	0.898	5.028	1.471	lag
27km	30.301	1.327	5.593	3.200	lag
9km	30.423	2.110	5.504	3.321	lag
3km	30.098	2.772	5.456	2.997	lag
WOCSS	--	--	--	--	--

Tables 6-4a, 6-4b, and 6-4c. TEST2 case statistics.

VNS	34.22N	118.49W	
	04/12Z	05/12Z	06/12Z
m AGL	Temp	Temp	Temp
158	27.58	29.60	29.52
263	28.27	31.63	31.74
368	29.03	31.99	32.65
473	29.59	31.91	32.76
578	29.45	31.96	34.47
683	28.83	32.07	34.81
788	28.47	32.06	33.48
893	27.67	32.08	33.37
998	26.93	31.57	33.89
1103	26.58	30.61	34.47
1208	26.30	31.08	34.34

Table 7-1. VNS profiler virtual temperatures for 04/12Z, 05/12Z, and 06/12Z.

VNS	34.22N		118.49W									
	04/12Z				05/12Z				06/12Z			
m AGL	Wspeed (m/s)		Wind Dir		Wspeed (m/s)		Wind Dir		Wspeed (m/s)		Wind Dir	
	OBS	MM5	OBS	MM5	OBS	MM5	OBS	MM5	OBS	MM5	OBS	MM5
152	0.73	3.10	14.21	33.20	0.74	4.80	328.79	27.30	2.64	1.30	86.07	75.20
210	0.95	3.00	18.77	47.80	2.47	6.70	346.05	48.40	1.73	2.40	55.96	113.00
268	1.39	3.30	65.12	68.20	3.97	8.40	350.59	59.50	2.53	3.30	42.07	94.70
326	0.76	4.70	14.23	88.50	5.15	9.10	348.79	65.60	2.77	4.00	44.34	90.40
384	1.48	6.40	34.24	99.00	5.65	9.40	349.33	70.40	2.97	4.50	41.52	88.50
442	2.10	7.40	79.10	103.30	6.21	9.20	354.42	73.80	3.30	5.00	49.82	85.50
500	3.44	8.10	107.66	106.60	7.16	8.90	356.81	77.00	3.04	5.50	35.52	83.40
558	3.01	8.10	113.96	109.50	7.20	8.50	2.24	78.80	5.77	5.80	5.97	82.30
616	1.65	8.10	105.43	112.50	5.75	8.10	357.63	80.60	5.11	6.10	9.93	81.40
674	0.88	8.30	197.20	113.50	3.77	7.70	2.49	81.20	3.54	6.30	3.78	81.40
732	1.02	8.60	216.50	114.40	3.73	7.30	22.36	81.60	4.48	6.50	20.15	81.40
790	2.38		252.90		3.24	6.90	11.54	81.80	4.97	6.60	9.12	81.50
848	3.49		251.73		3.66		7.66		5.12	6.60	15.53	81.70
906	2.54		244.73		3.89		0.78		4.90	6.60	19.39	81.90
964	3.75		241.74		4.04		350.78		4.21	6.60	351.62	82.10
1022	4.26		245.93		4.28		337.57		4.83	6.70	10.66	82.40
1080	3.86		248.80		3.71		342.47		5.46		10.11	
1138	5.05		252.15		3.64		323.34		4.48		350.38	
1196	5.68		256.75		4.20		312.64		5.48		13.38	
1254	999.00		999.00		3.27		308.10		5.69		359.17	
1312	4.86		242.08		3.88		299.36		6.63		0.84	
1370	4.67		237.57		3.60		277.18		5.90		348.54	
1428	4.24		173.65		3.24		271.82		6.24		343.27	
1486	4.41		173.94		3.75		273.59		4.21		6.58	
1544	4.53		177.63		2.87		262.13		2.95		356.91	
1602	3.91		174.53		2.35		257.32		2.31		1.38	
1660	4.14		177.05		2.89		251.80		2.85		9.36	
1718	3.80		178.76		1.78		240.30		3.26		32.62	
1776	4.01		196.47		2.42		216.75		3.66		33.39	
1834	3.33		187.17		1.81		202.52		3.27		22.93	
1892	3.37		189.00		1.65		182.46		2.78		21.09	
1950	2.94		189.45		1.69		172.06		2.76		31.59	
2008	2.94		179.13		2.09		166.30		0.44		48.18	
2066	2.85		179.69		1.97		162.79		1.73		204.43	
2124	3.21		184.54		2.55		146.41		3.88		220.08	
2182	3.64		188.35		2.61		146.62		2.44		161.28	
2240	3.89		191.42		2.46		168.29		2.95		163.52	
2298	4.02		192.40		2.51		165.14		2.96		168.35	

Table 7-2. VNS profiler winds for 04/12Z, 05/12Z, and 06/12Z

APPENDIX B. FIGURES

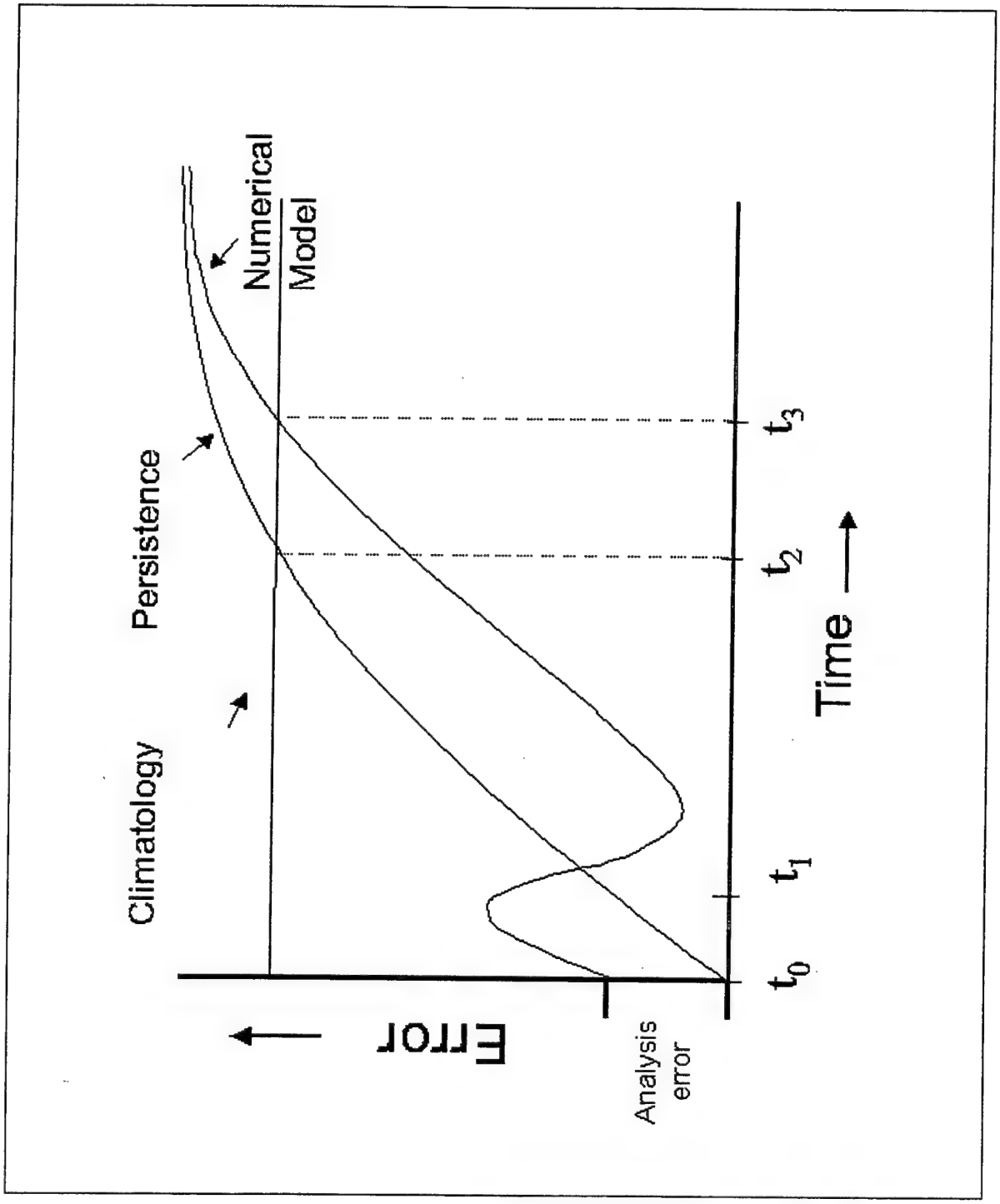

Figure 1-1. Numerical Model Forecast Error.

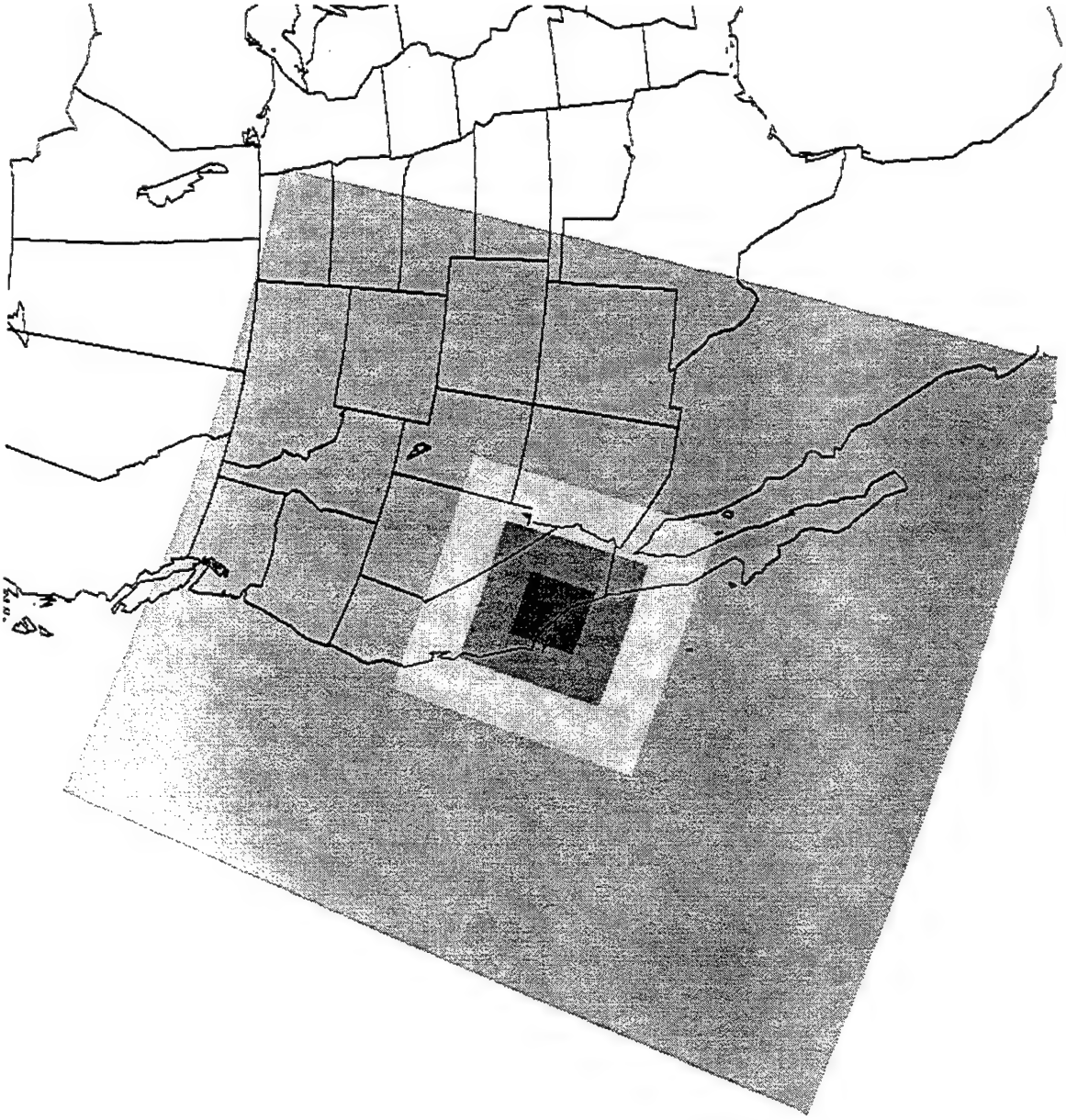

Figure 2-1. Concentric domain boxes: 81km (outermost), 27km, 9km, and 3km (innermost).

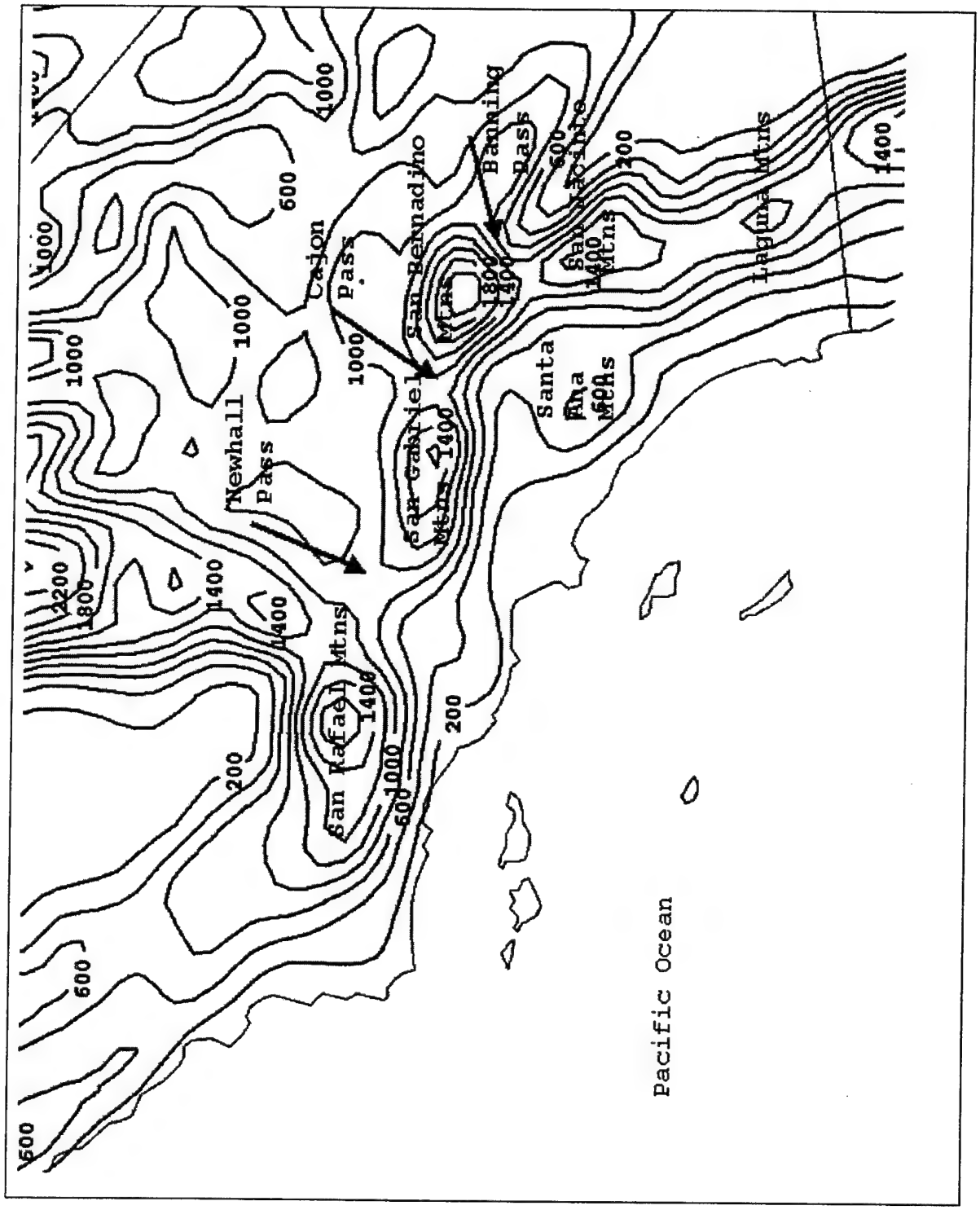

Figure 3-1. Major topography of LA basin.

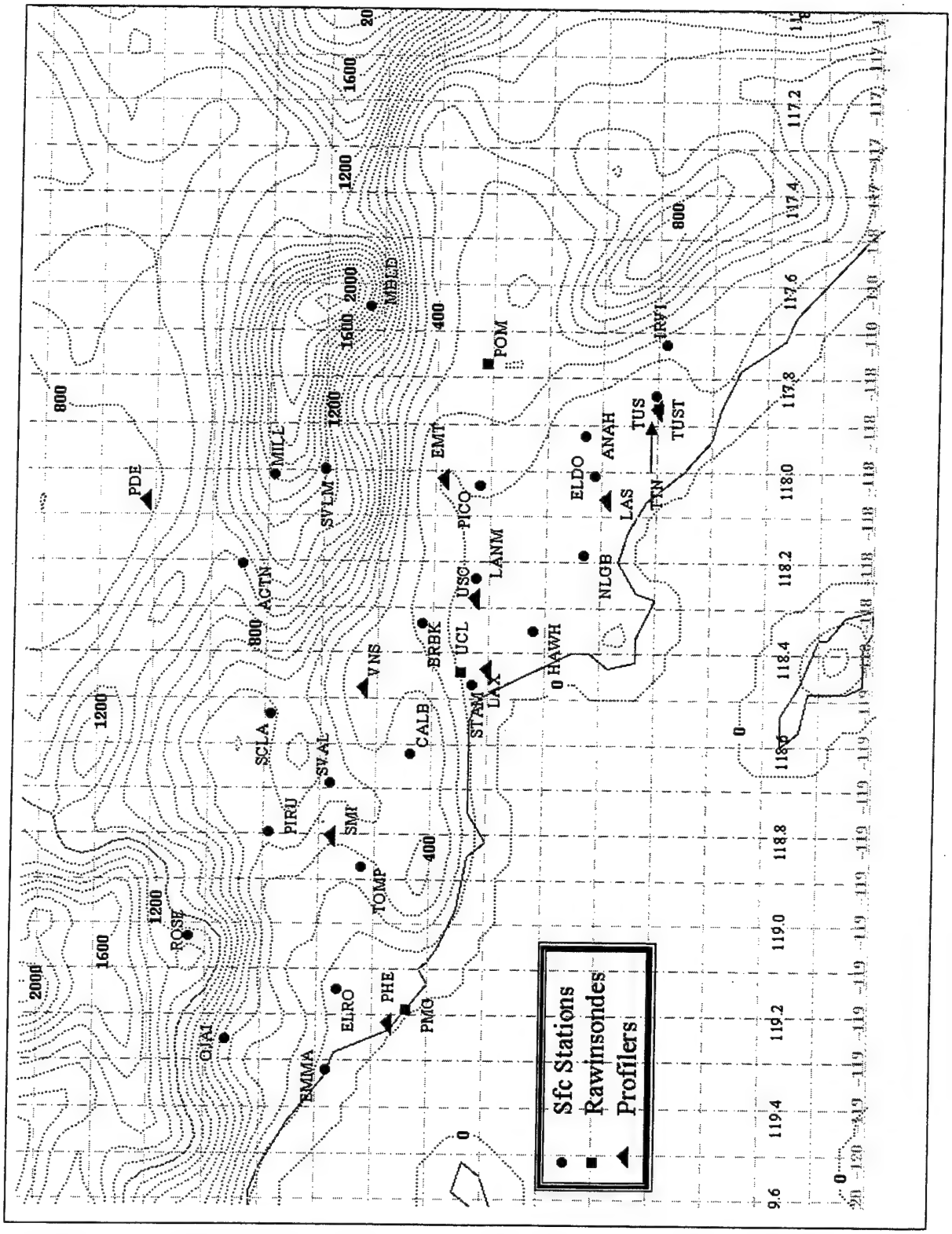

Figure 3-2. Geographic location of observation stations. Height contours (200m) from MM5 3km domain.

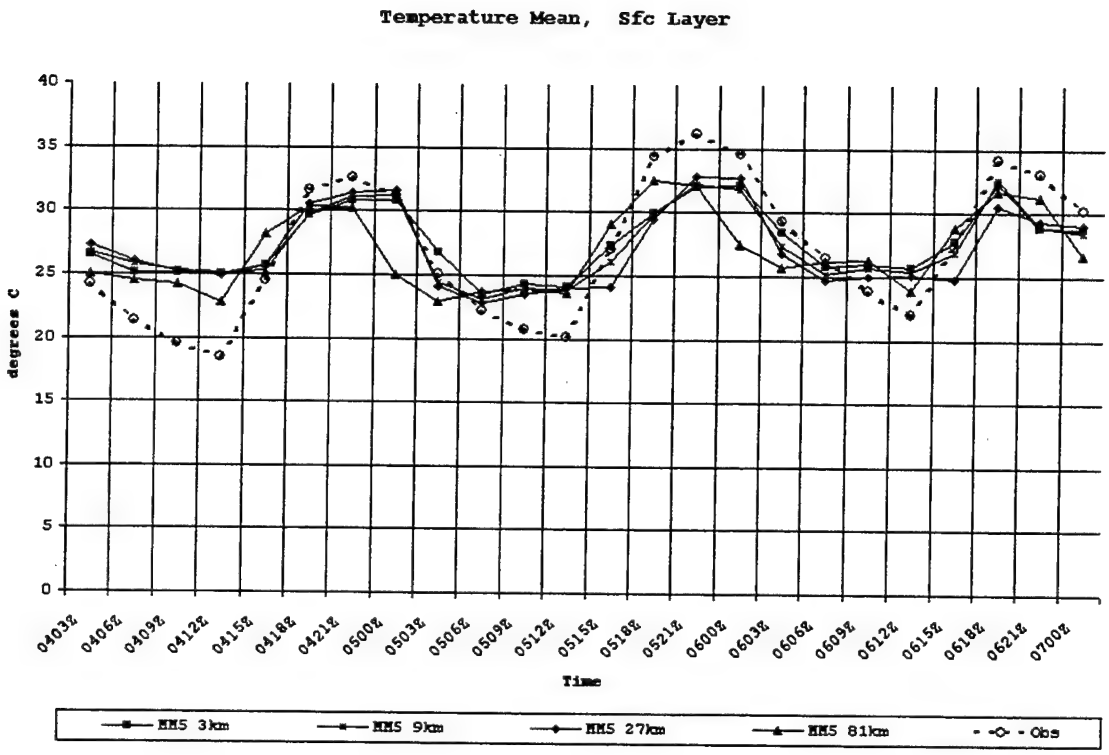

Figure 4-1. Mean surface temperature, 4 domains and observations.

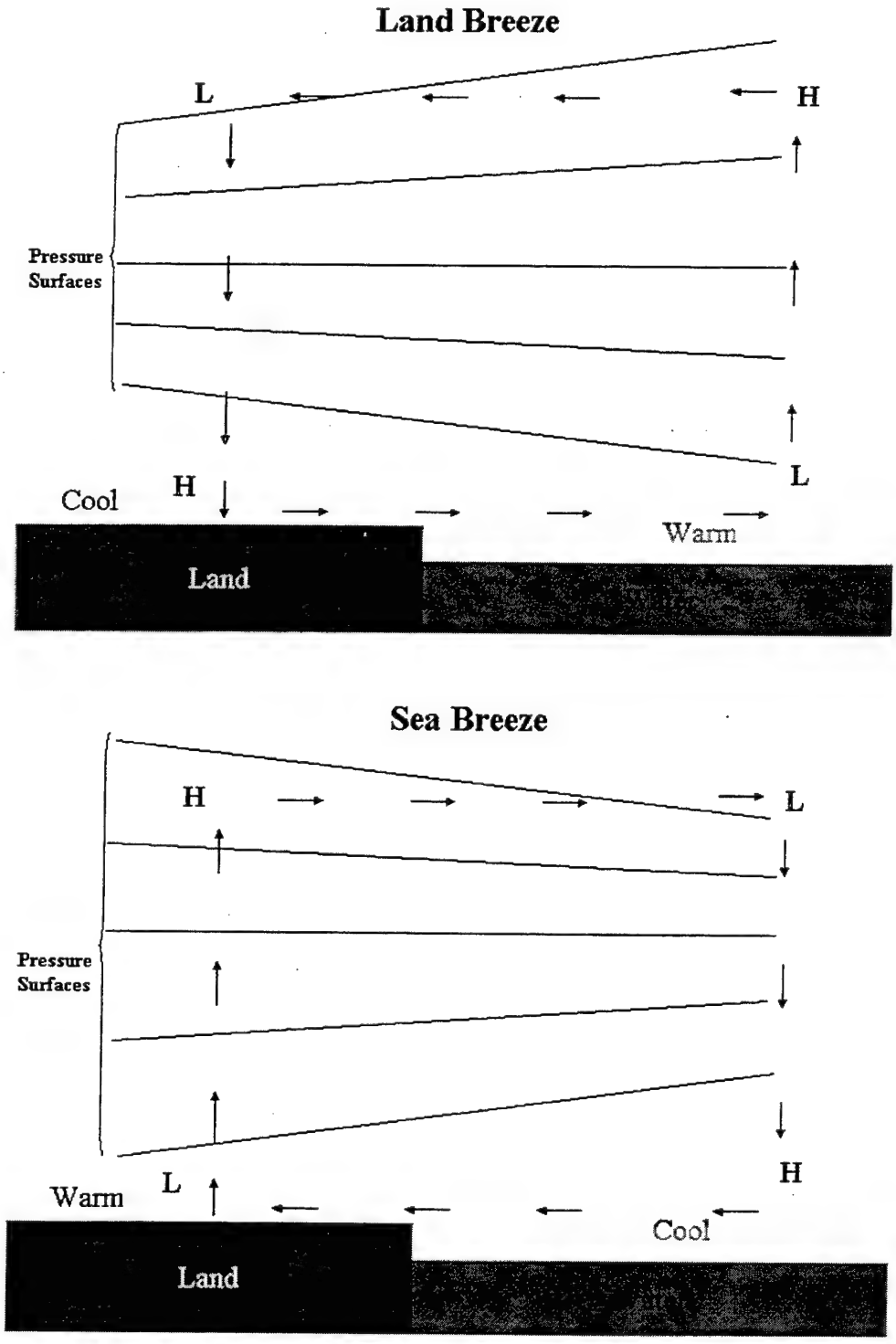

Figure 5-1. Land Breeze / Sea Breeze schematic.

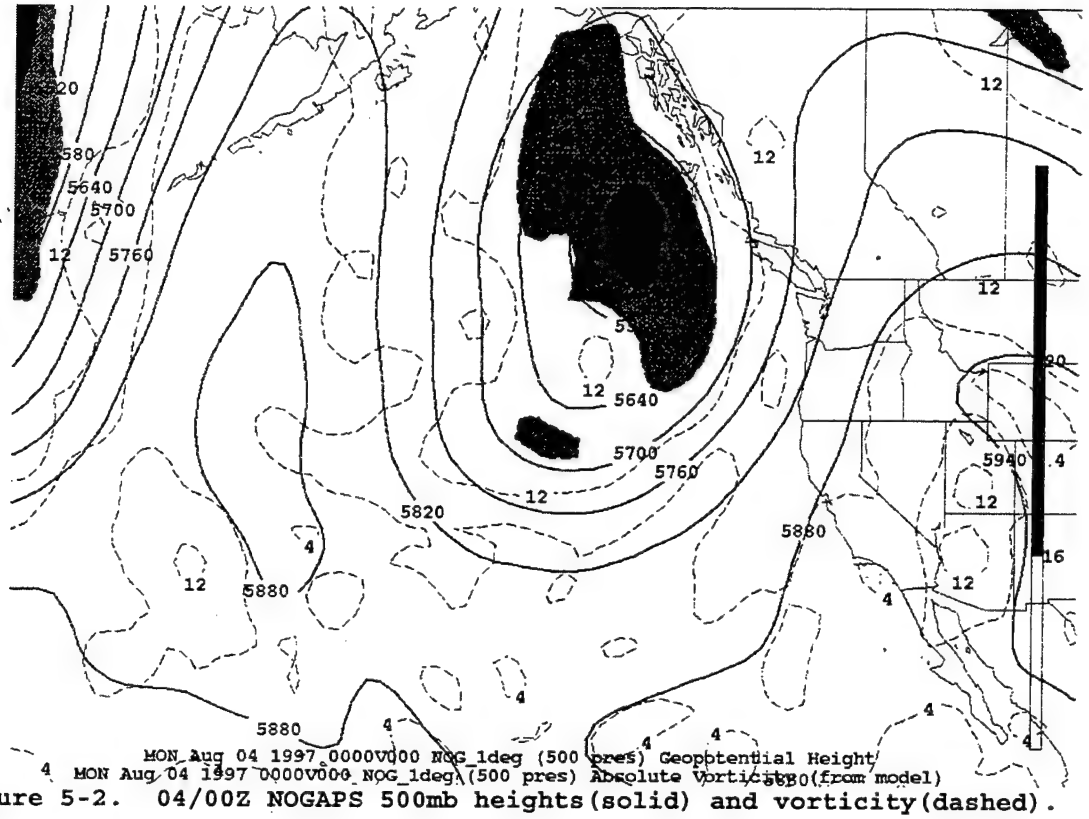

Figure 5-2. 04/00Z NOGAPS 500mb heights(solid) and vorticity(dashed).

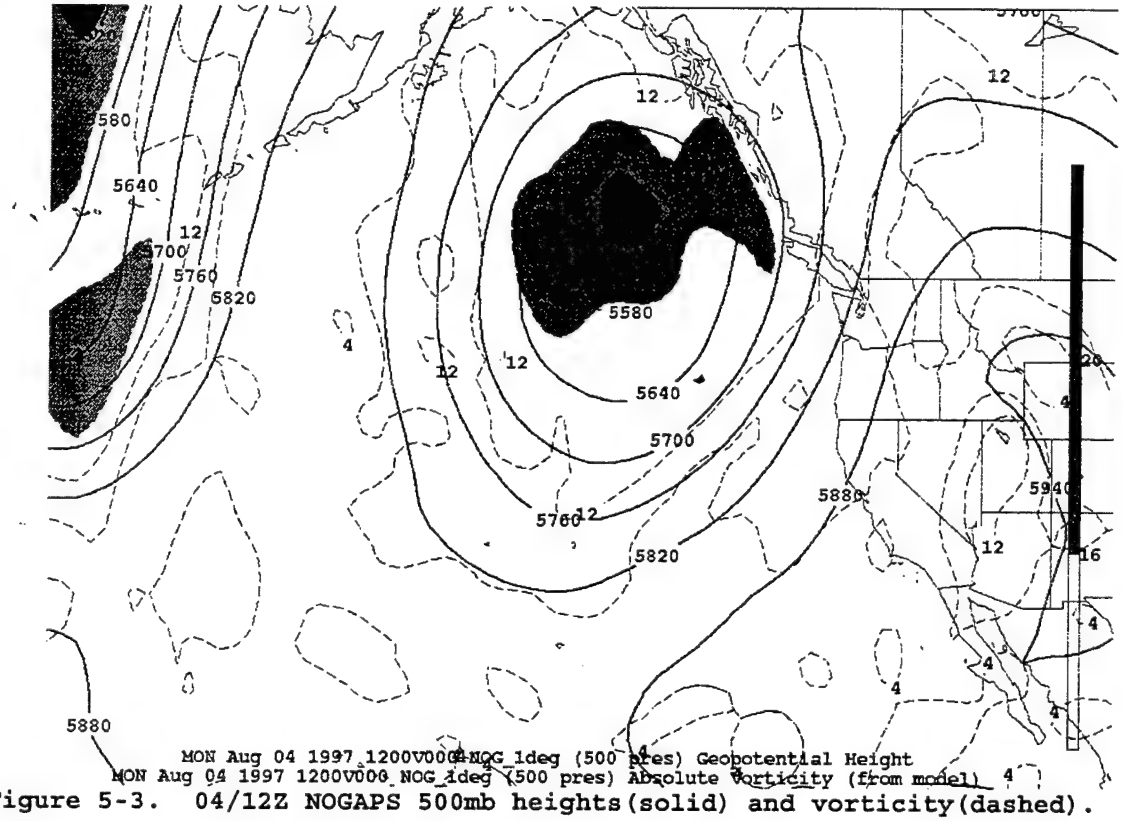

Figure 5-3. 04/12Z NOGAPS 500mb heights(solid) and vorticity(dashed).

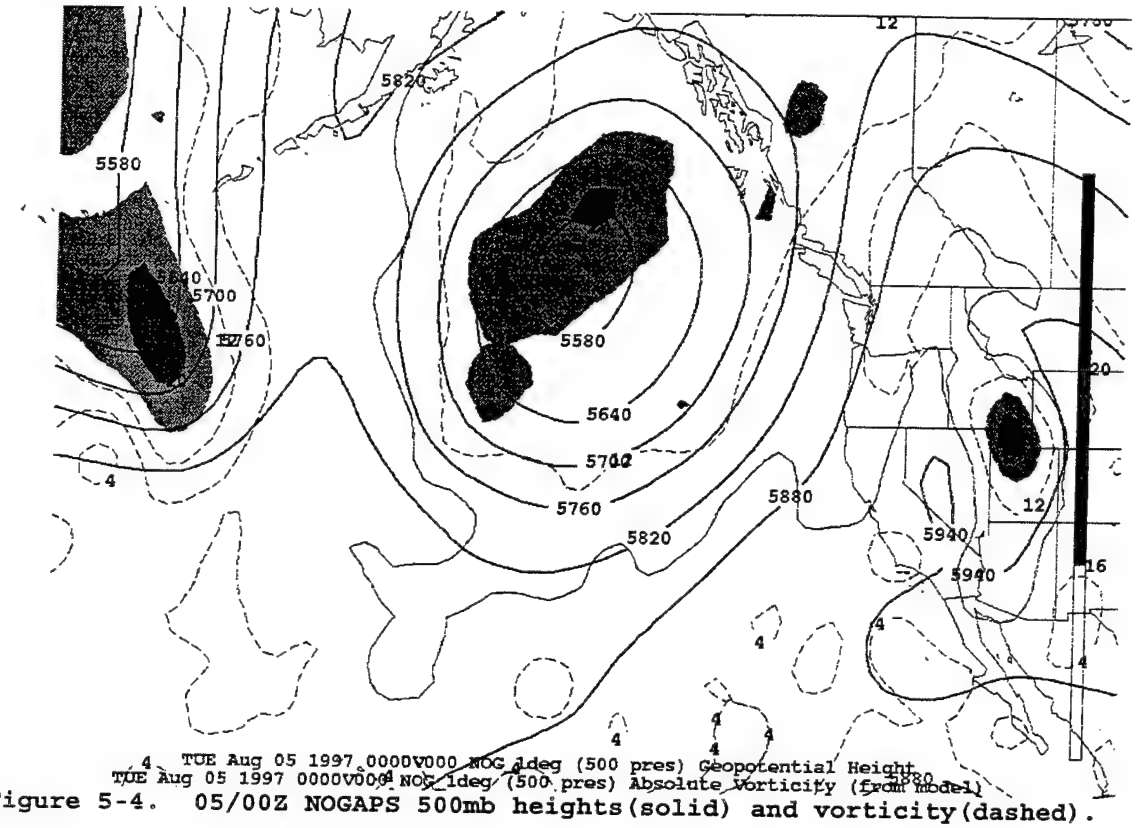

Figure 5-4. 05/00Z NOGAPS 500mb heights(solid) and vorticity(dashed).

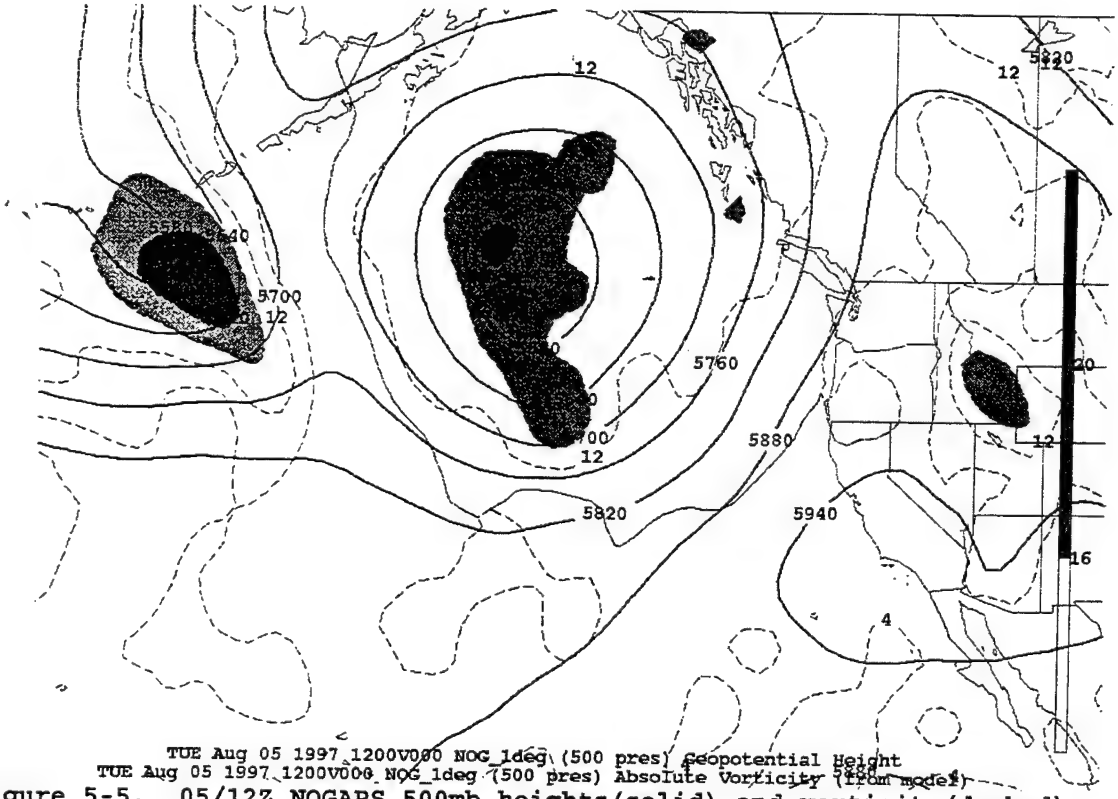

Figure 5-5. 05/12Z NOGAPS 500mb heights(solid) and vorticity(dashed).

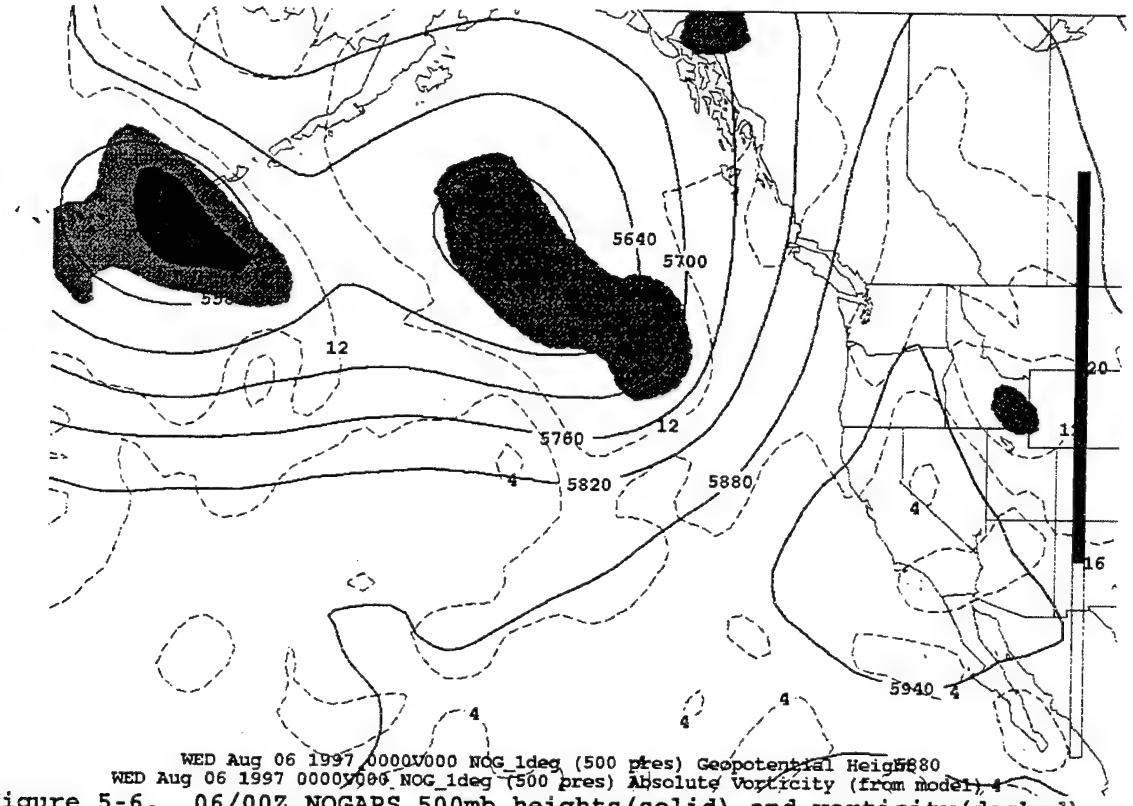

Figure 5-6. 06/00Z NOGAPS 500mb heights(solid) and vorticity(dashed).

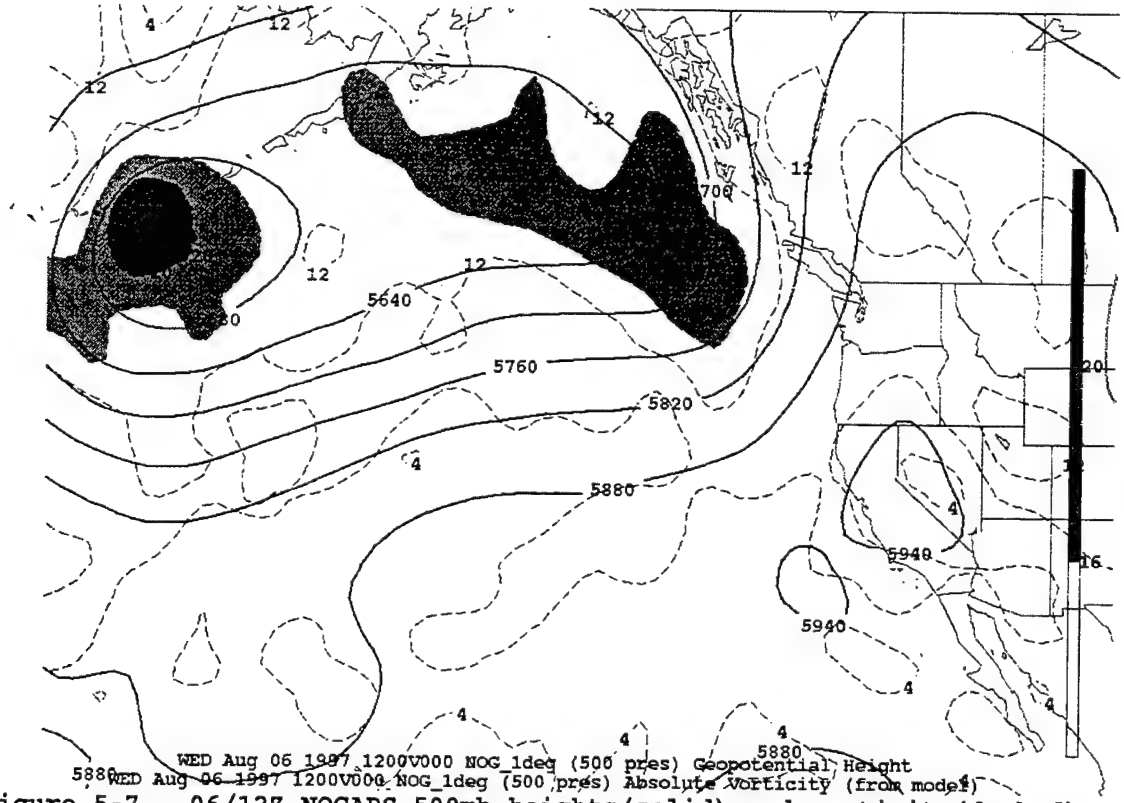

Figure 5-7. 06/12Z NOGAPS 500mb heights(solid) and vorticity(dashed).

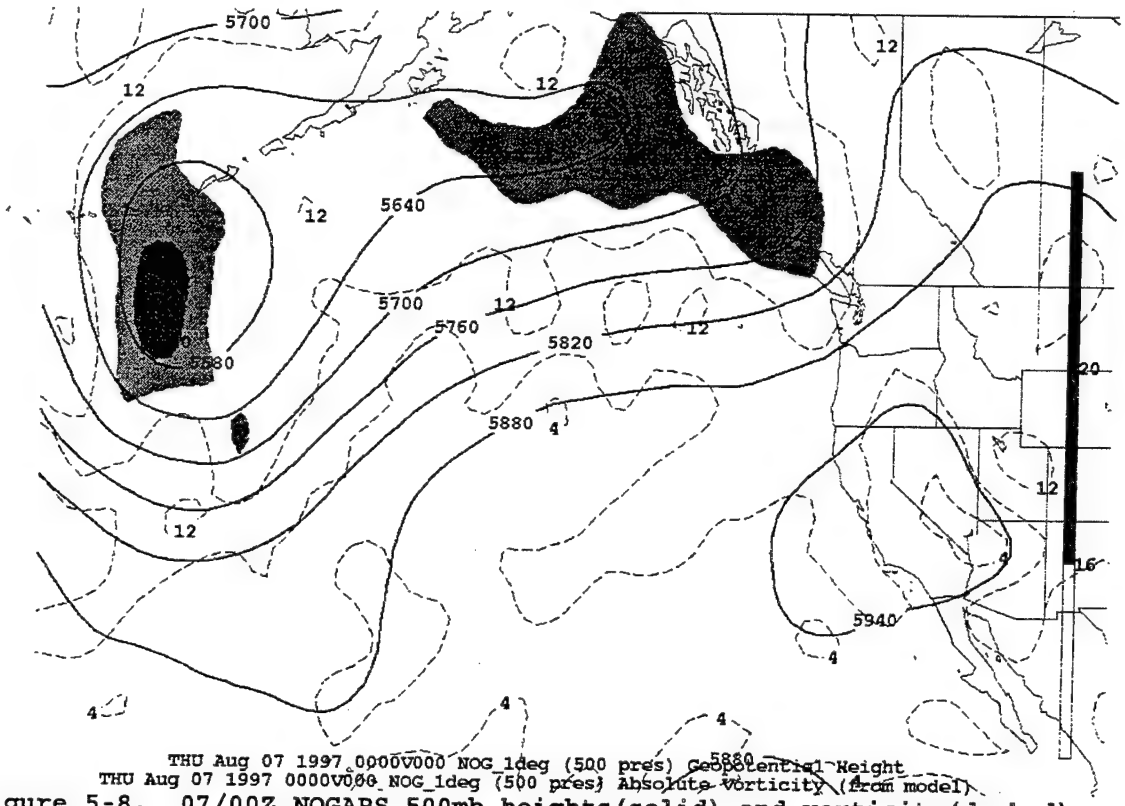

Figure 5-8. 07/00Z NOGAPS 500mb heights(solid) and vorticity(dashed).

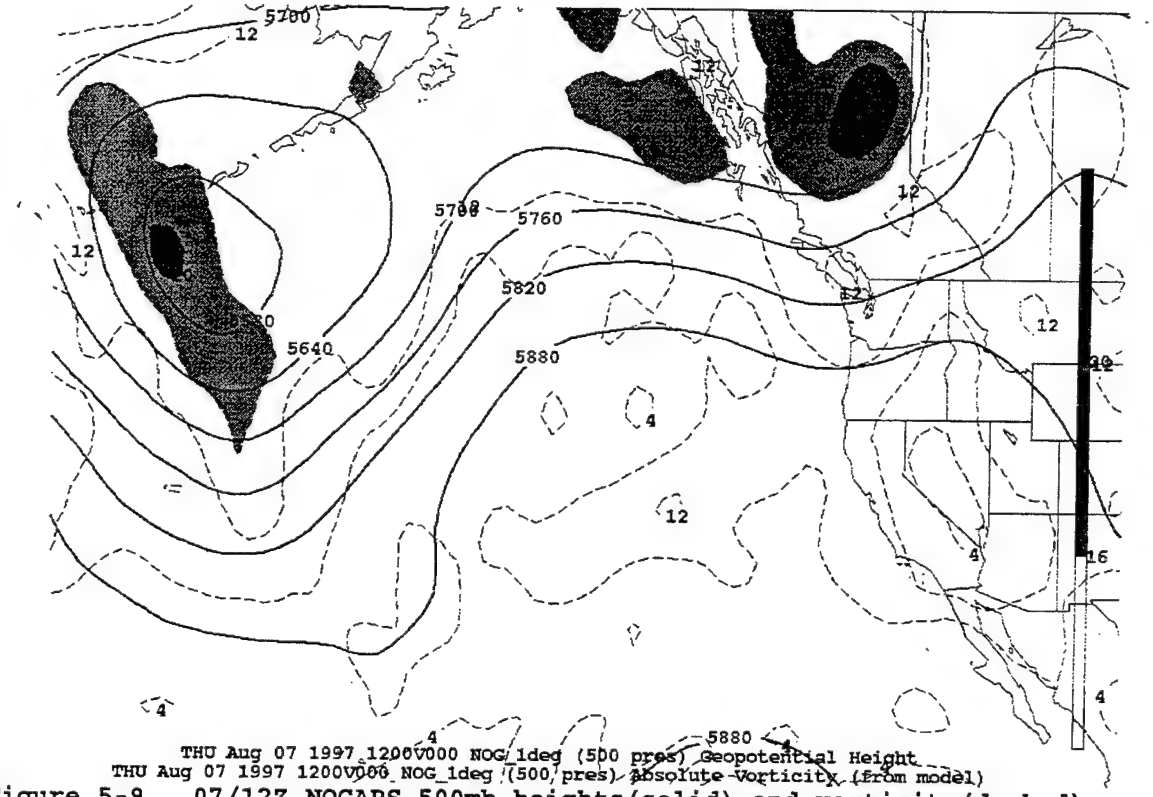

Figure 5-9. 07/12Z NOGAPS 500mb heights(solid) and vorticity(dashed).

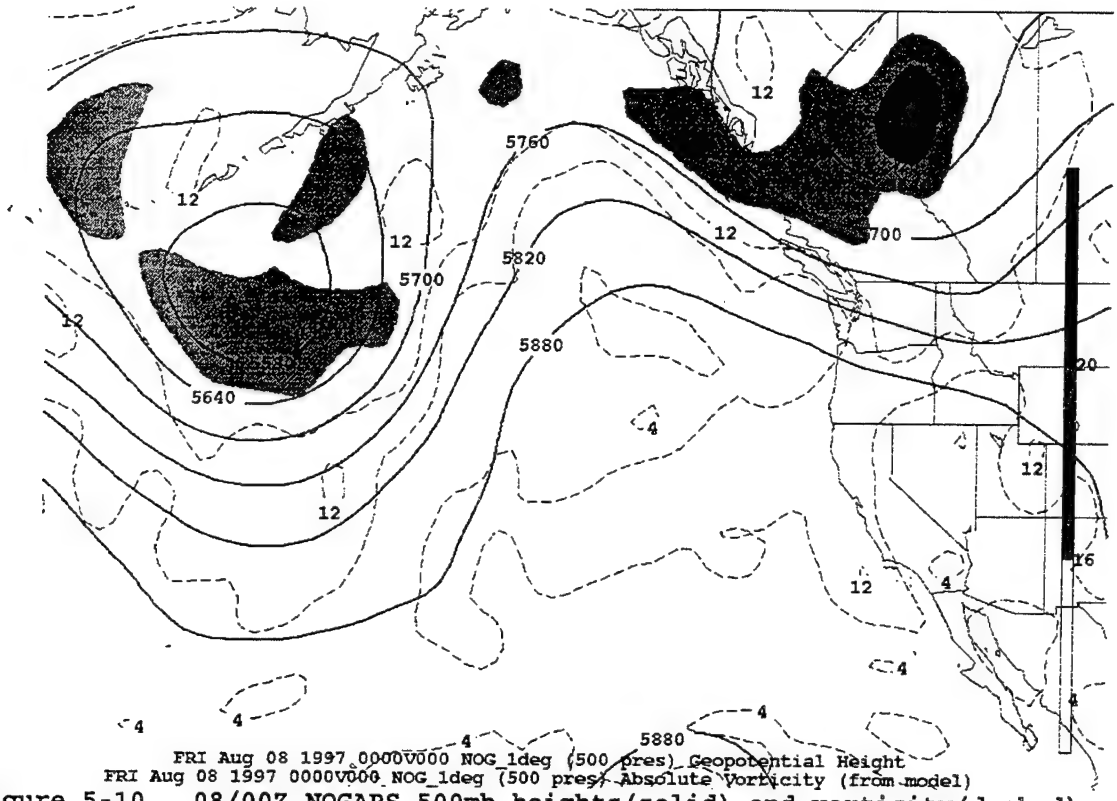

Figure 5-10. 08/00Z NOGAPS 500mb heights(solid) and vorticity(dashed).

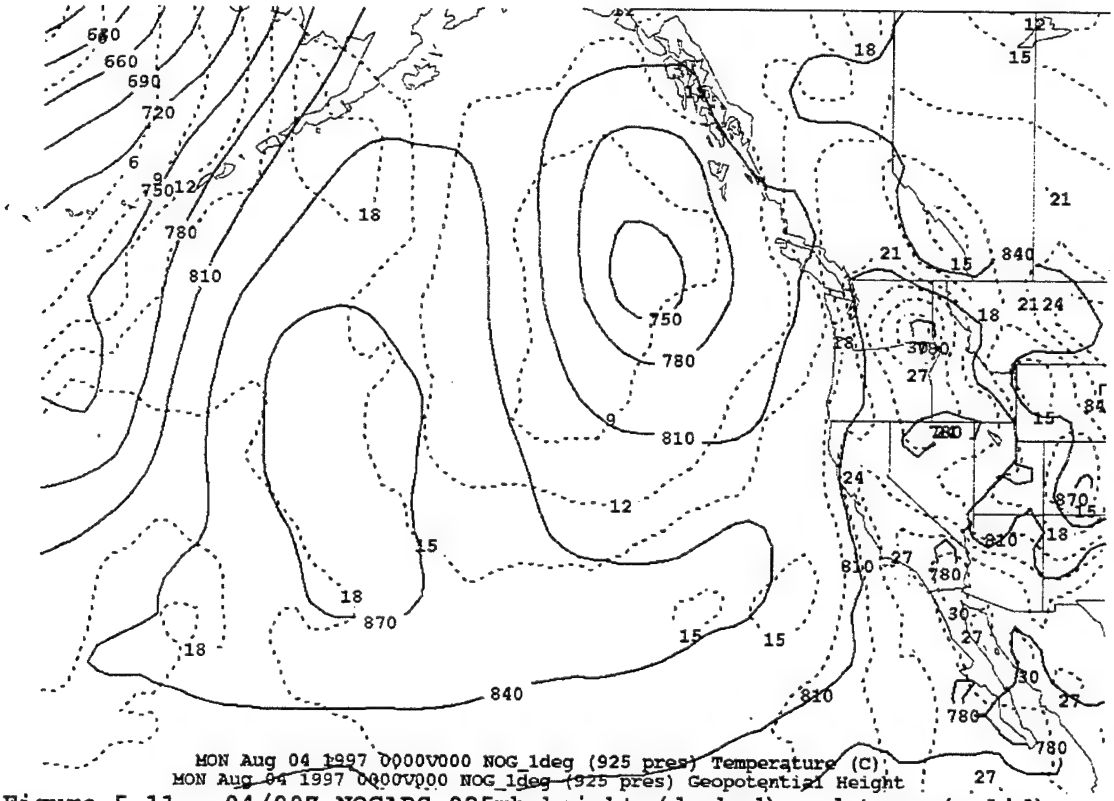

Figure 5-11. 04/00Z NOGAPS 925mb heights(dashed) and temps(solid).

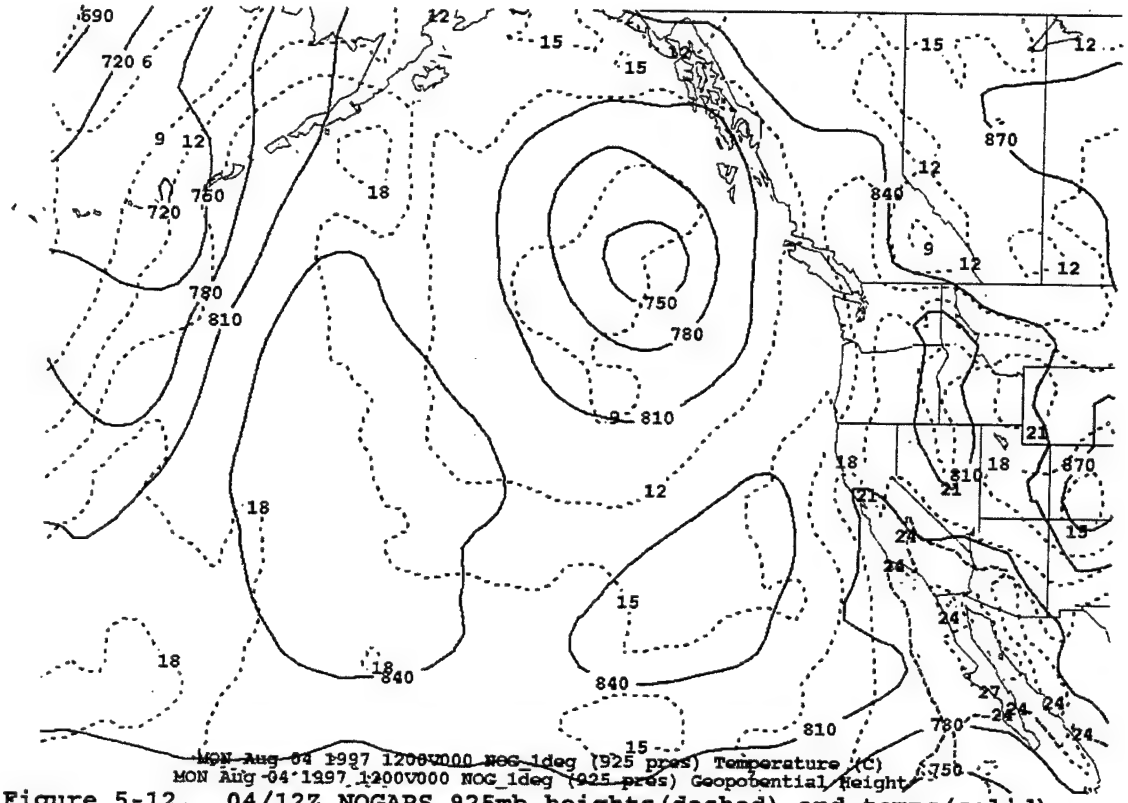

Figure 5-12. 04/12Z NOGAPS 925mb heights(dashed) and temps(solid).

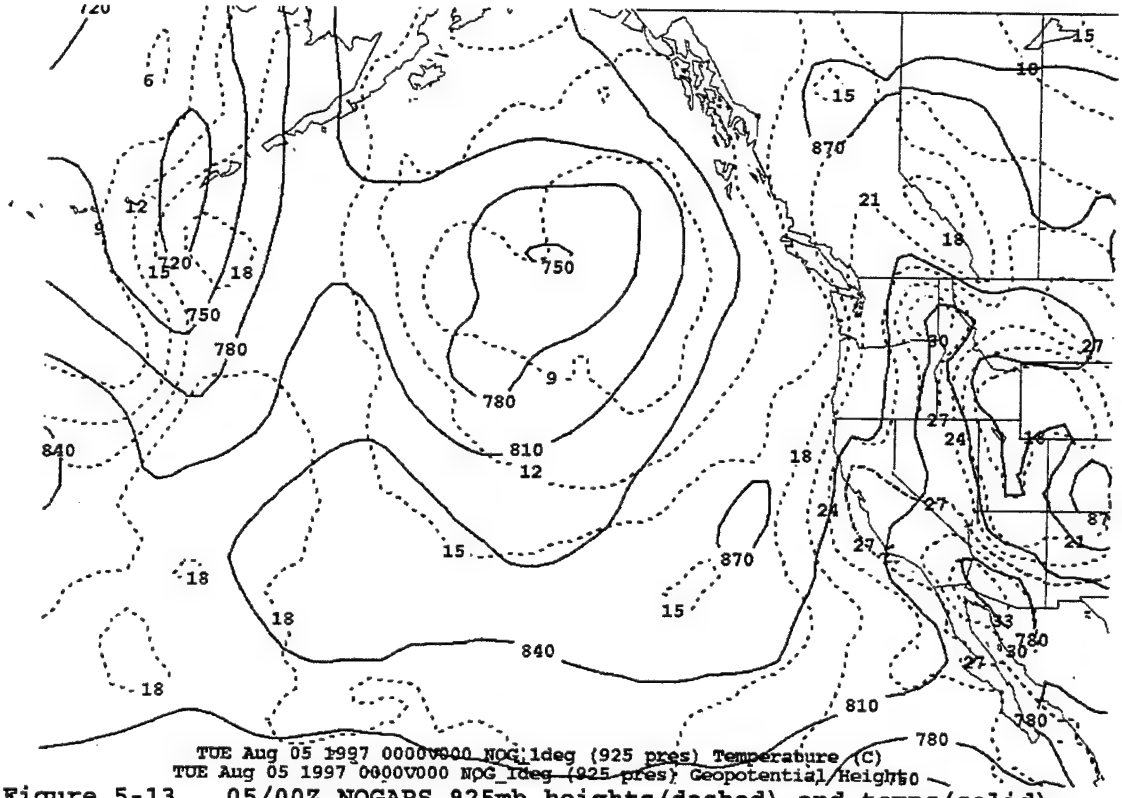

Figure 5-13. 05/00Z NOGAPS 925mb heights(dashed) and temps(solid).

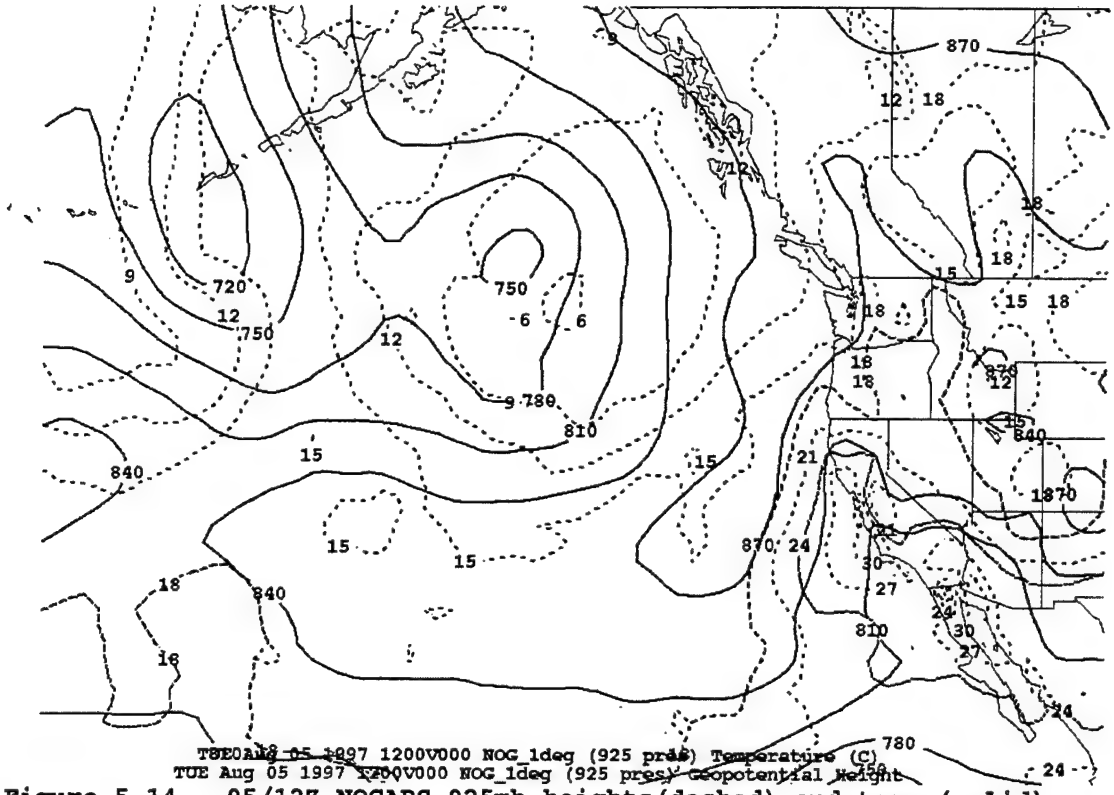

Figure 5-14. 05/12Z NOGAPS 925mb heights(dashed) and temps(solid).

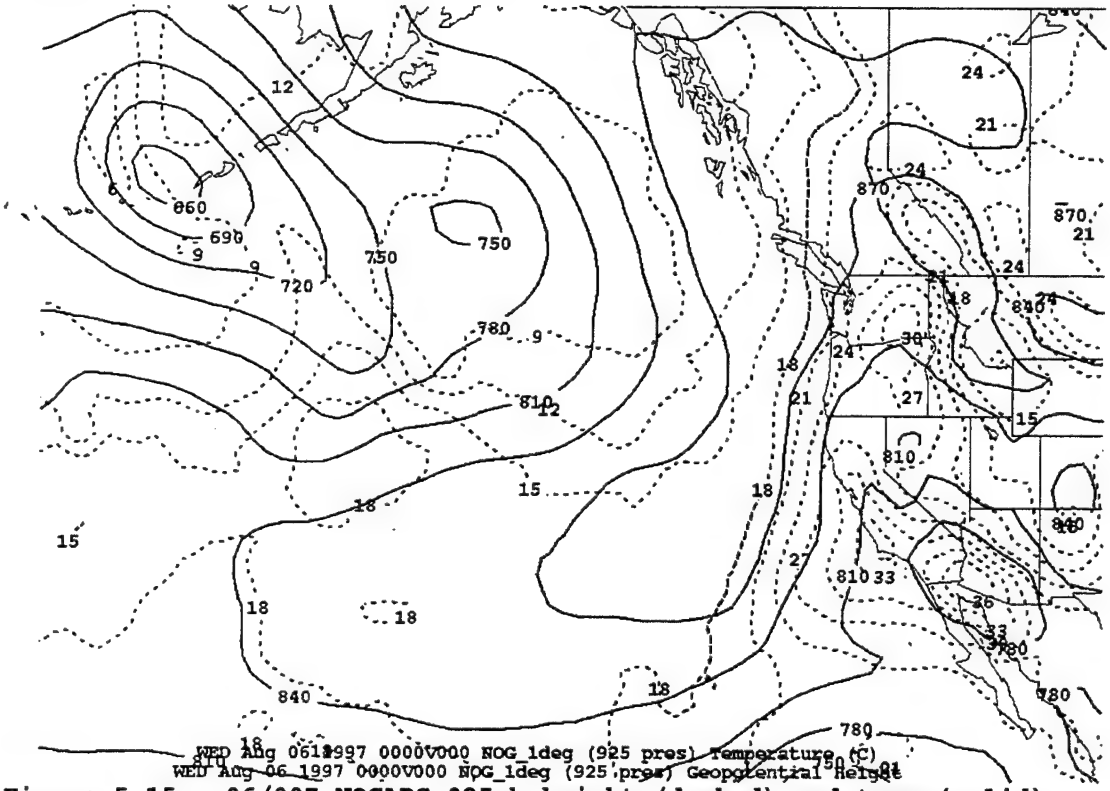

Figure 5-15. 06/00Z NOGAPS 925mb heights(dashed) and temps(solid).

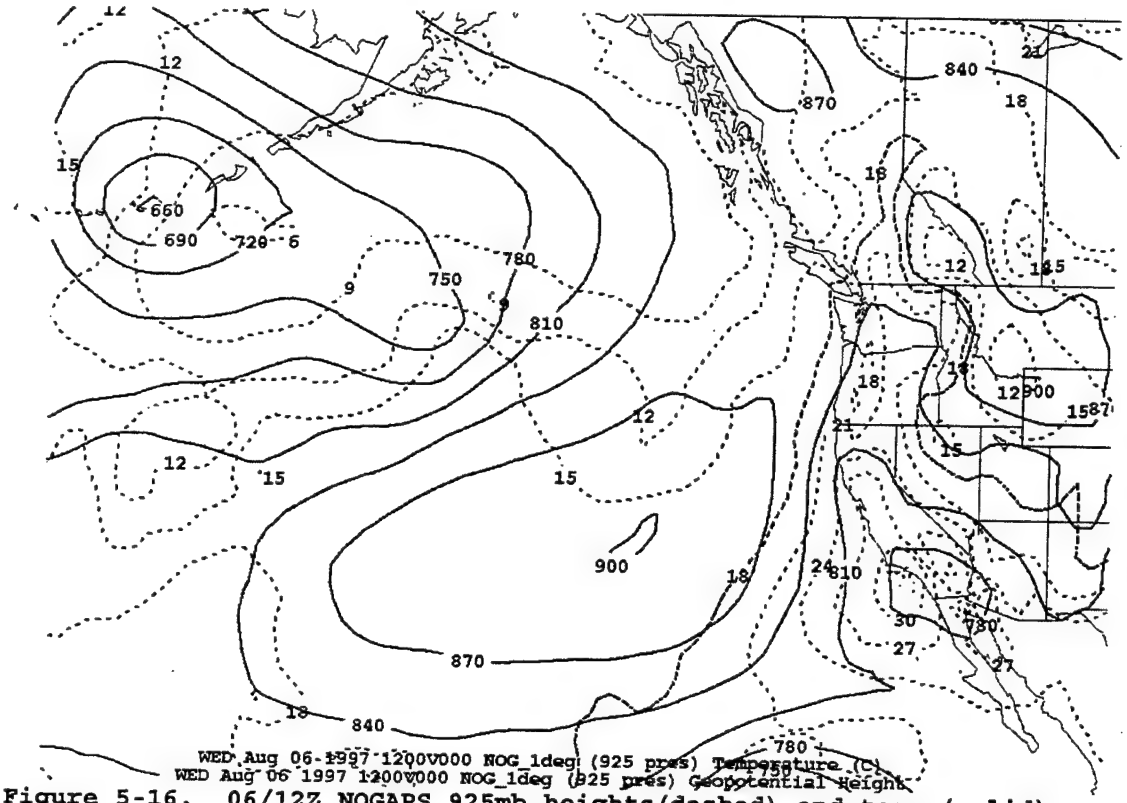

Figure 5-16. 06/12Z NOGAPS 925mb heights(dashed) and temps(solid).

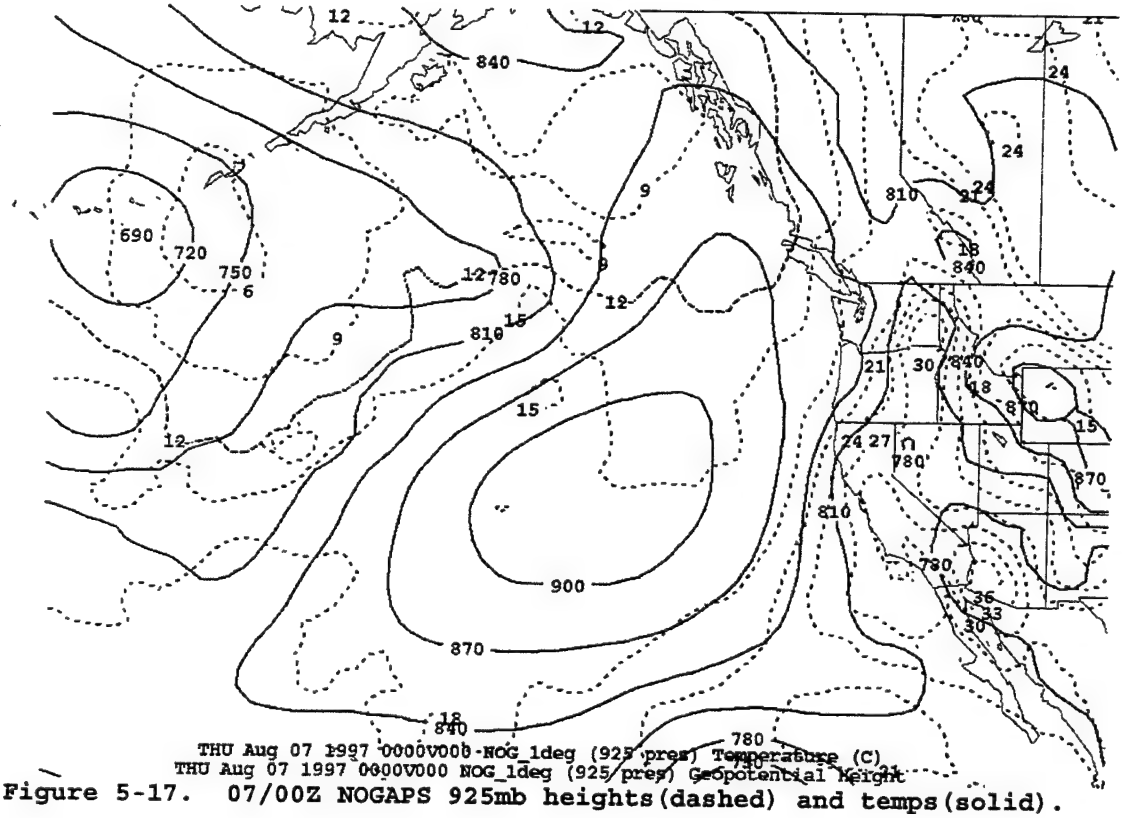

Figure 5-17. 07/00Z NOGAPS 925mb heights(dashed) and temps(solid).

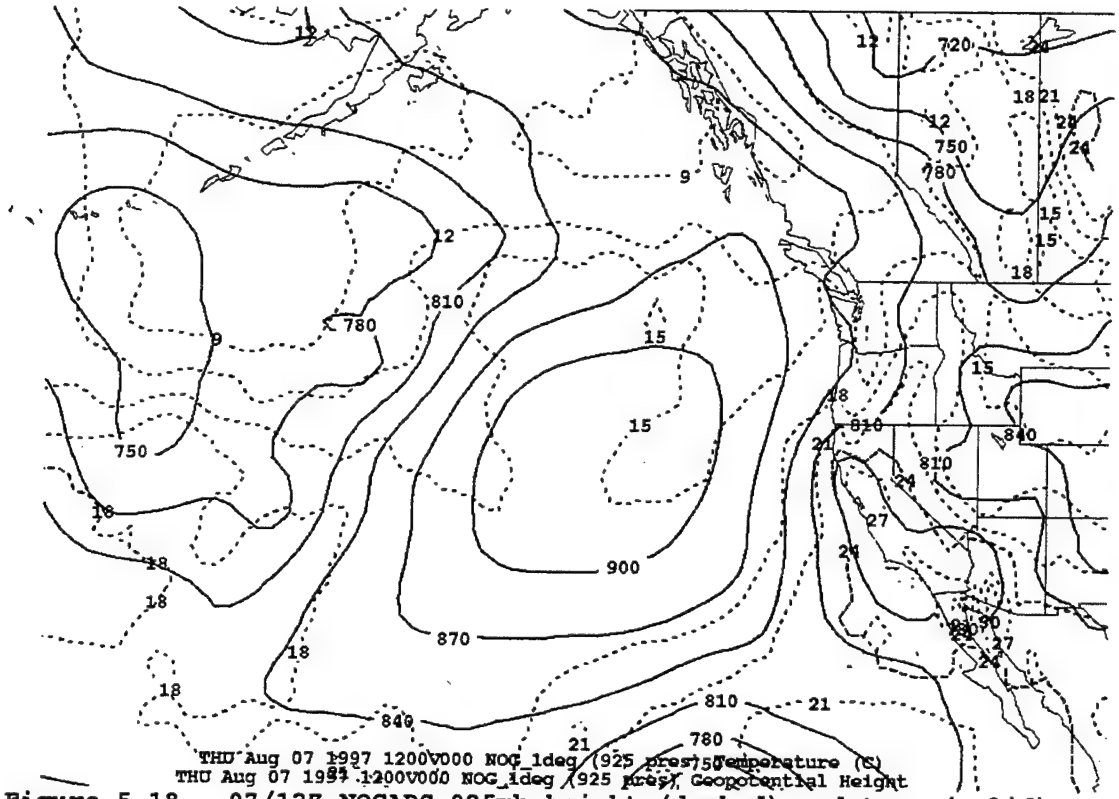

Figure 5-18. 07/12Z NOGAPS 925mb heights(dashed) and temps(solid).

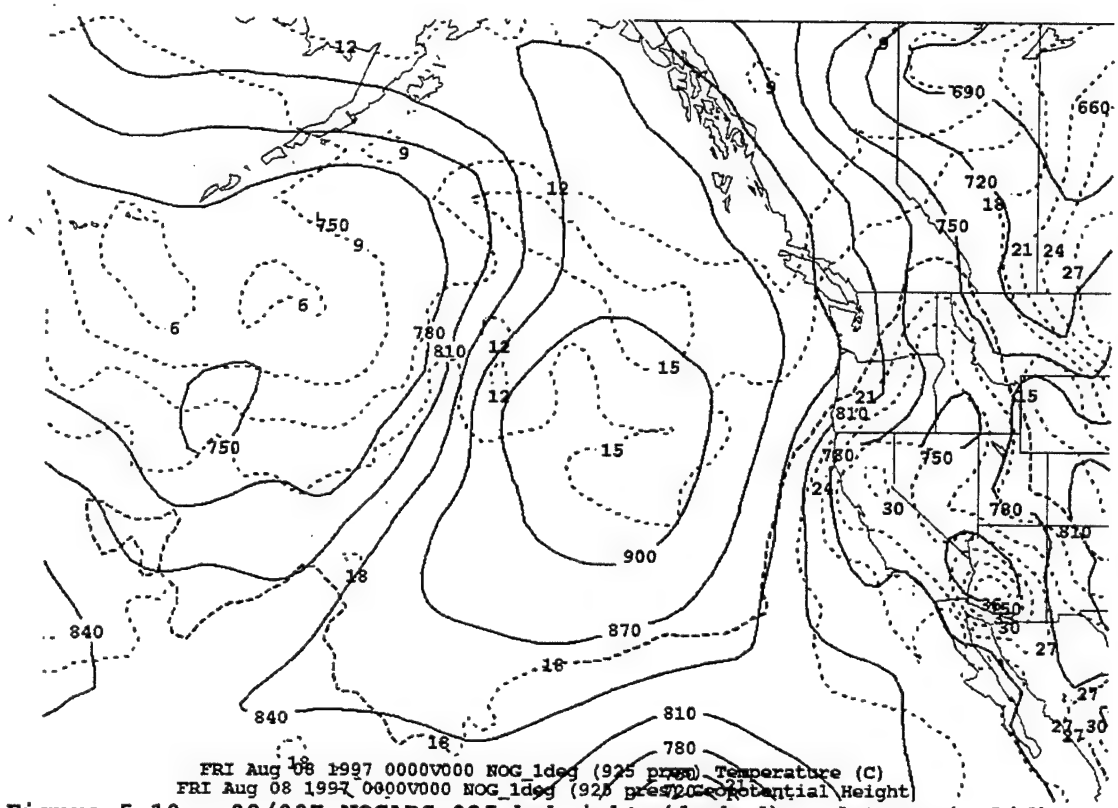

Figure 5-19. 08/00Z NOGAPS 925mb heights(dashed) and temps(solid).

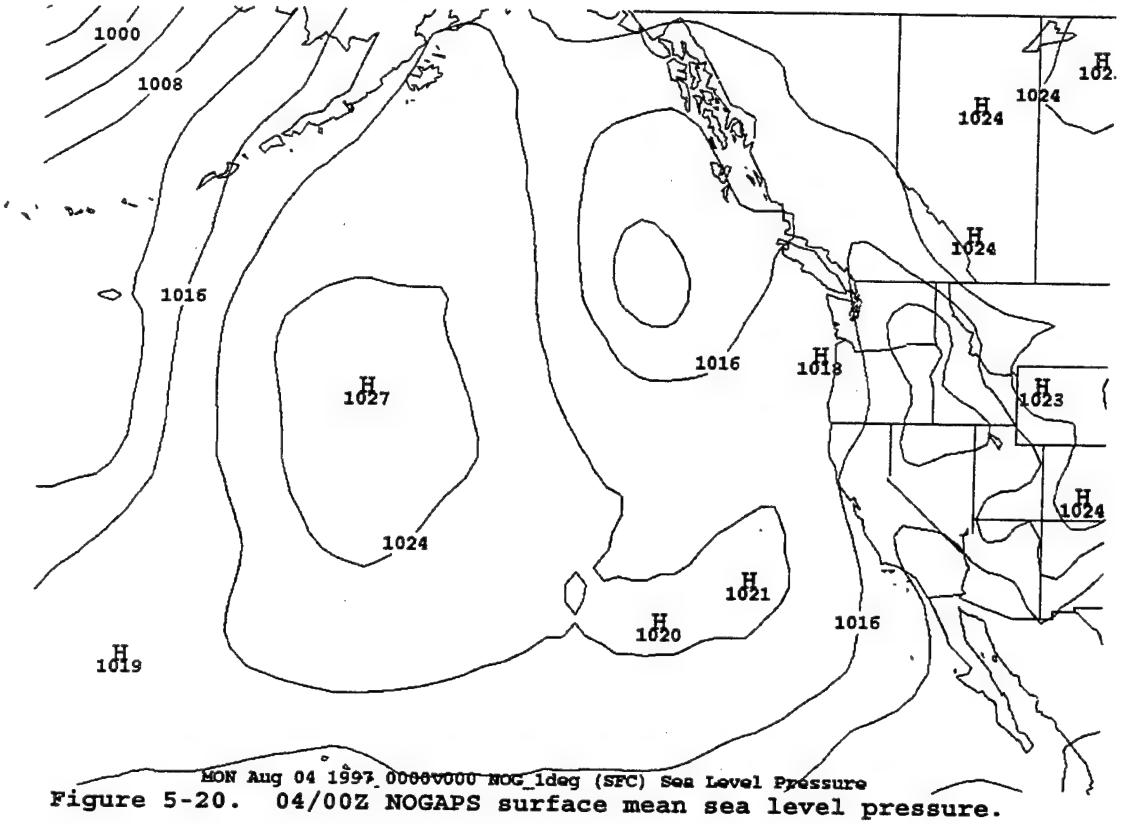

Figure 5-20. 04/00Z NOGAPS surface mean sea level pressure.

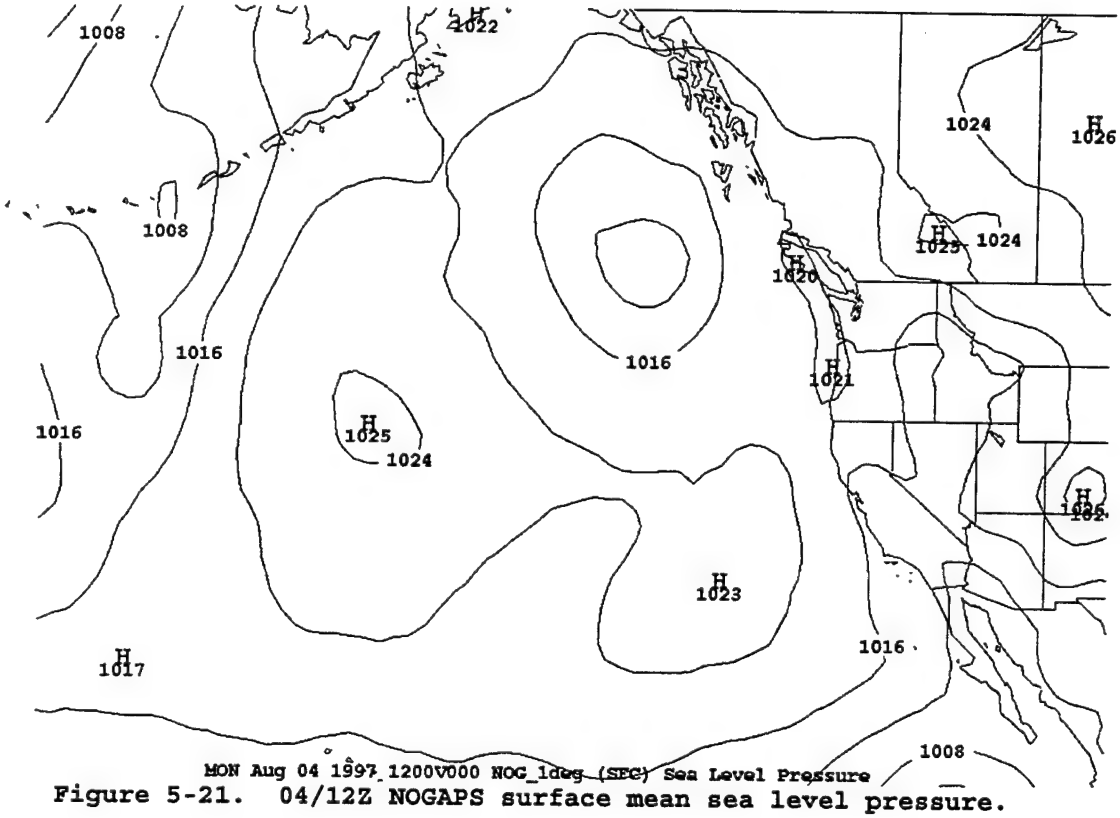

Figure 5-21. 04/12Z NOGAPS surface mean sea level pressure.

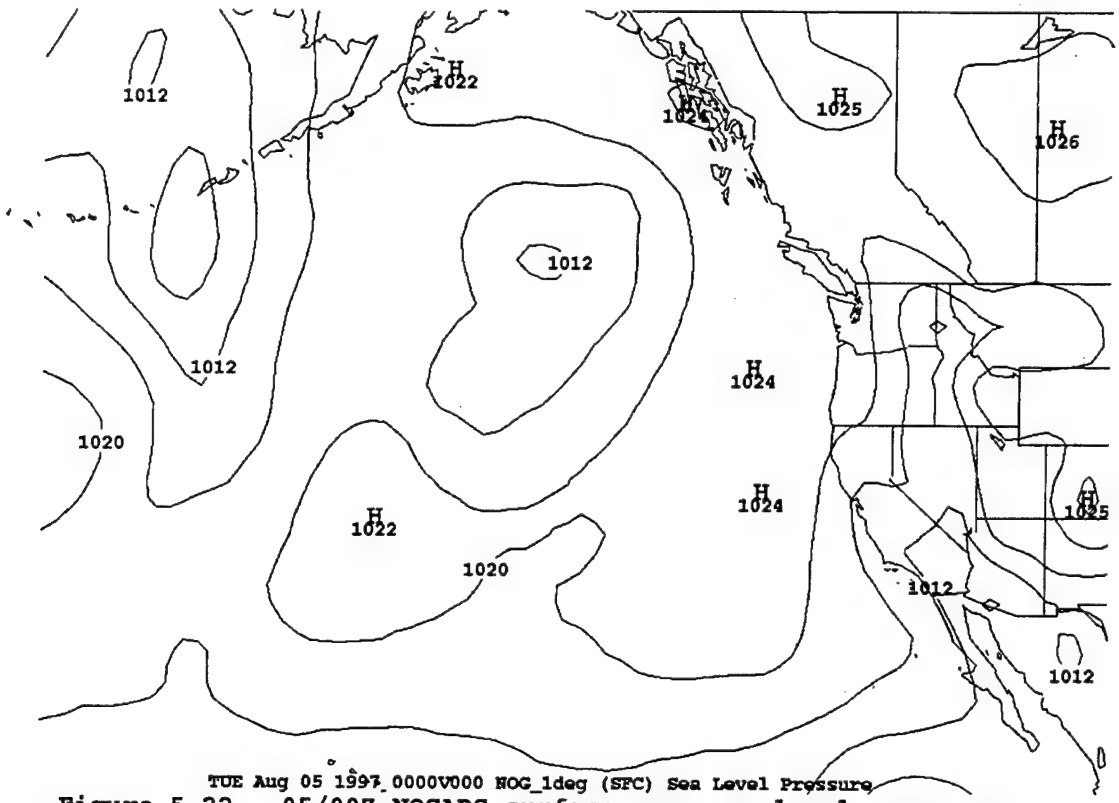

TUE Aug 05 1997 0000V000 NOG_1deg (SFC) Sea Level Pressure

Figure 5-22. 05/00Z NOGAPS surface mean sea level pressure.

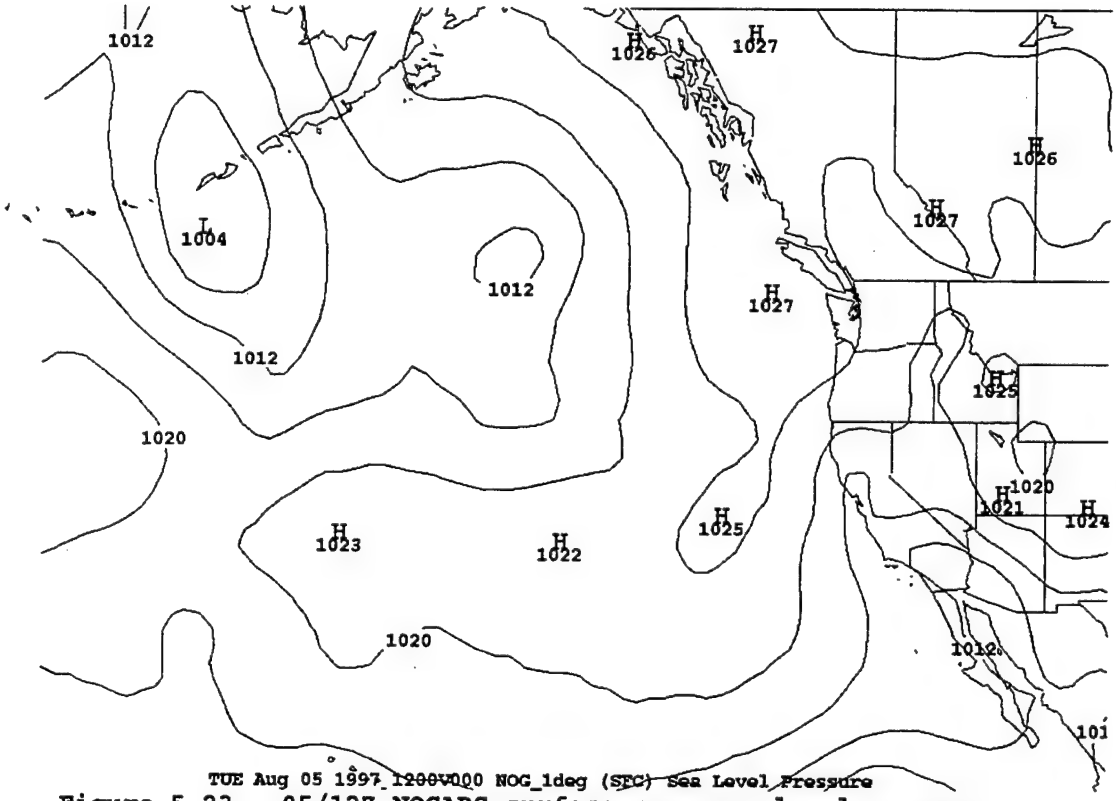

TUE Aug 05 1997 1200V000 NOG_1deg (SFC) Sea Level Pressure

Figure 5-23. 05/12Z NOGAPS surface mean sea level pressure.

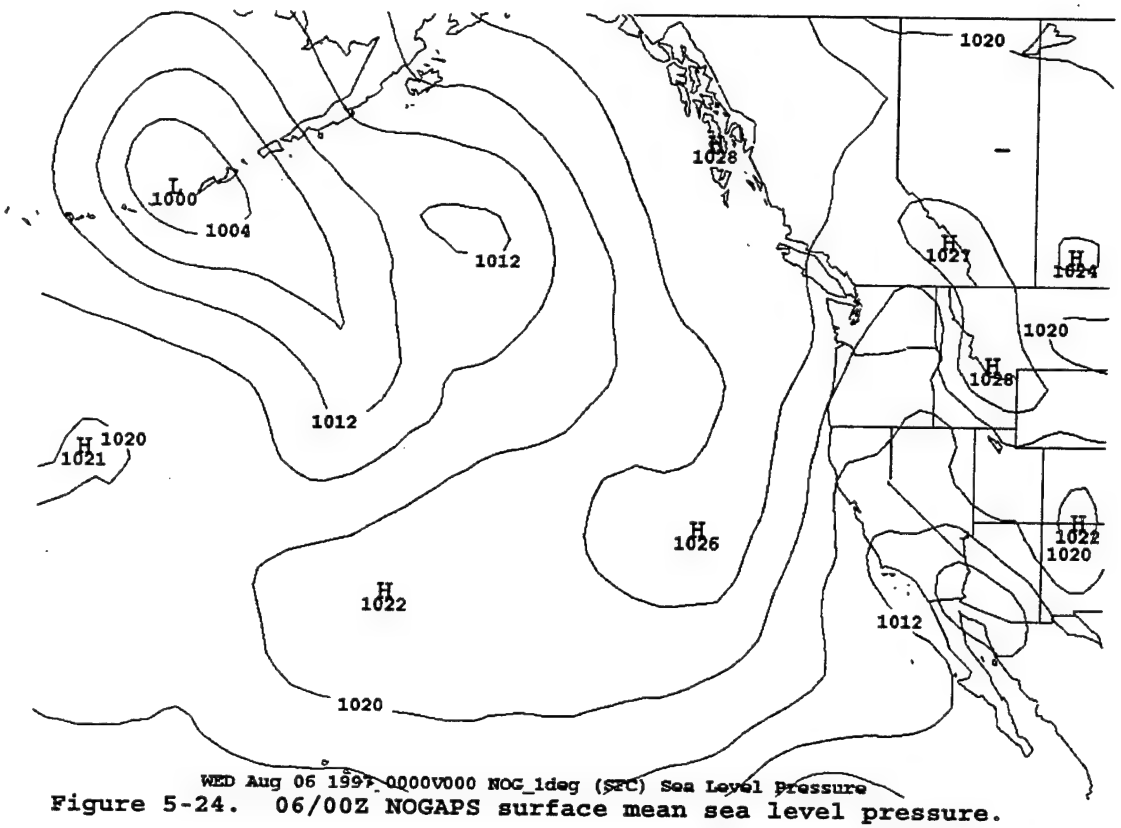

Figure 5-24. 06/00Z NOGAPS surface mean sea level pressure.

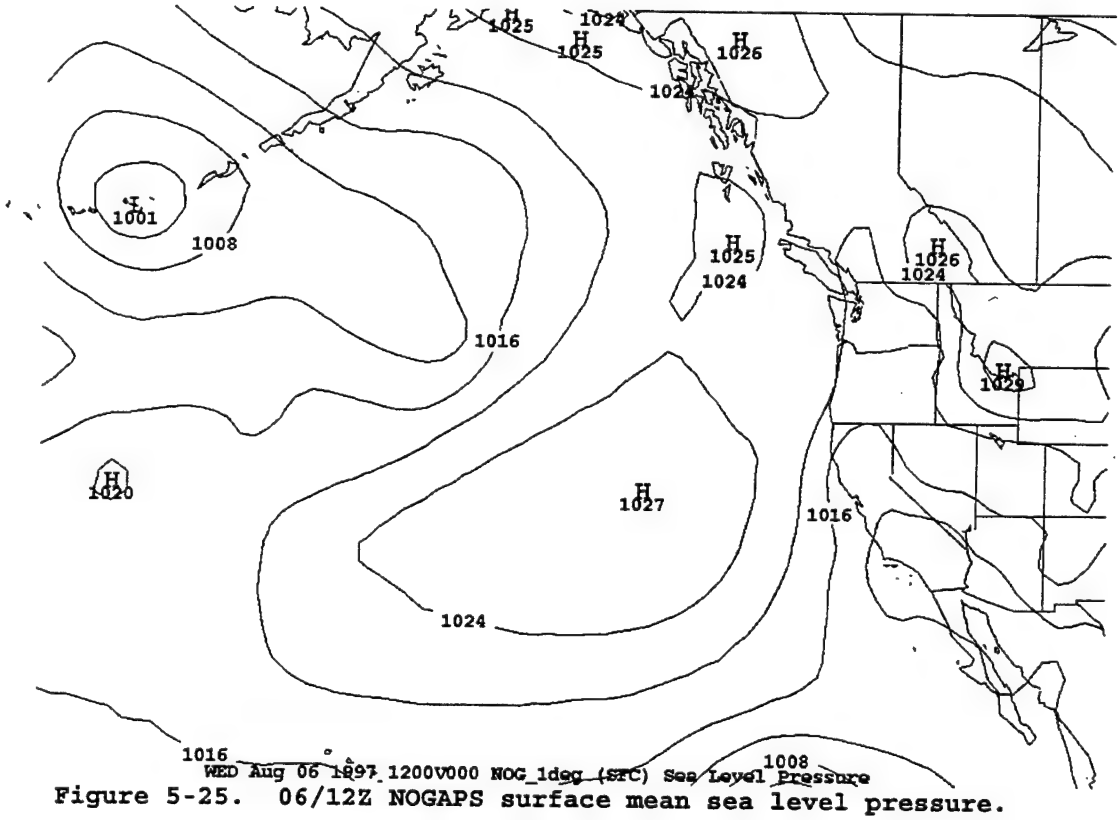

Figure 5-25. 06/12Z NOGAPS surface mean sea level pressure.

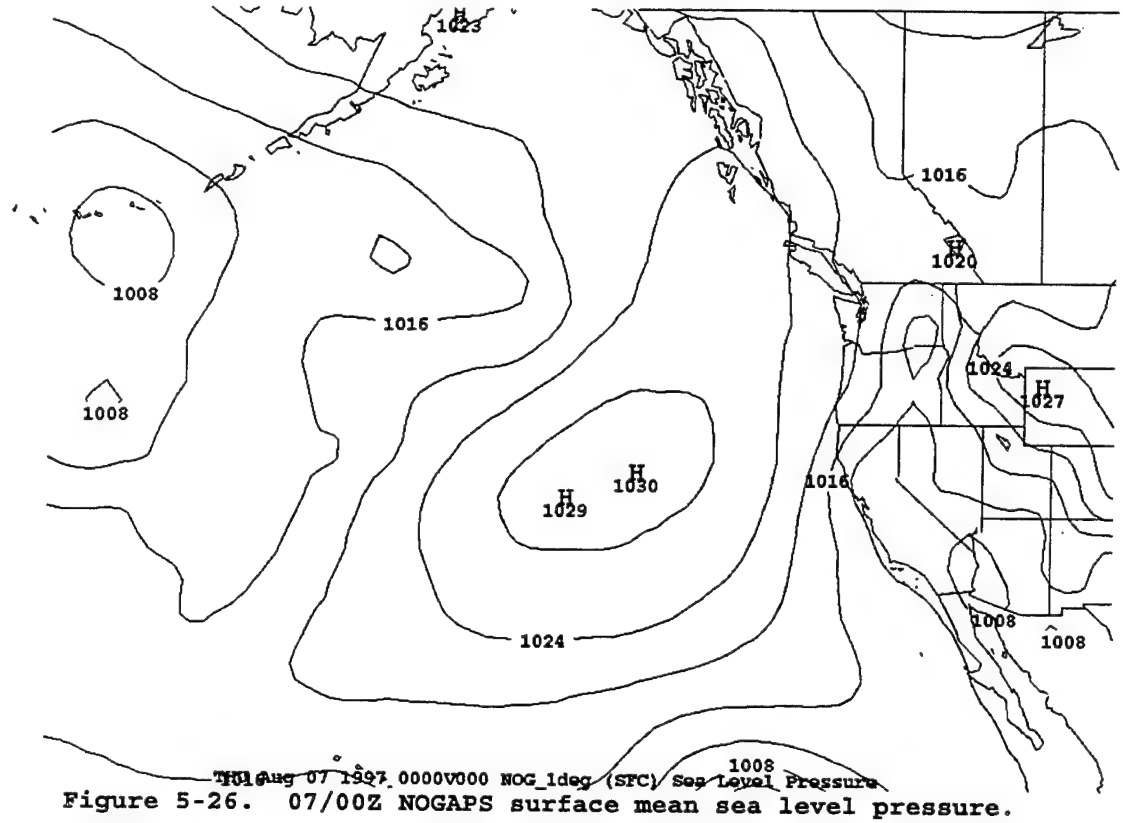

Figure 5-26. 07/00Z NOGAPS surface mean sea level pressure.

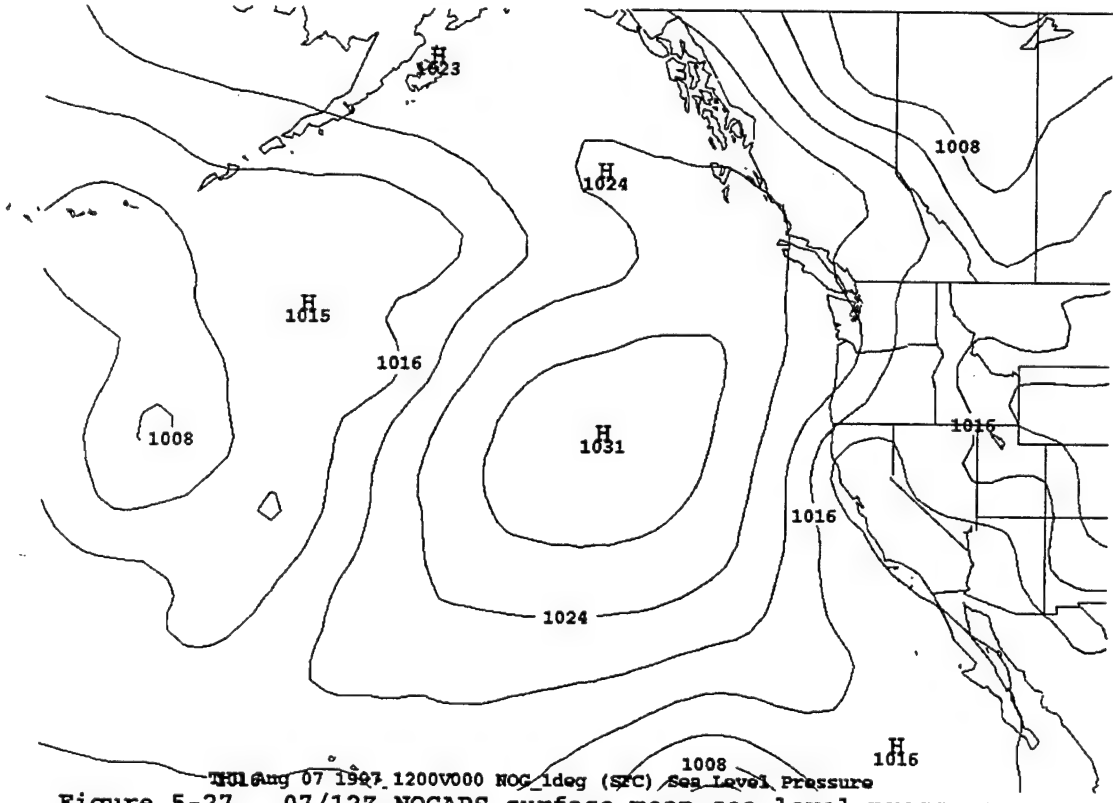

Figure 5-27. 07/12Z NOGAPS surface mean sea level pressure.

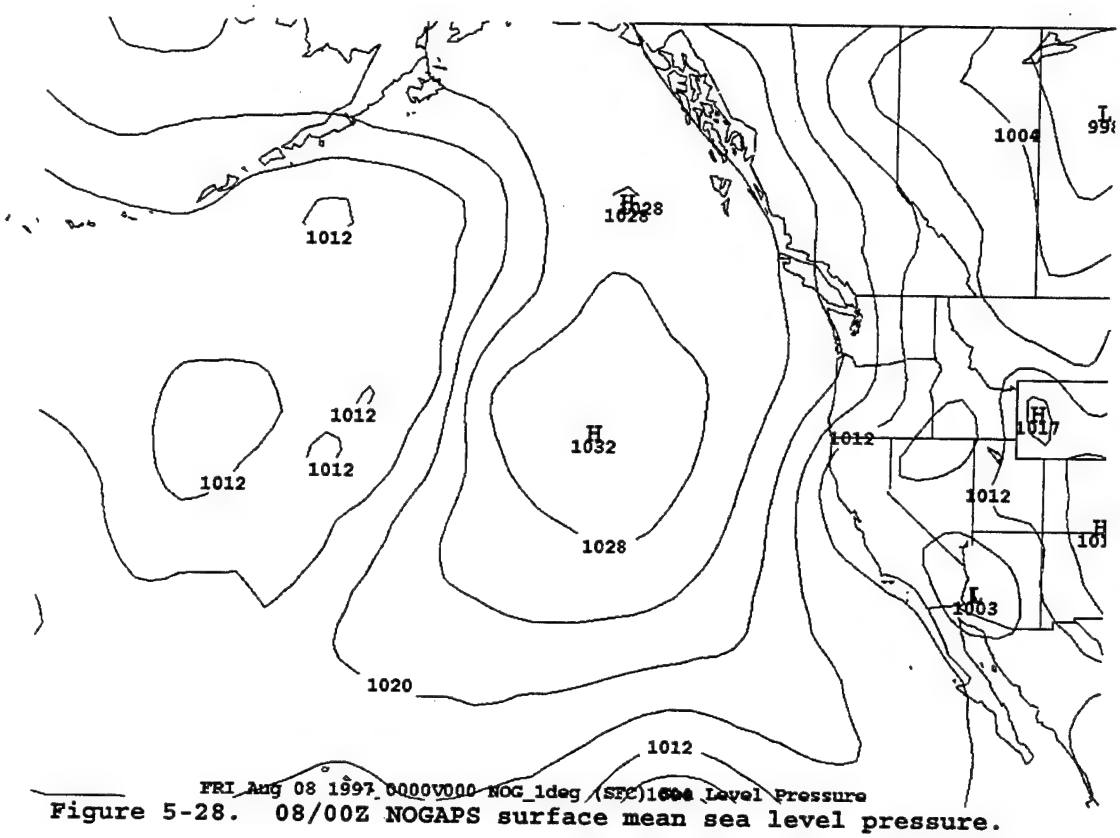

Figure 5-28. 08/00Z NOGAPS surface mean sea level pressure.

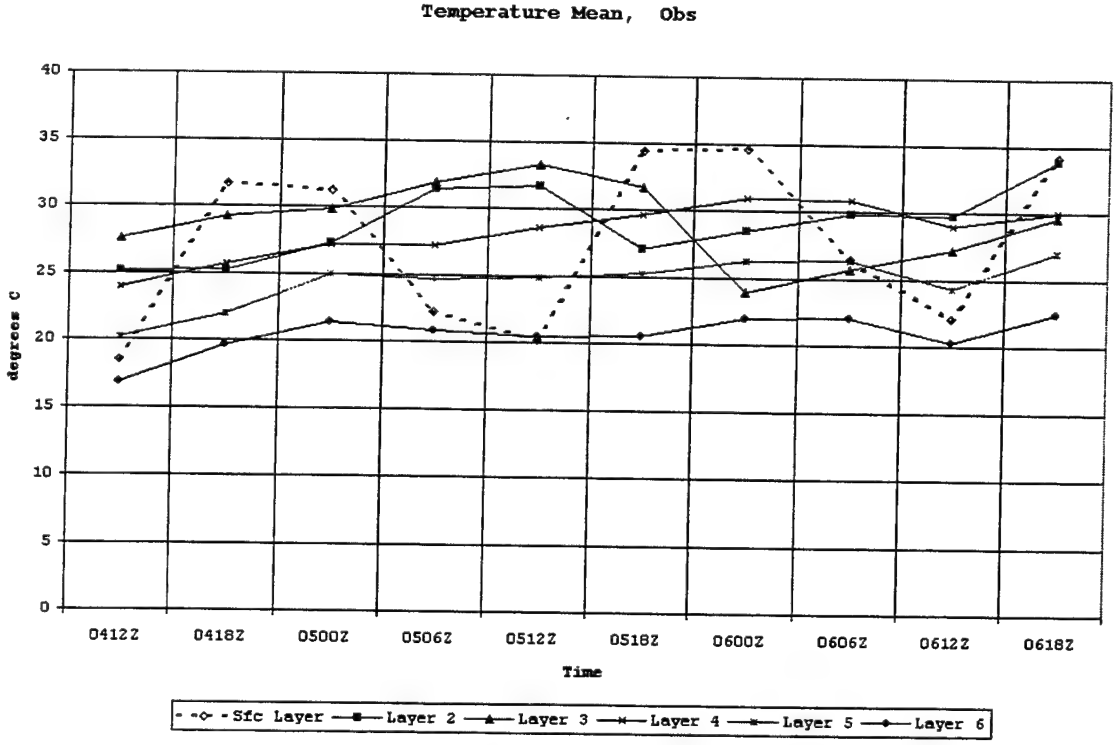

Figure 5-29. Mean temperature, observations.

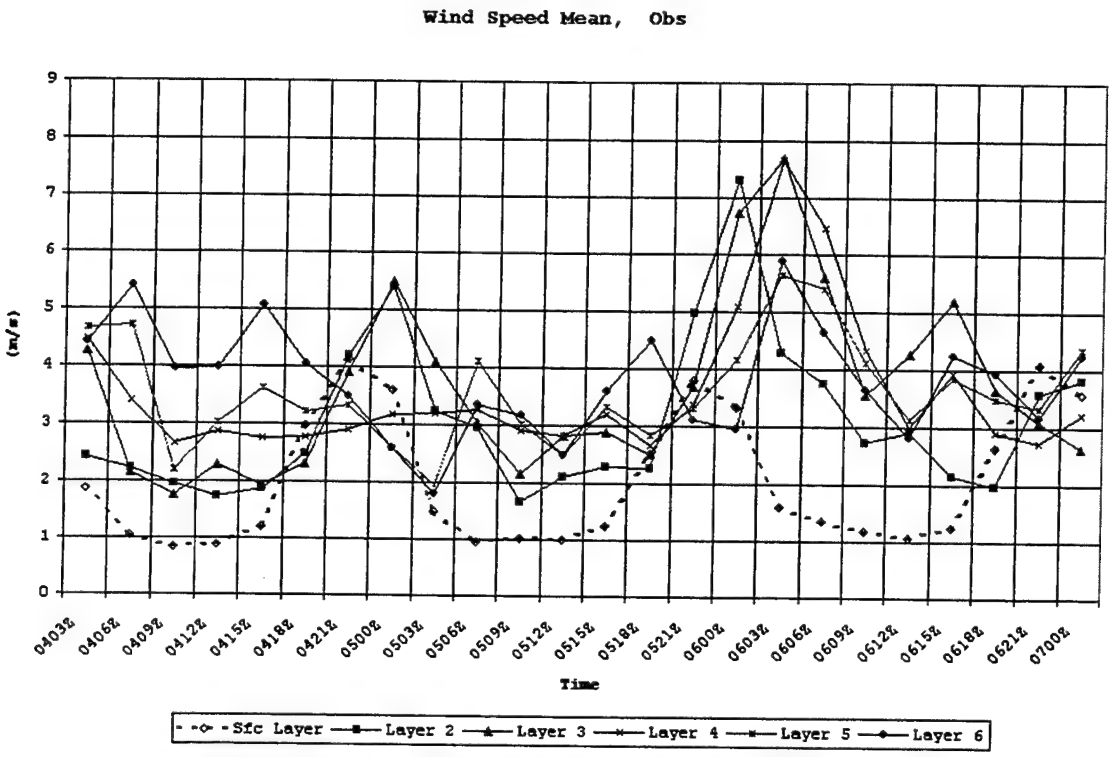

Figure 5-30. Mean wind speed, observations.

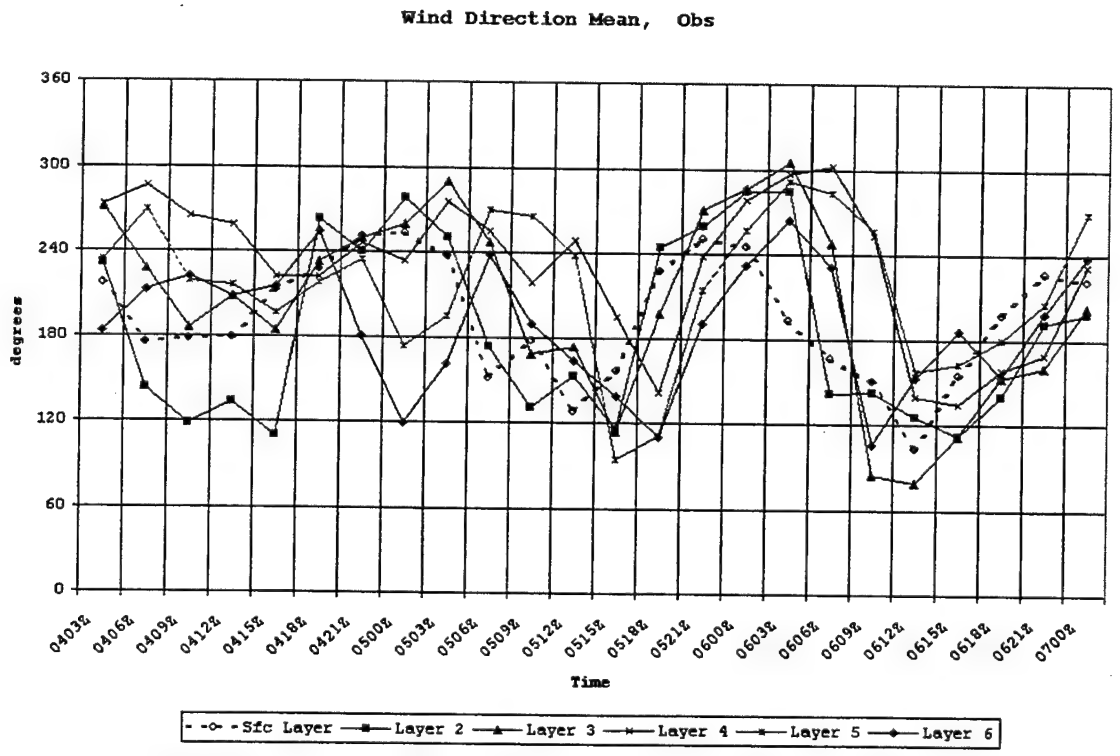

Figure 5-31. Mean wind direction, observations.

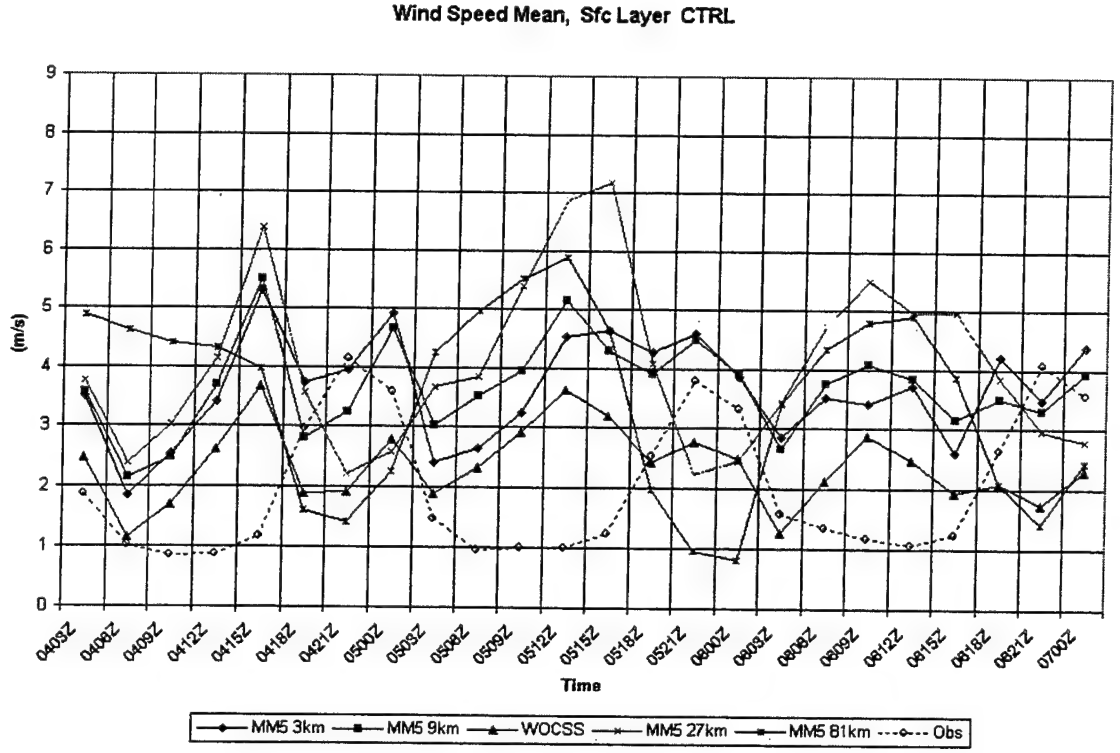

Figure 6-1. CTRL mean wind speed.

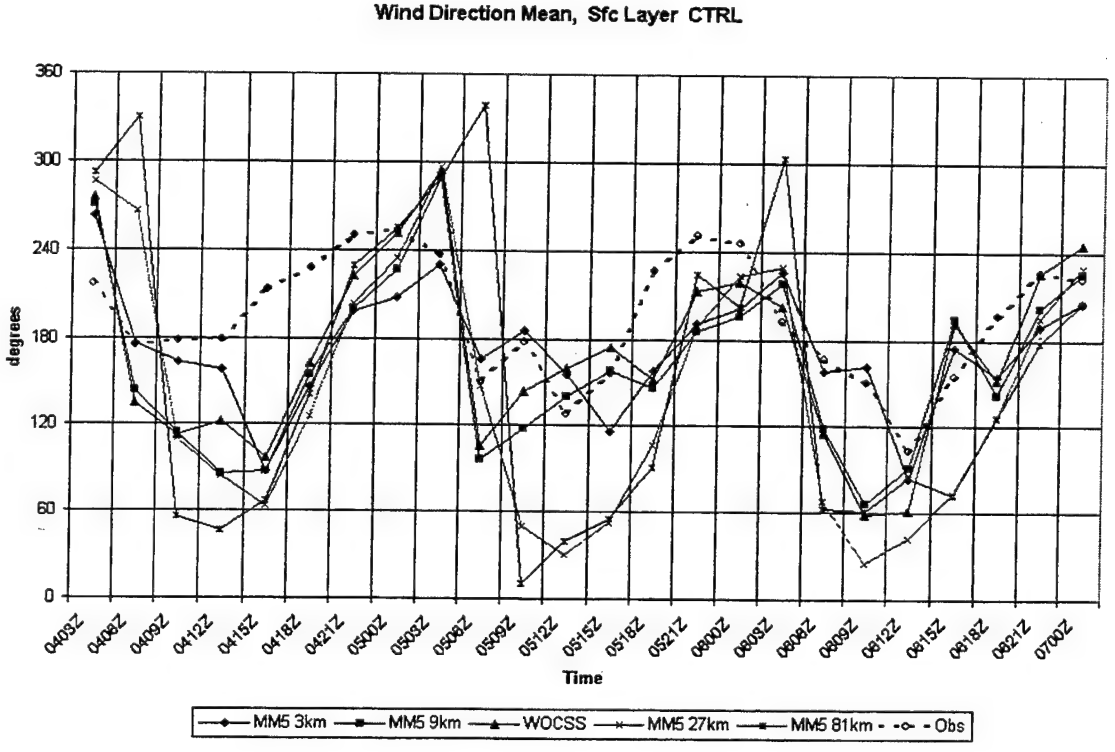

Figure 6-2. CTRL mean wind direction.

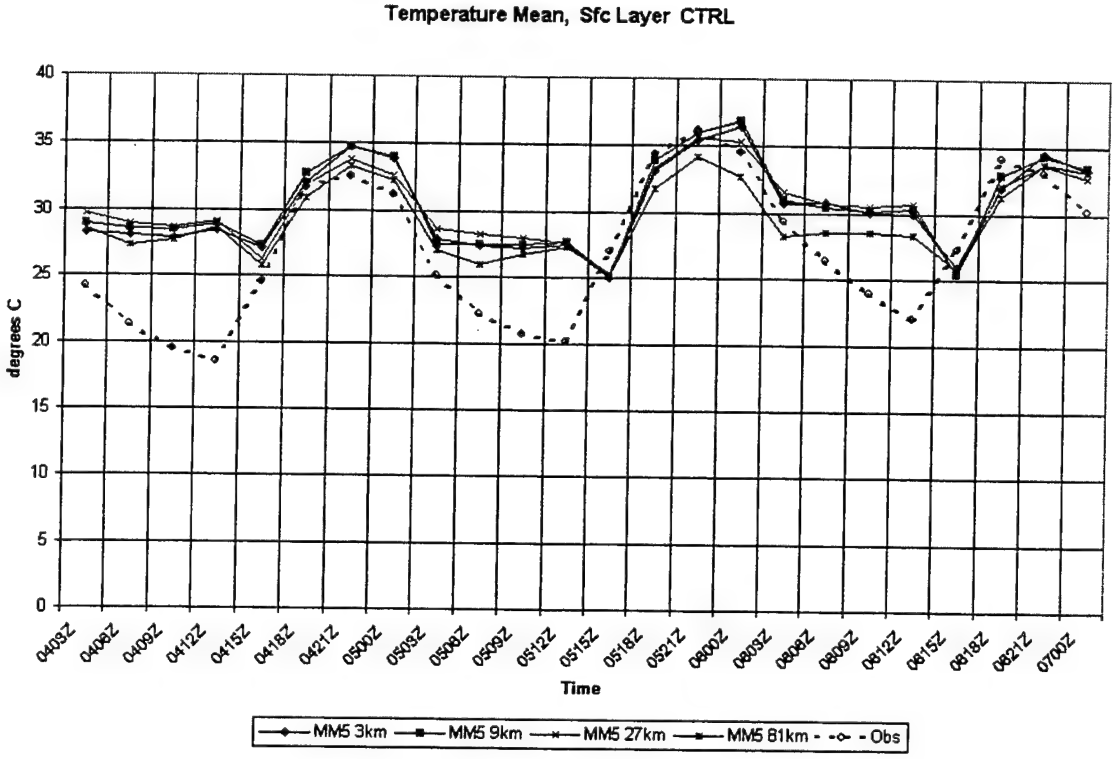

Figure 6-3. CTRL mean temperature.

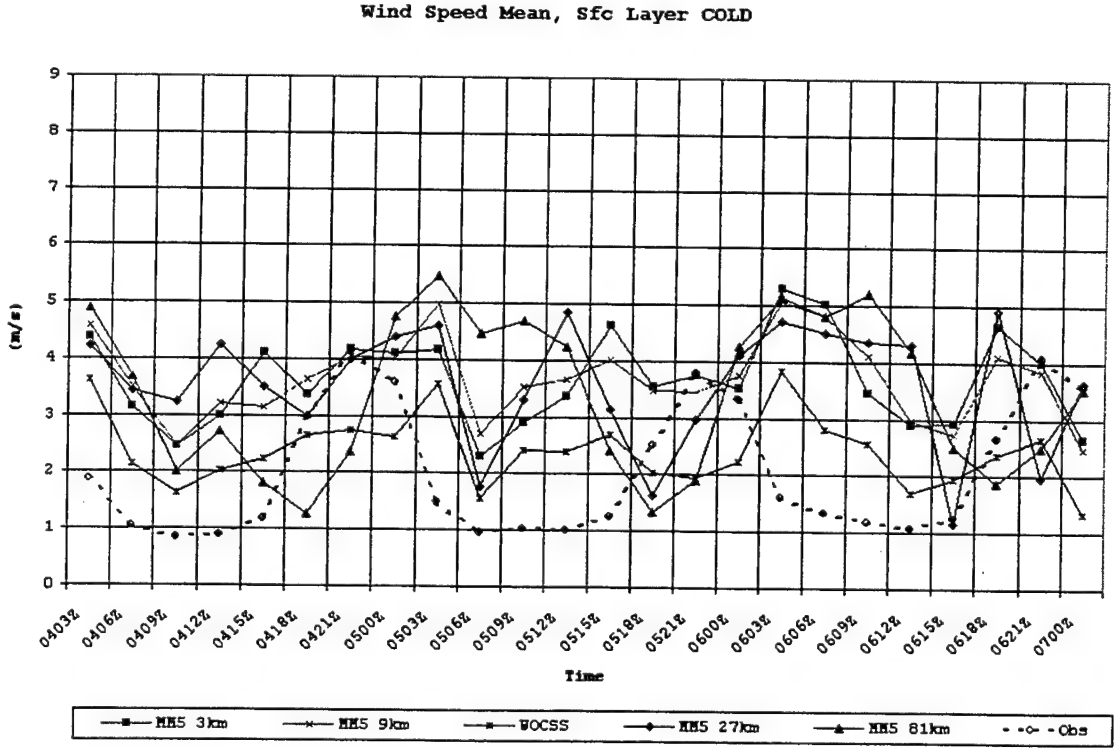

Figure 6-4. COLD mean wind speed.

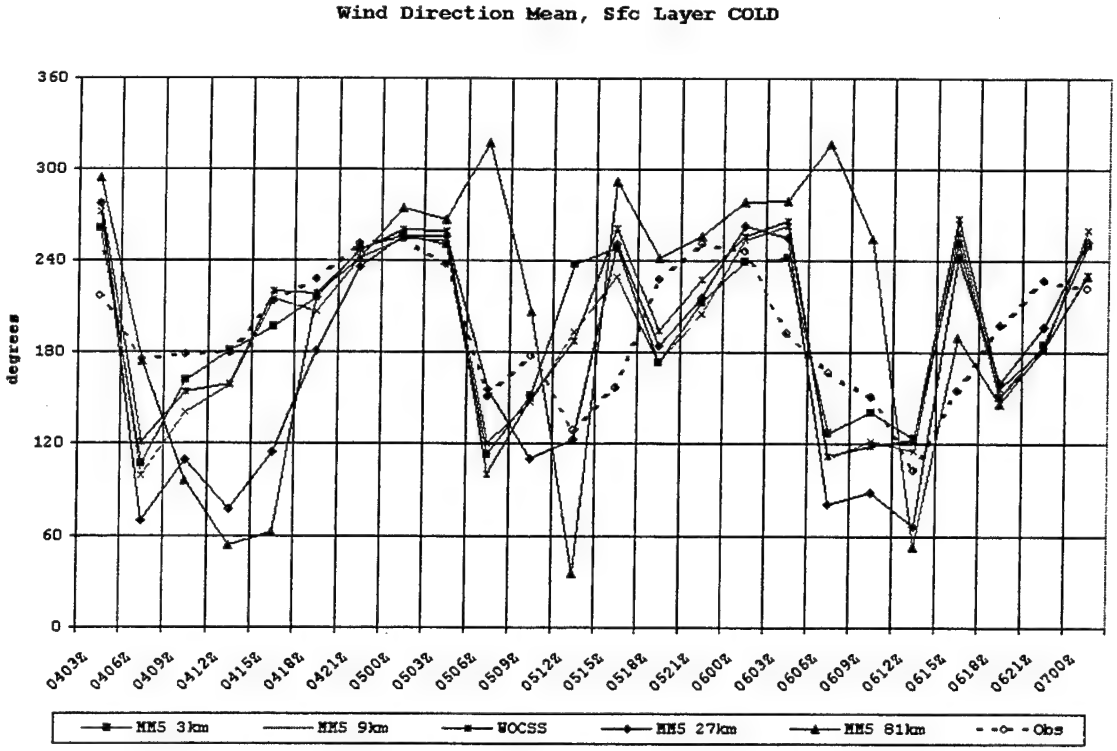

Figure 6-5. COLD mean wind direction.

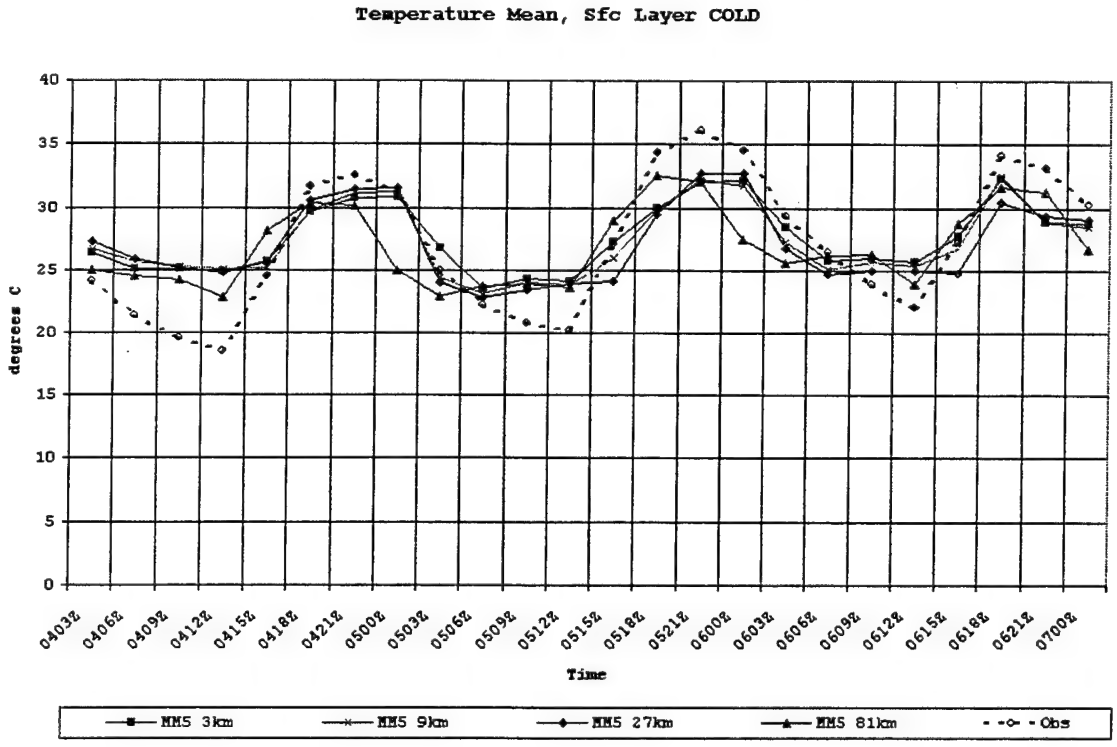

Figure 6-6. COLD mean temperature.

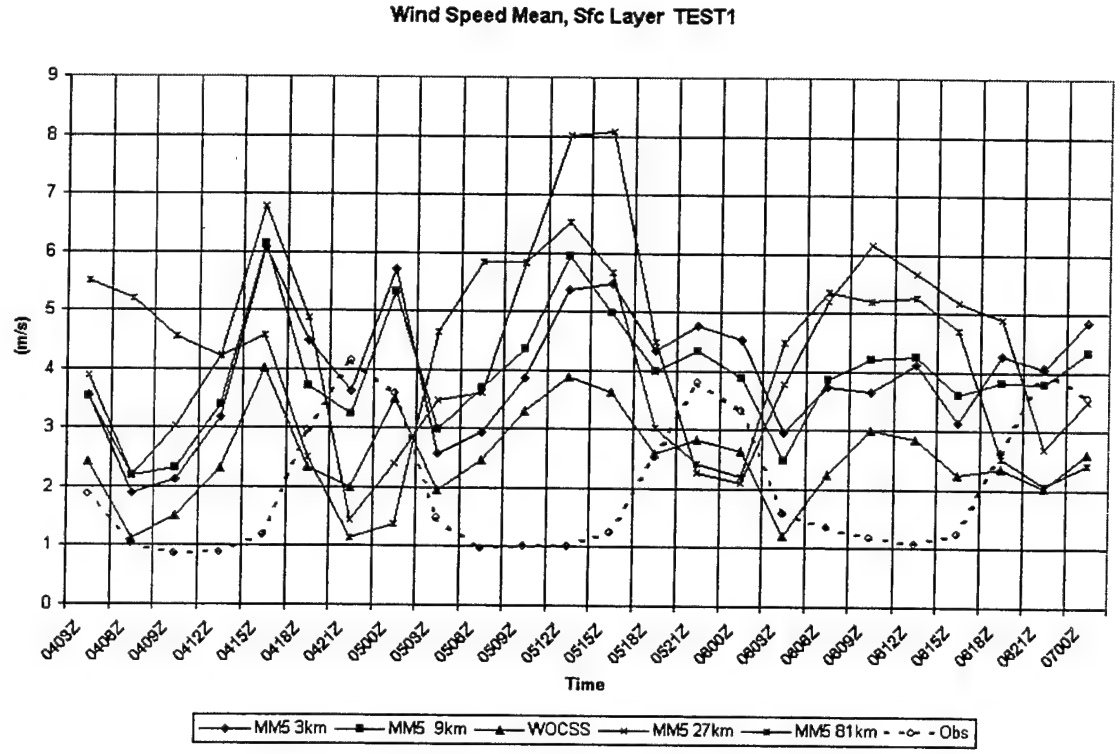

Figure 6-7. TEST1 mean wind speed.

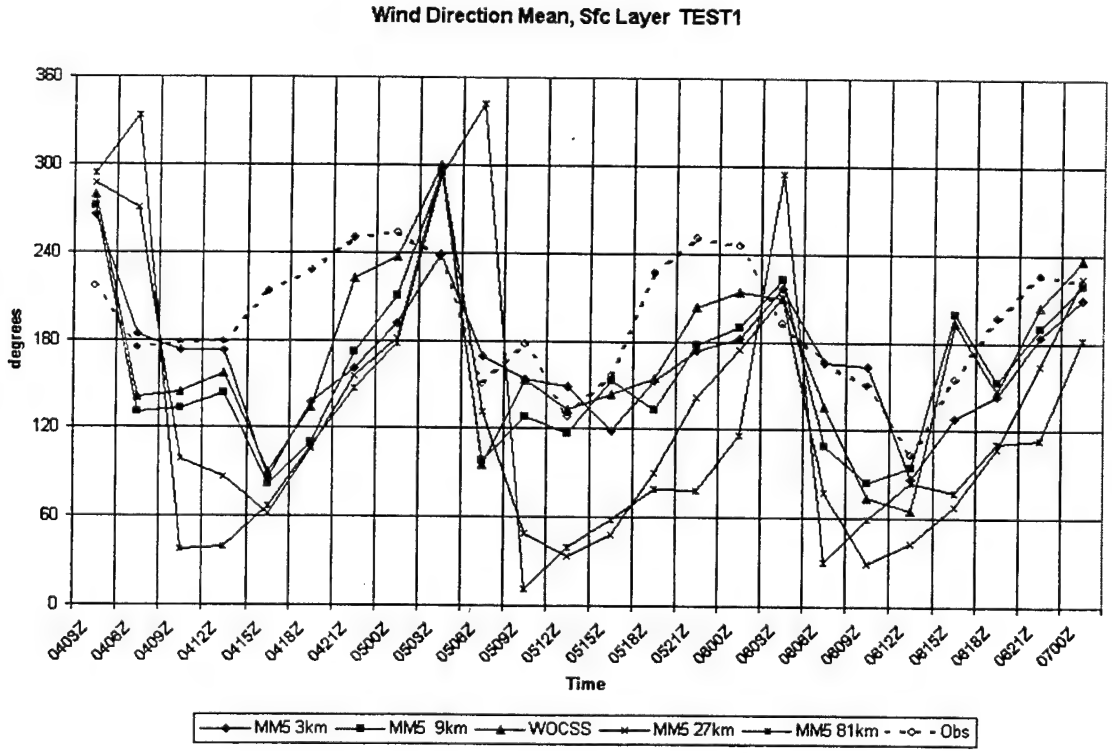

Figure 6-8. TEST1 mean wind direction.

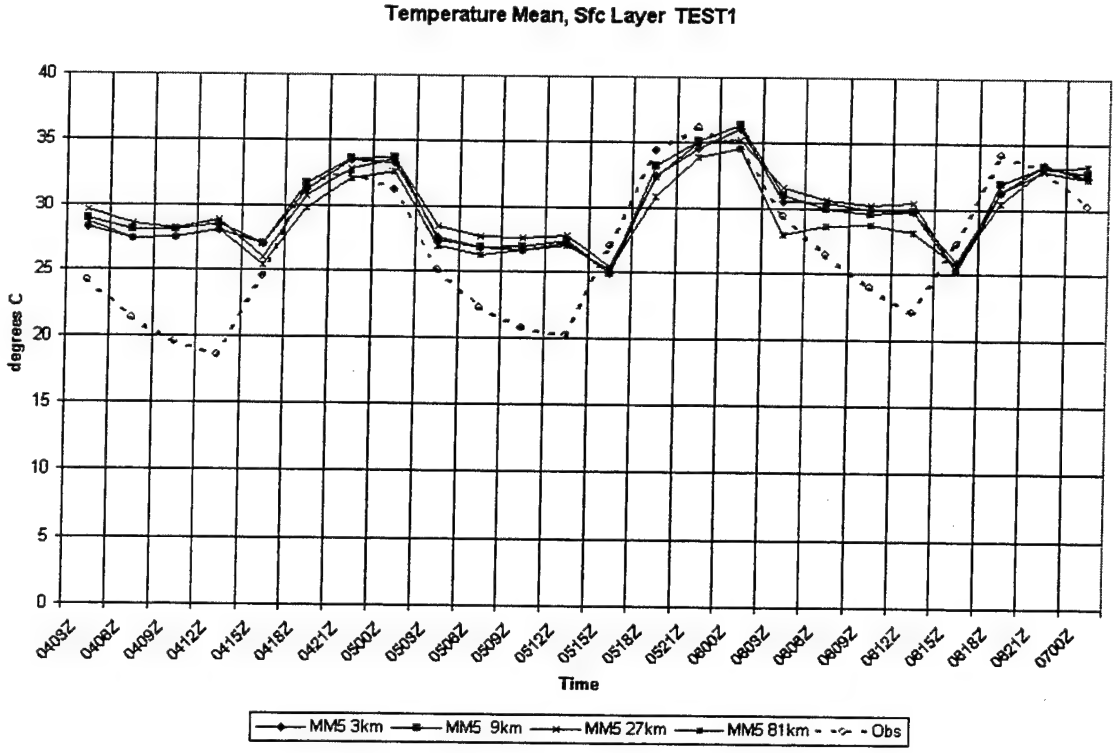

Figure 6-9. TEST1 mean temperature.

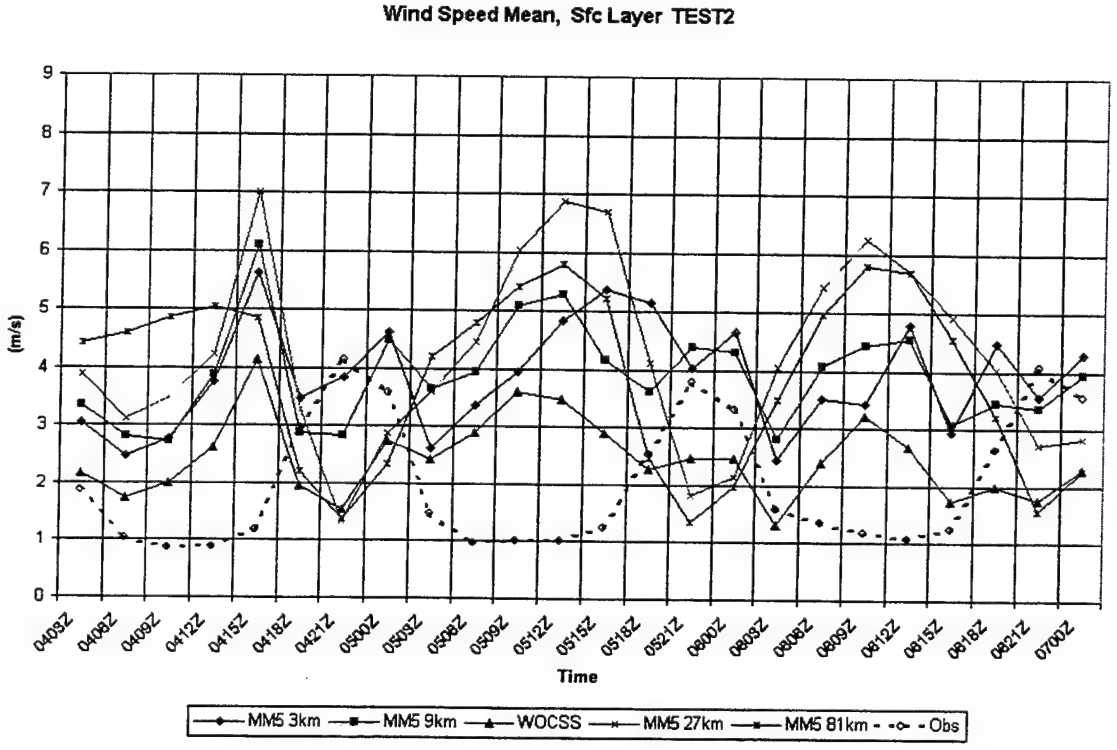

Figure 6-10. TEST2 mean wind speed.

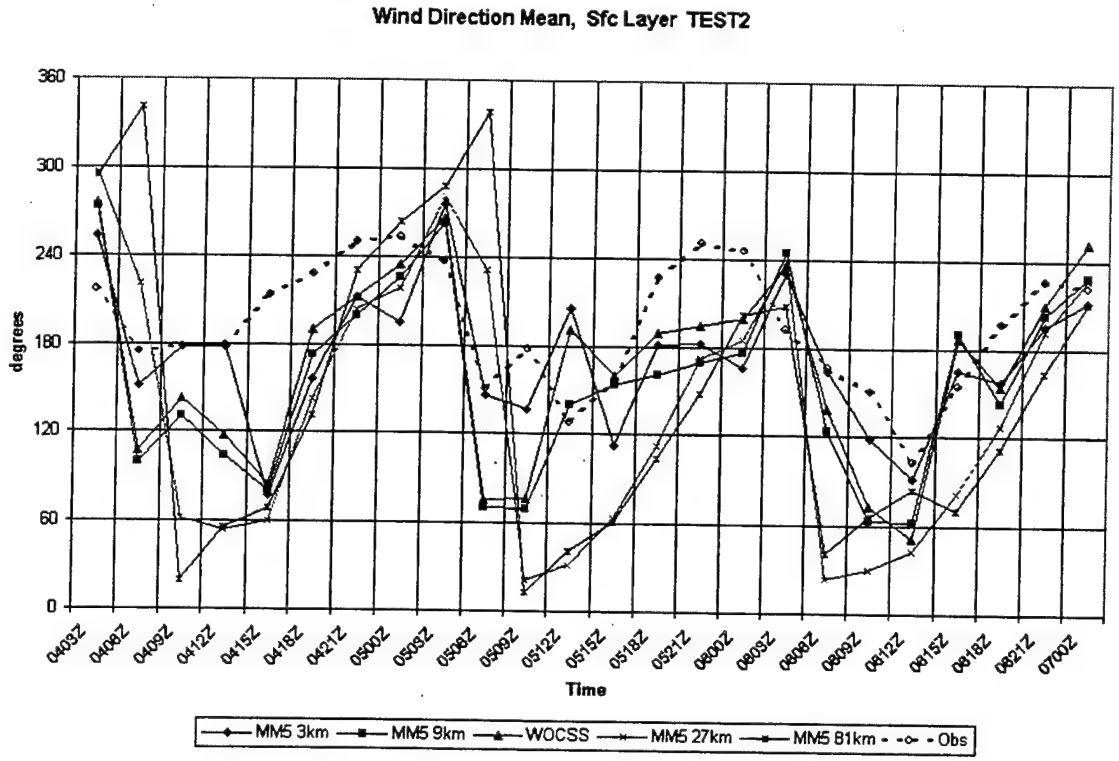

Figure 6-11. TEST2 mean wind direction.

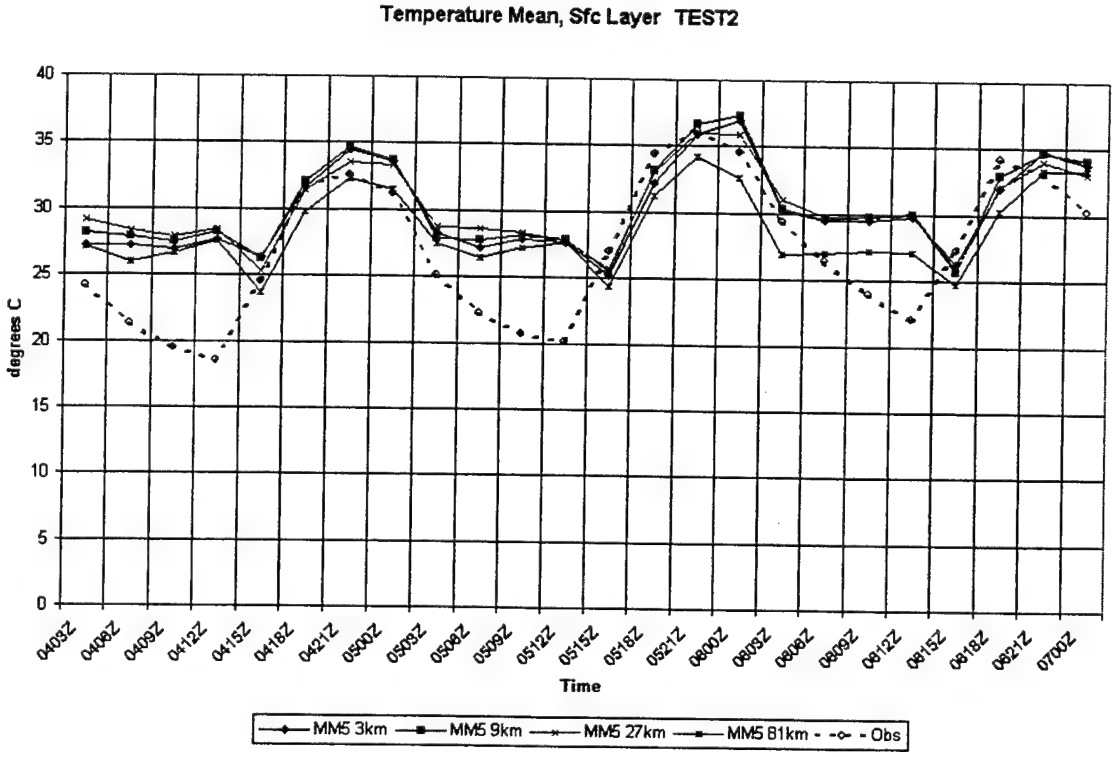

Figure 6-12. TEST2 mean temperature.

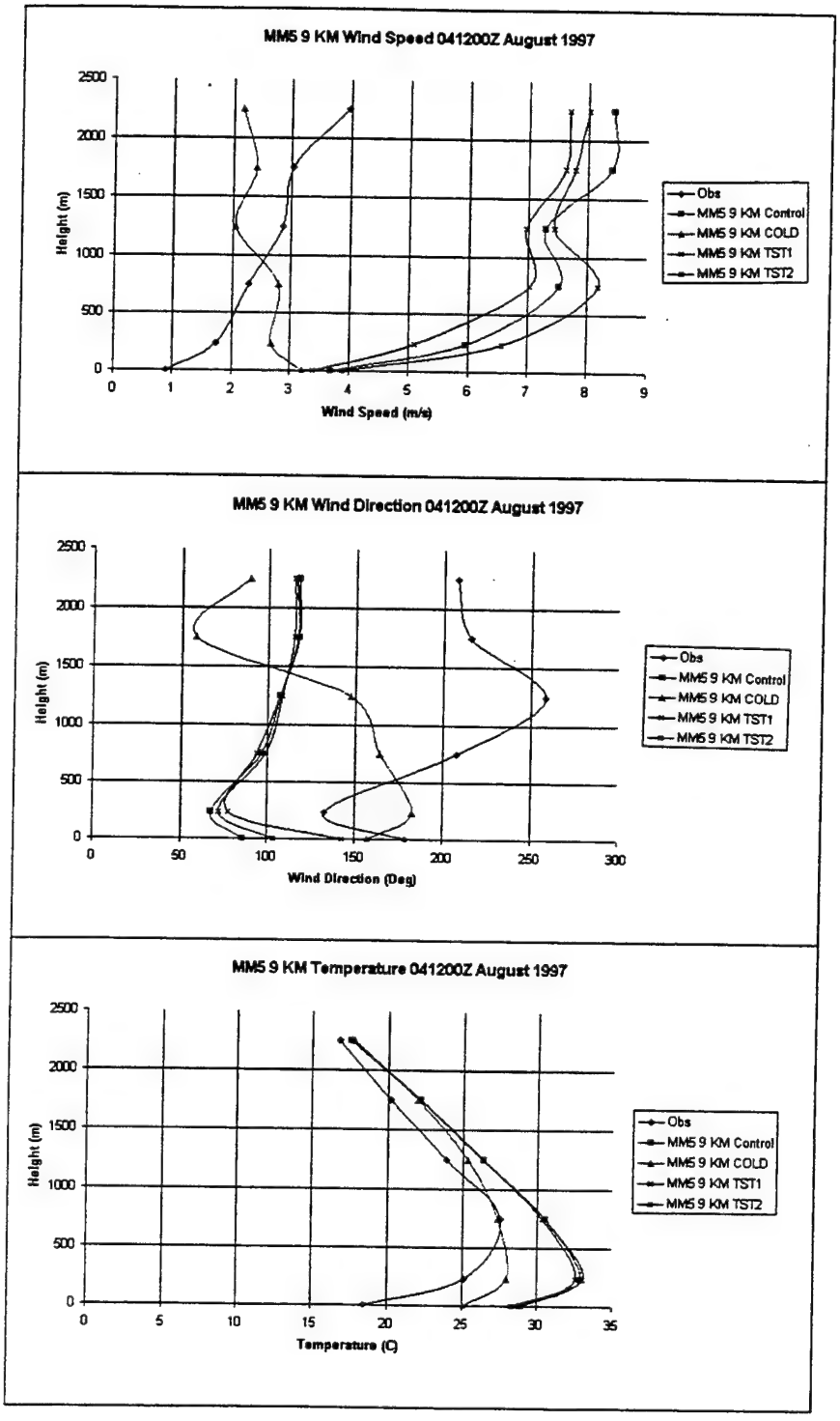

Figure 6-13. 04/12Z 9km mean vertical profiles.

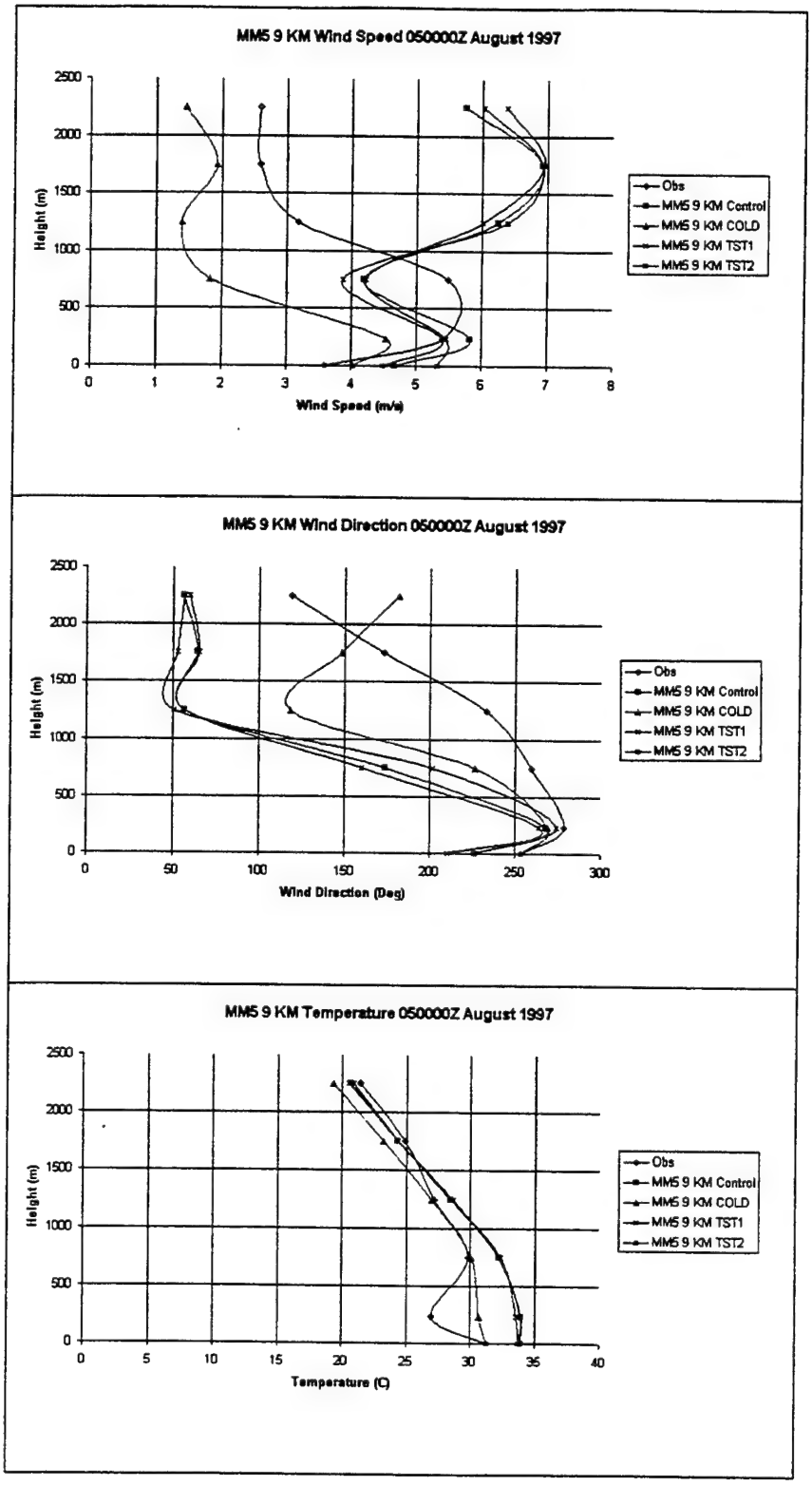

Figure 6-14. 05/00Z 9km mean vertical profiles.

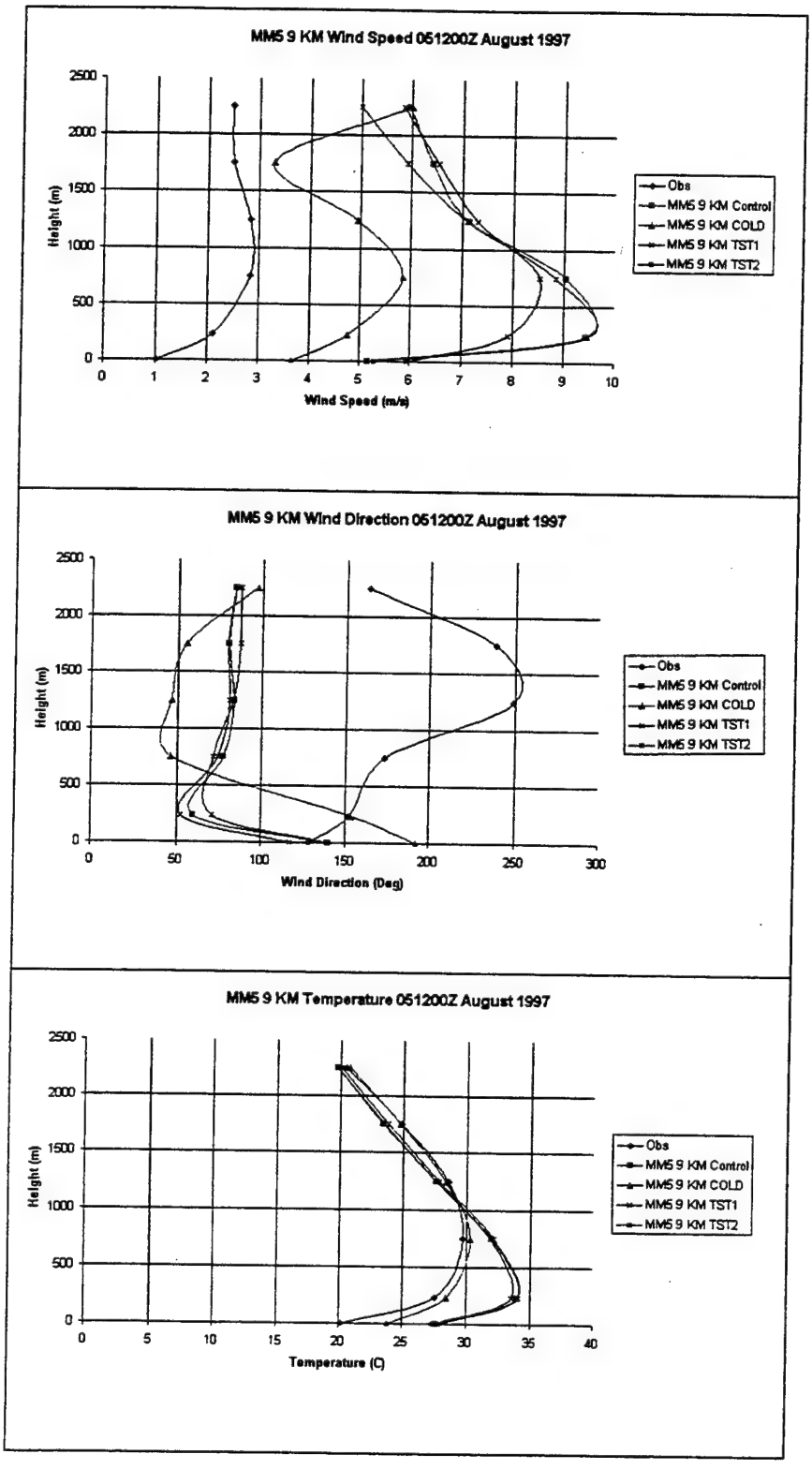

Figure 6-15. 05/12Z 9km mean vertical profiles.

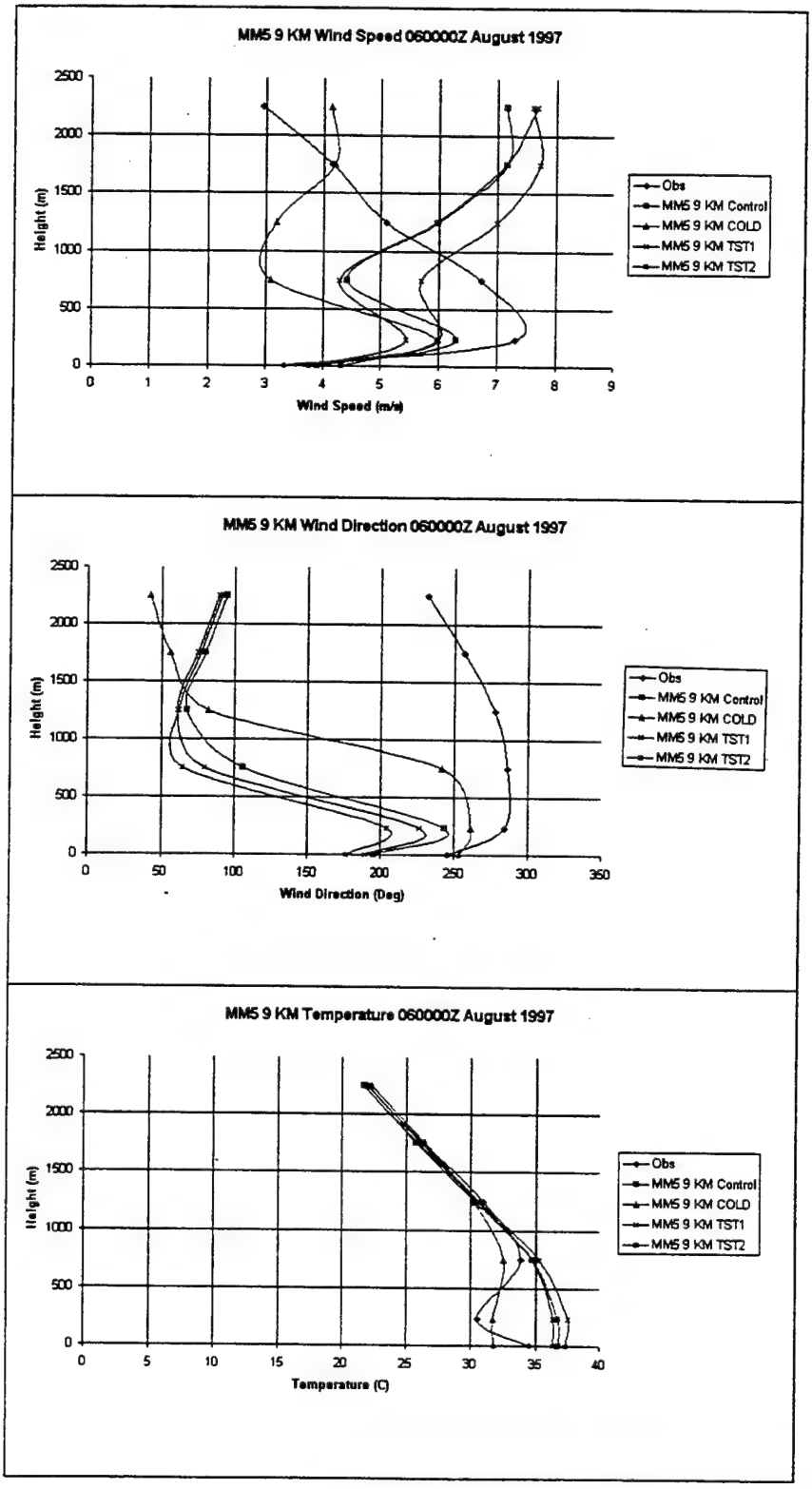

Figure 6-16. 06/00Z 9km mean vertical profiles.

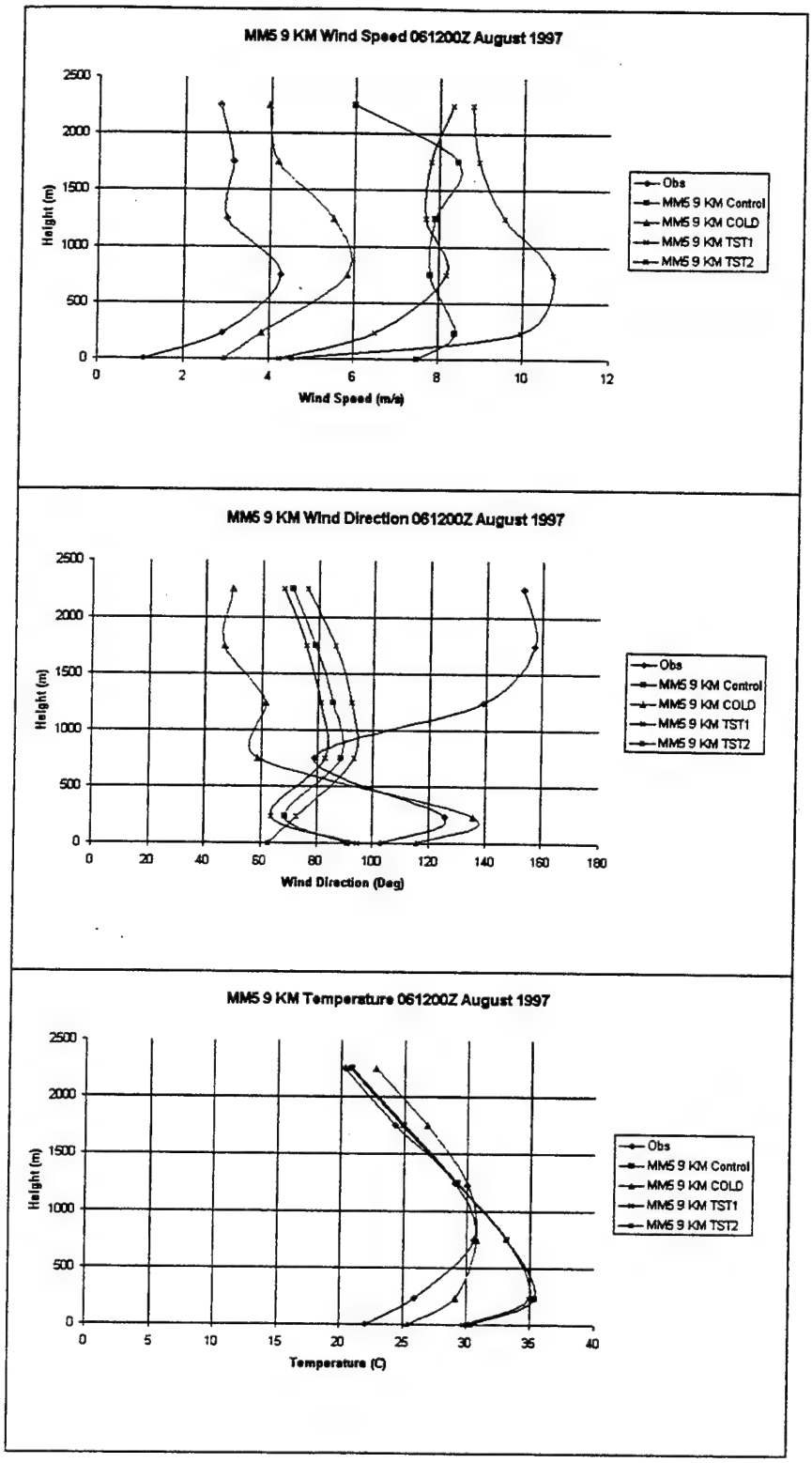

Figure 6-17. 06/12Z 9km mean vertical profiles.

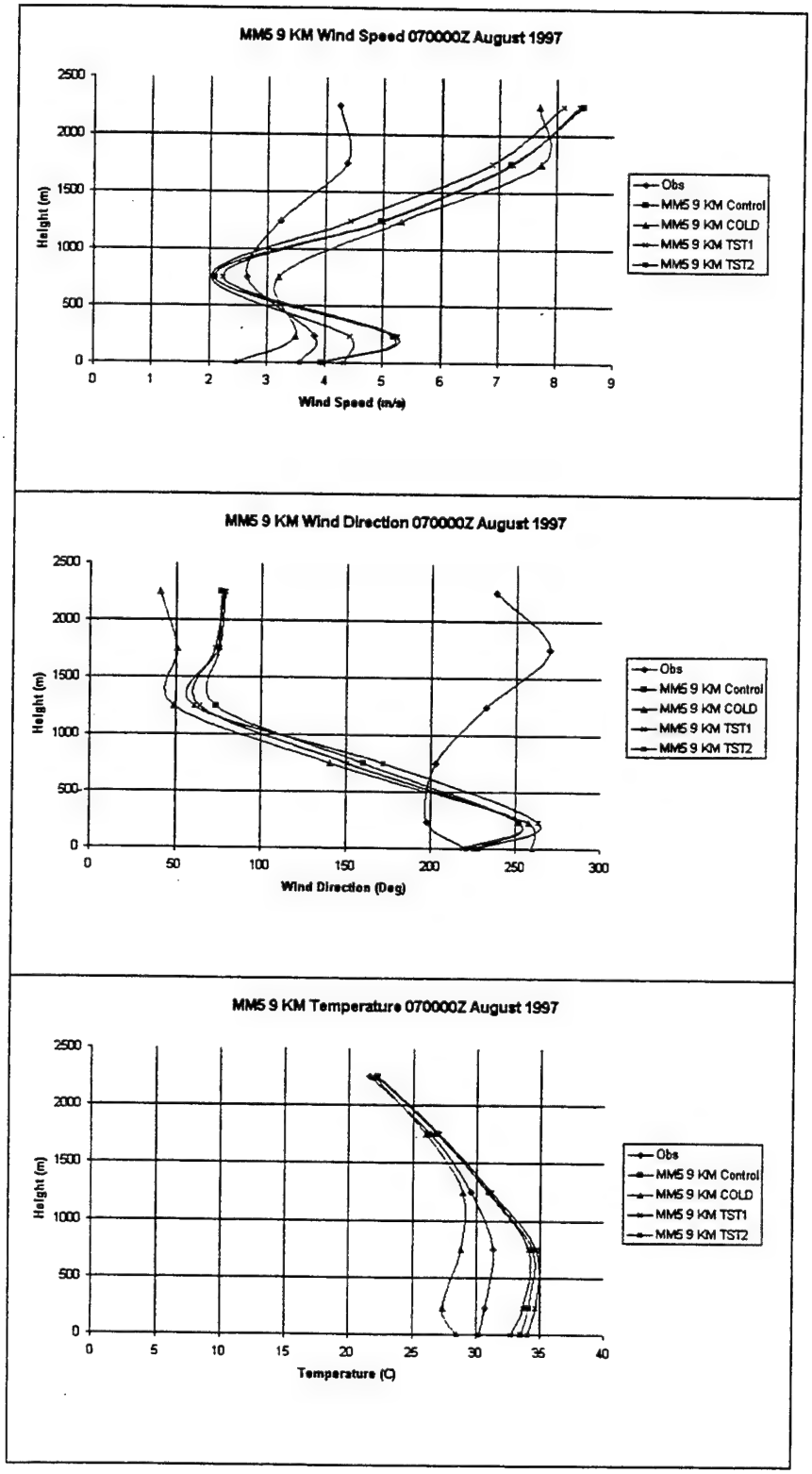

Figure 6-18. 07/00Z 9km mean vertical profiles.

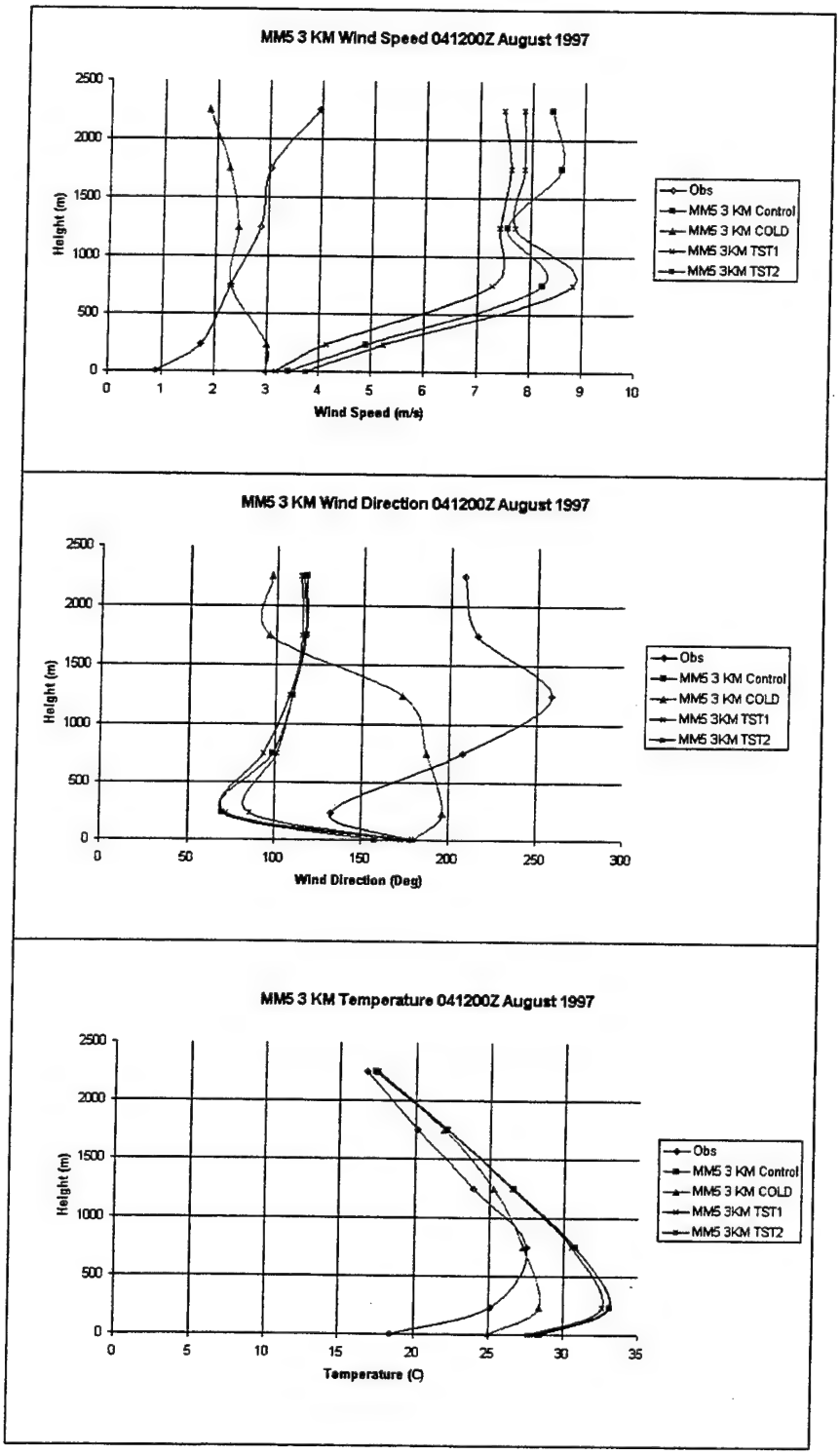

Figure 6-19. 04/12Z 3km mean vertical profiles.

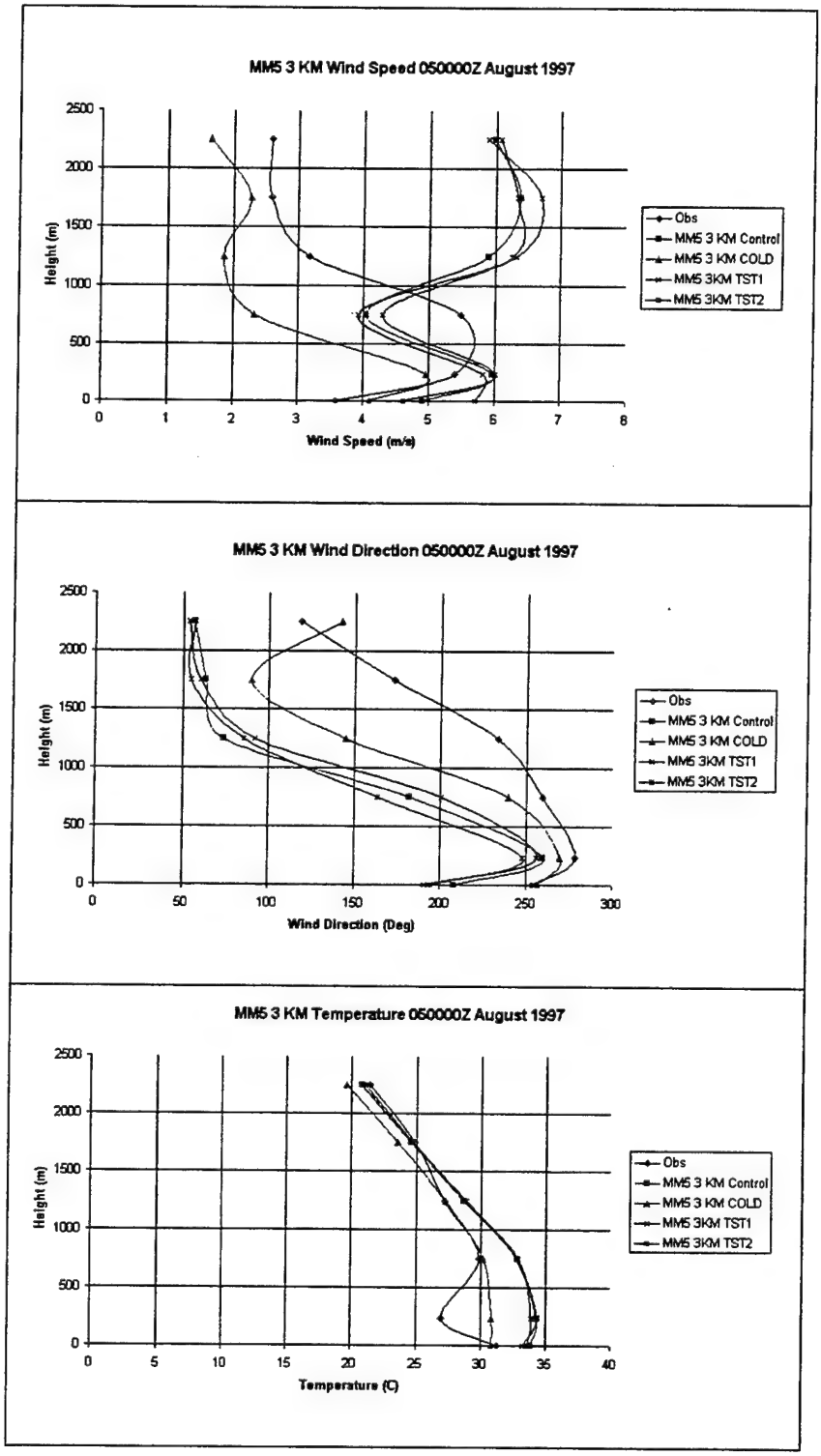

Figure 6-20. 05/00Z 3km mean vertical profiles.

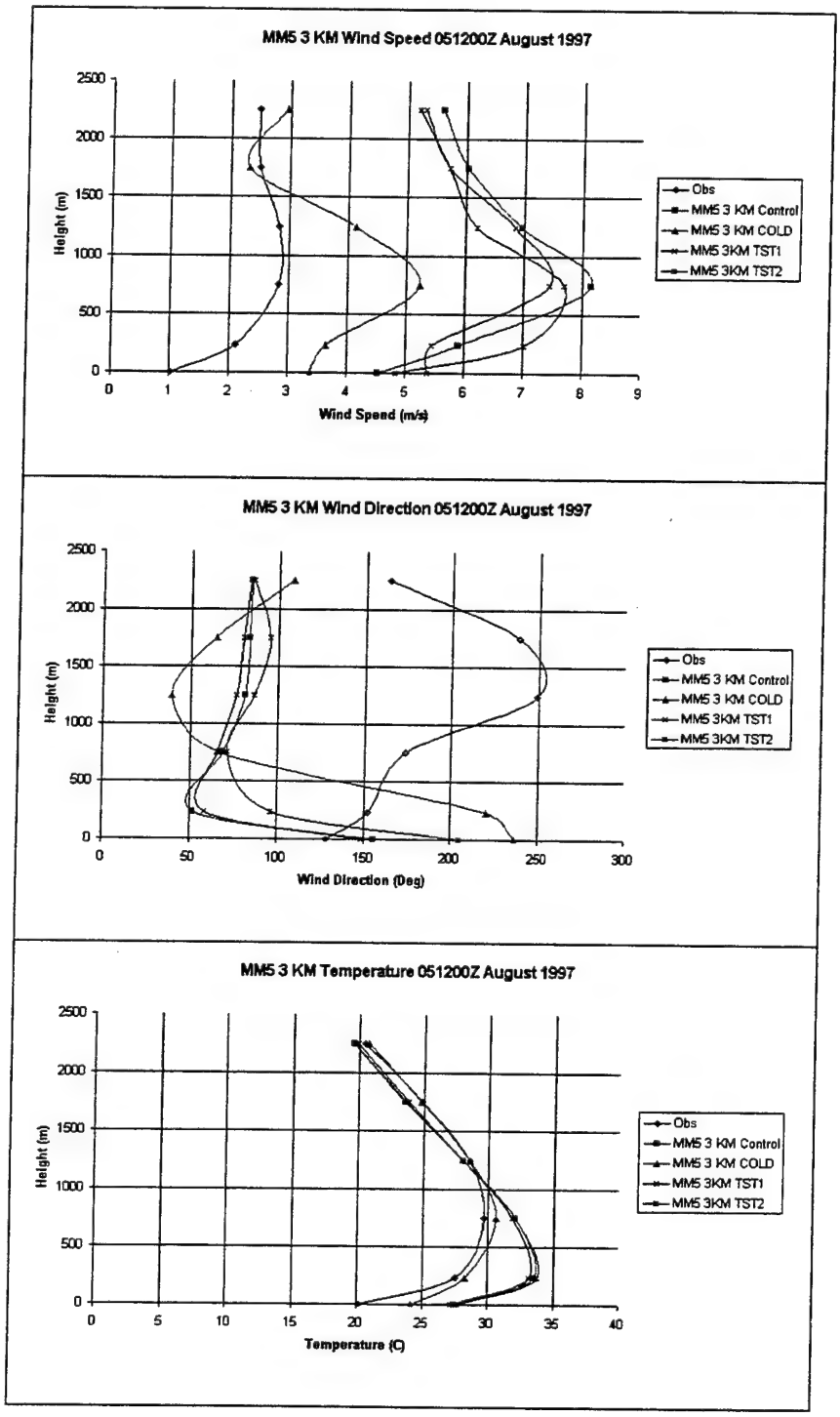

Figure 6-21. 05/12Z 3km mean vertical profiles.

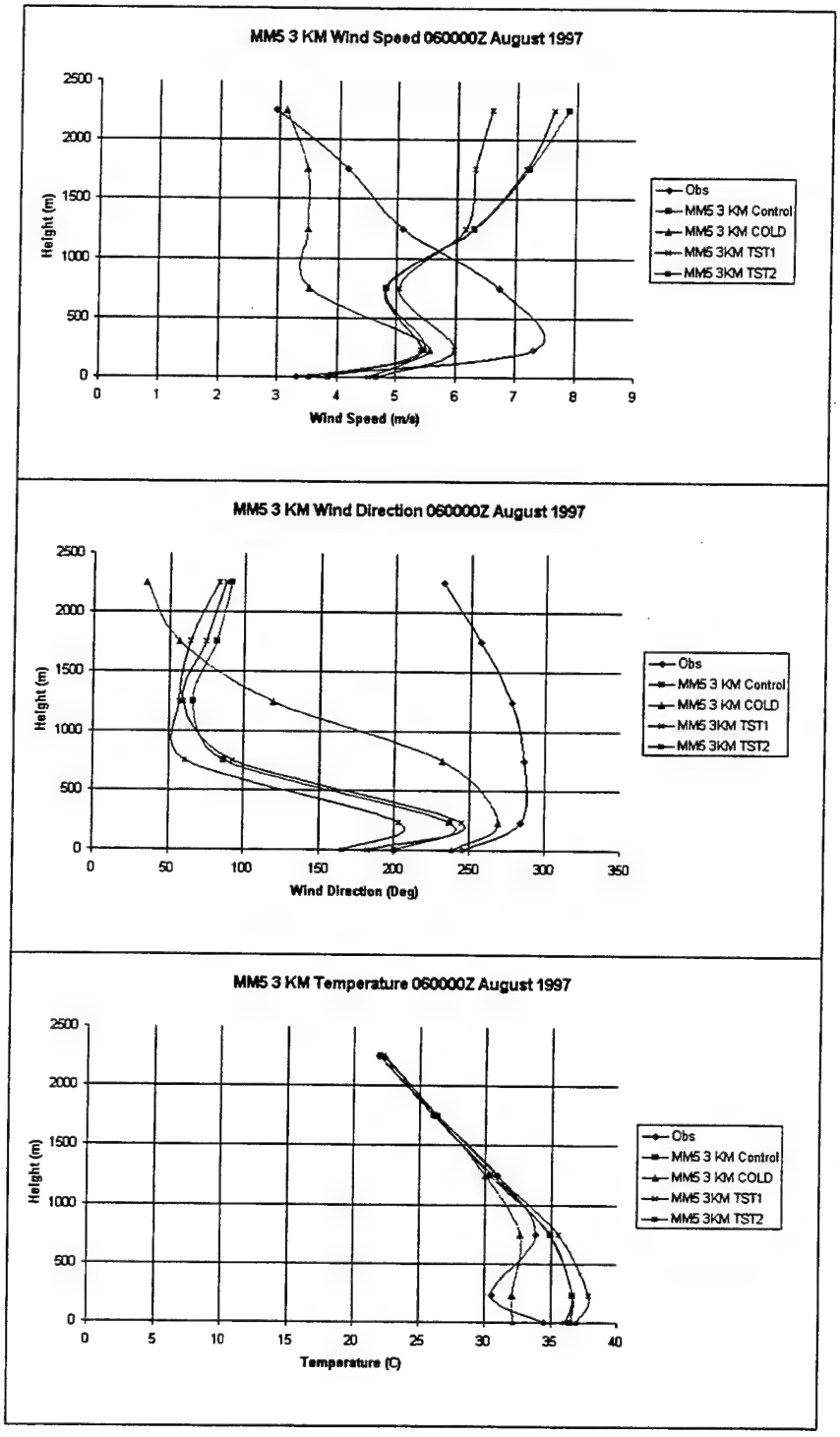

Figure 6-22. 06/00Z 3km mean vertical profiles.

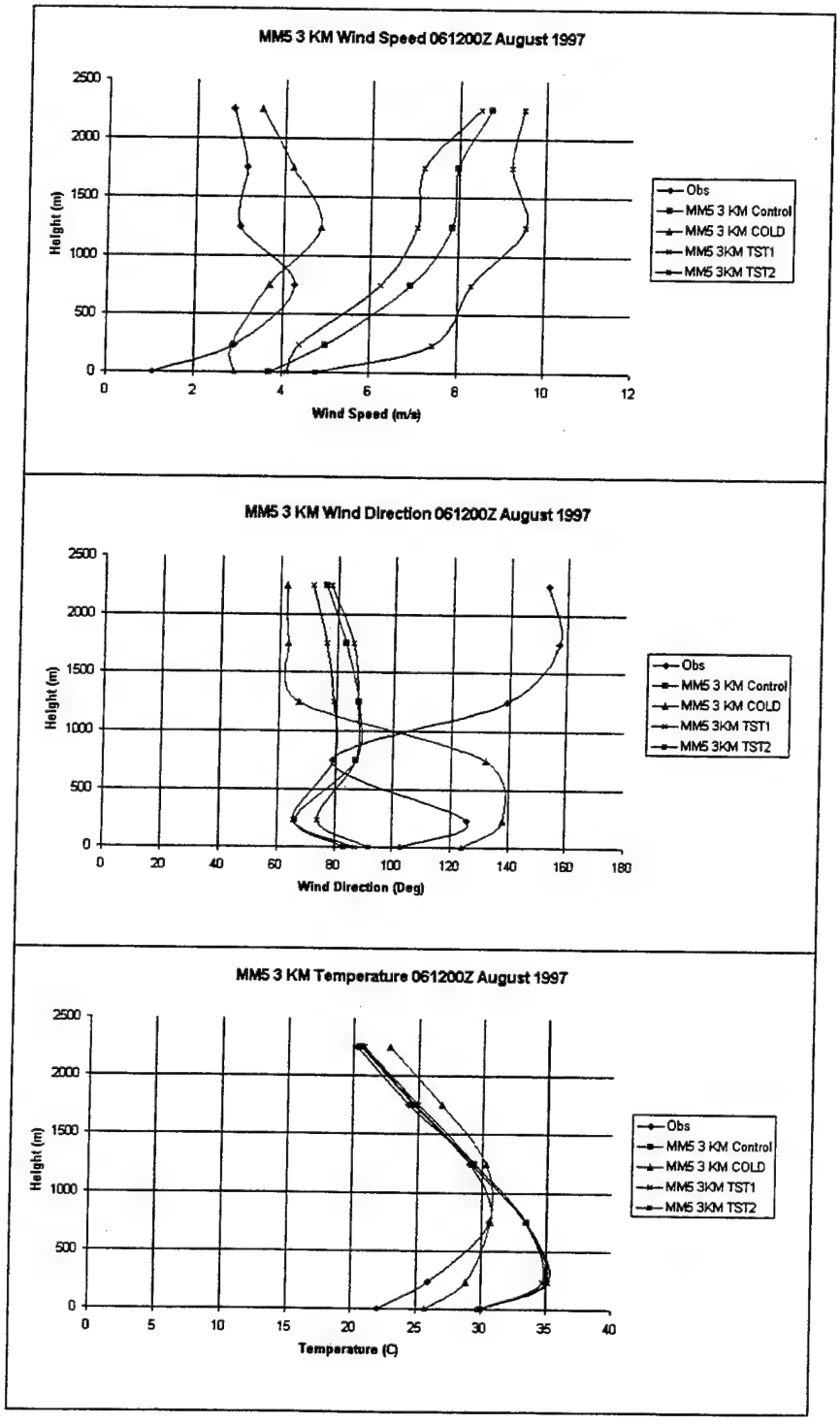

Figure 6-23. 06/12Z 3km mean vertical profiles.

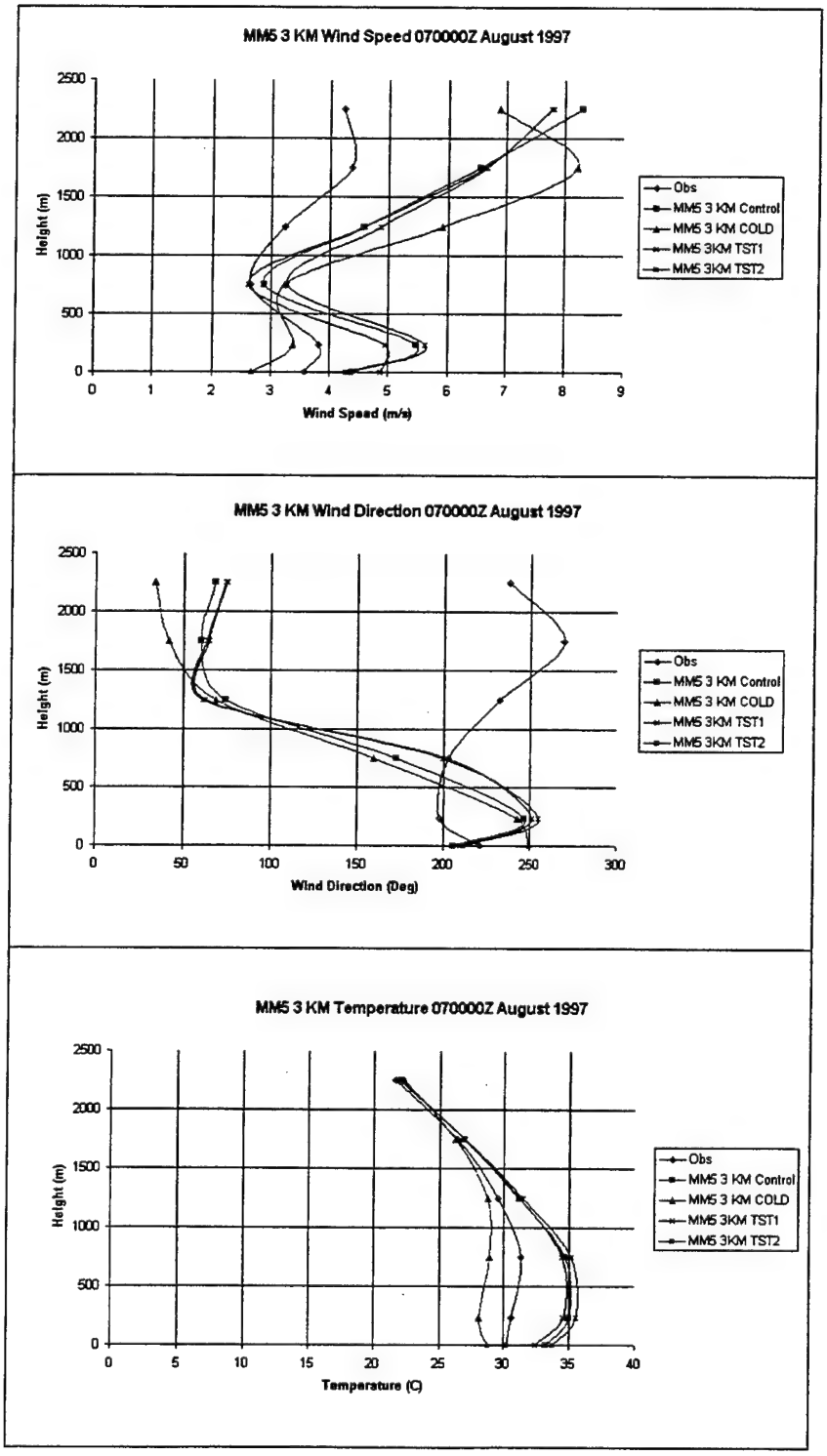

Figure 6-24. 07/00Z 3km mean vertical profiles.

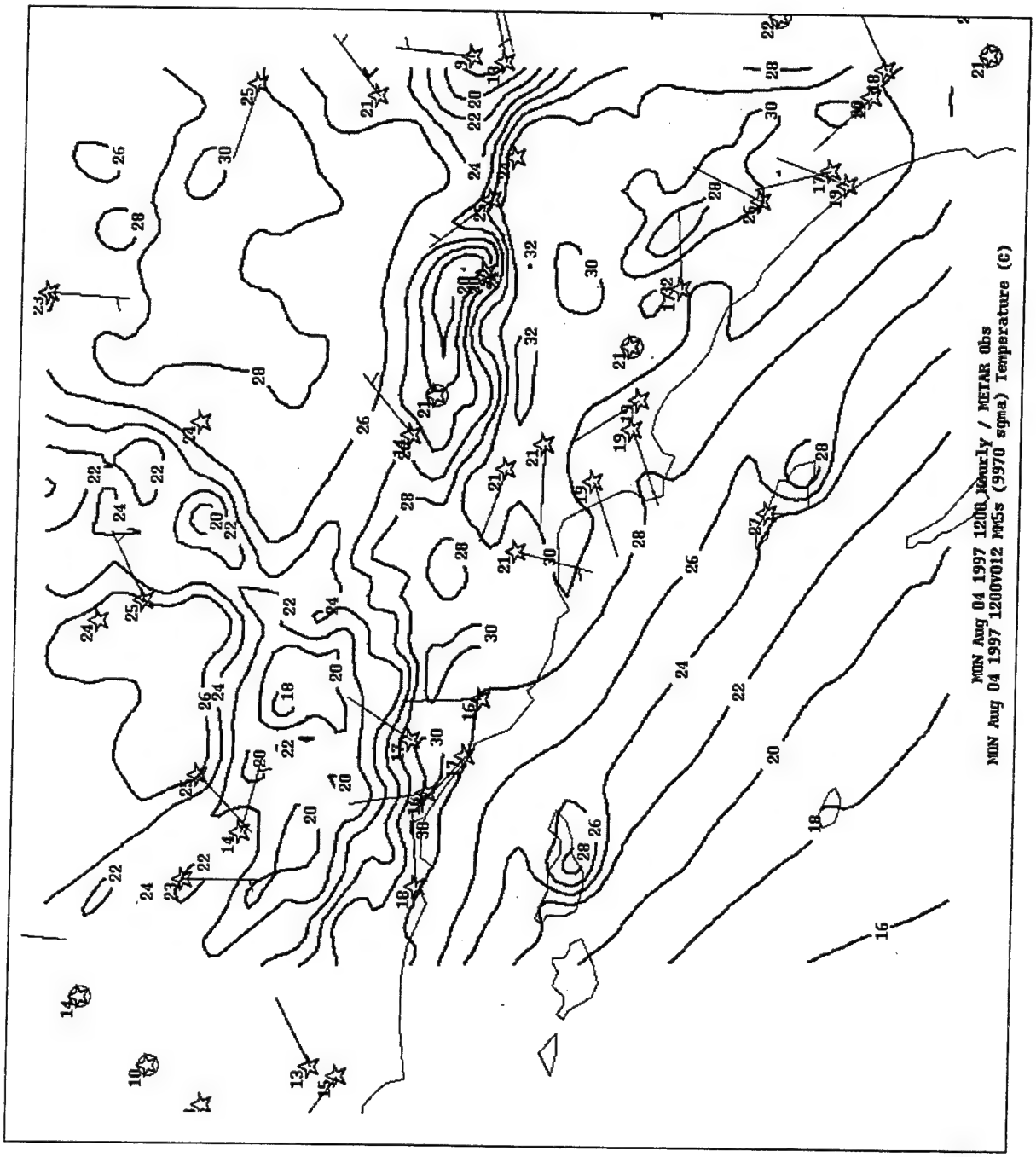

Figure 7-1. 04/12Z MM5 CTRL 3km 12 hour temperature forecast for sigma level 9970 (approx. 22m AGL) with surface observations.

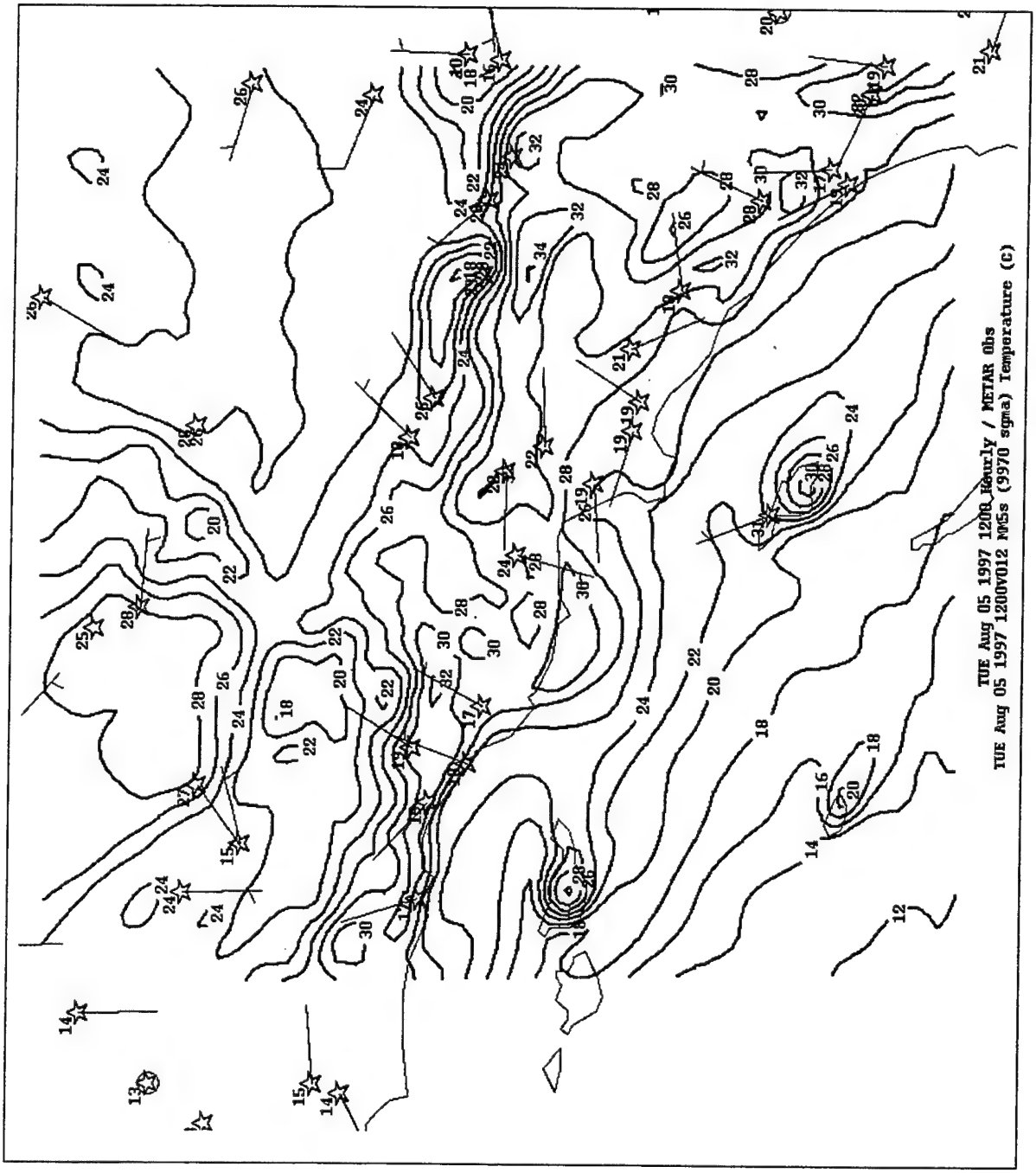

Figure 7-2. 05/12Z MM5 CTRL 3km 12 hour temperature forecast for sigma level 9970 (approx. 22m AGL) with surface observations.

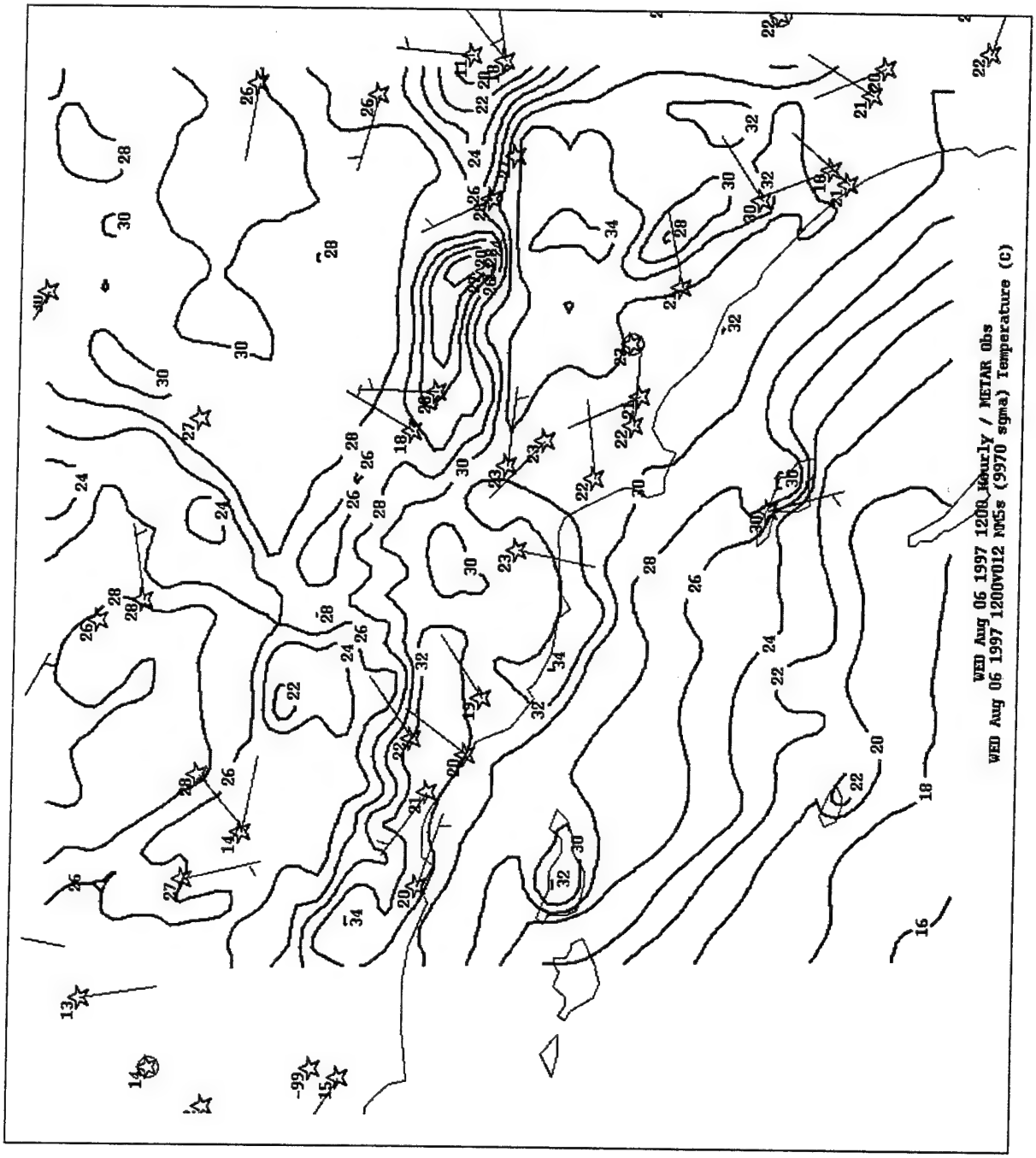

Figure 7-3. 06/12Z MM5 CTRL 3km 12 hour temperature forecast for sigma level 9970 (approx. 22m AGL) with surface observations.

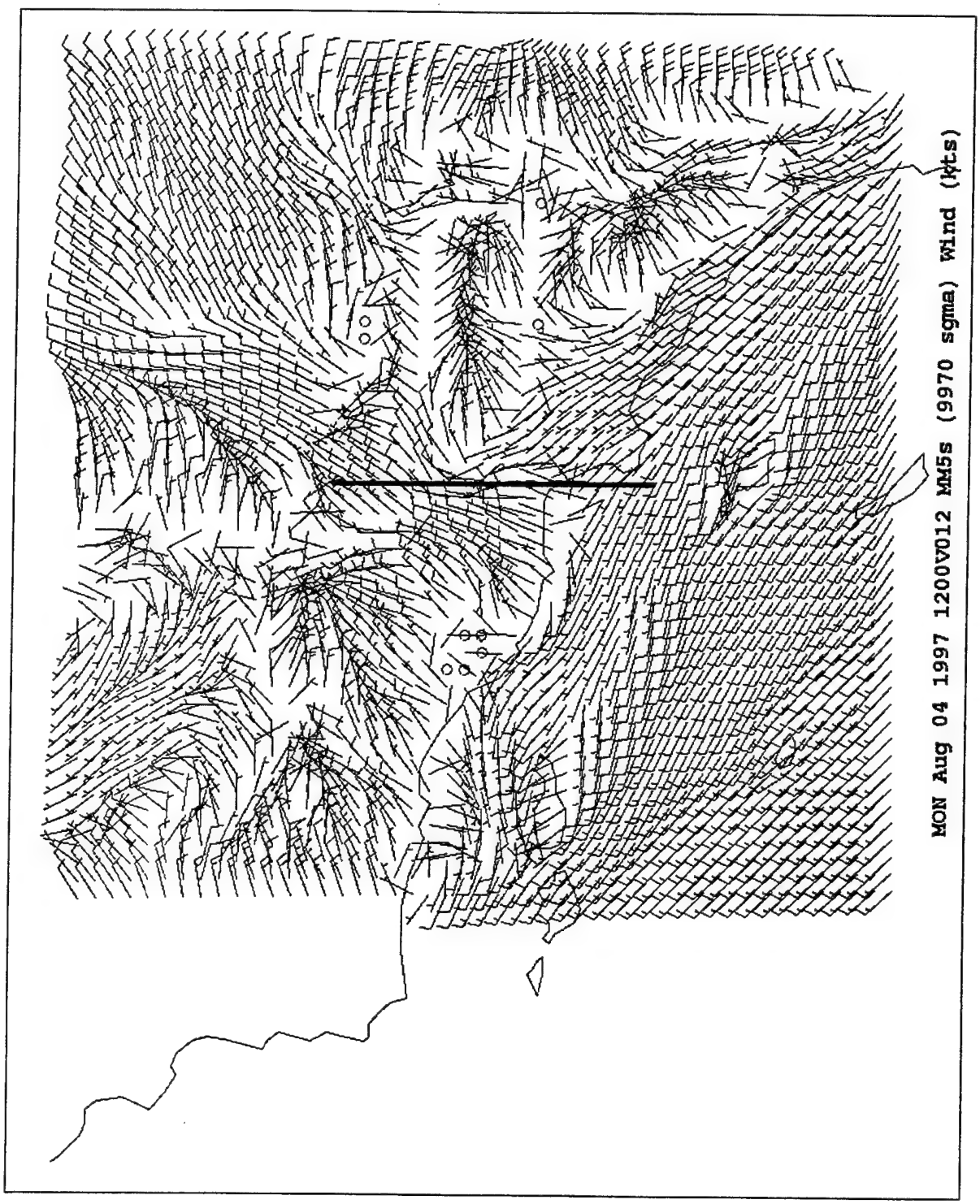

Figure 7-4. 04/12Z MM5 CTRL 3km 12 hour wind (kts) forecast for sigma level 9970 (approx. 22m AGL).

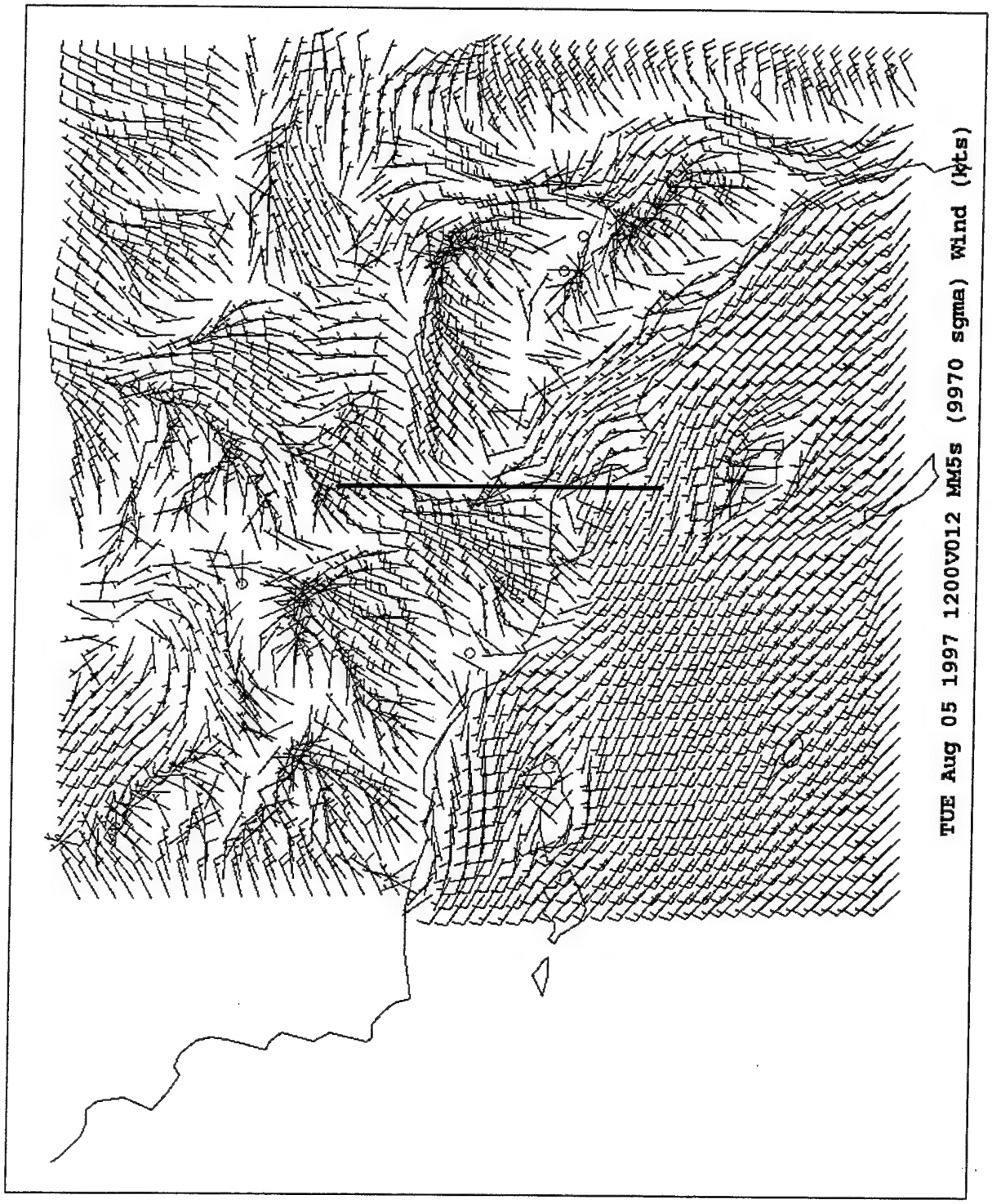

Figure 7-5. 05/12Z MM5 CTRL 3km 12 hour wind (kts) forecast for sigma level 9970 (approx. 22m AGL).

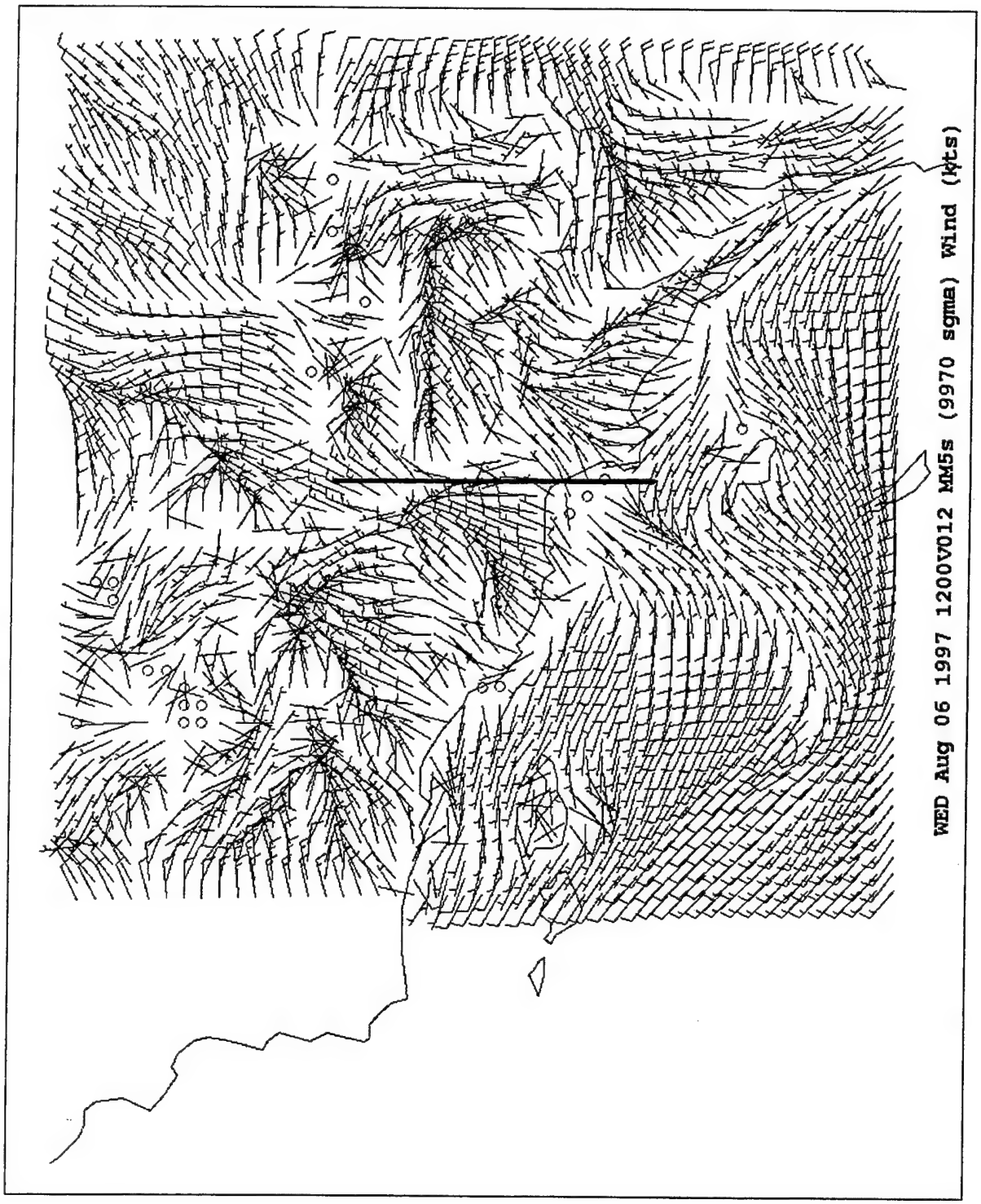

Figure 7-6. 06/12Z MM5 CTRL 3km 12 hour wind (kts) forecast for sigma level 9970 (approx. 22m AGL).

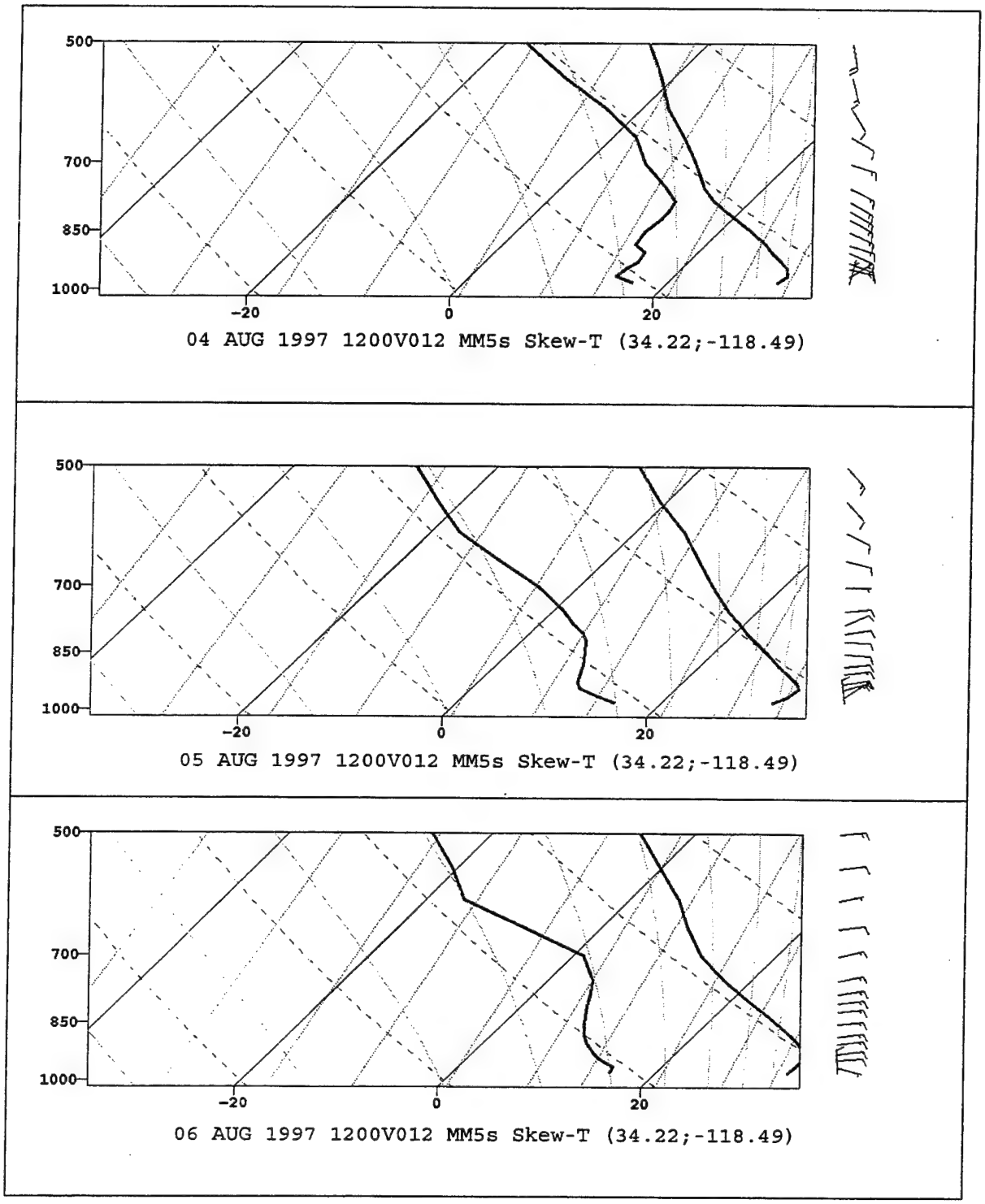

Figures 7-7a, 7-7b, and 7-7c. MM5 CTRL 3km domain vertical profile 12 hour forecasts at same lat/long of VNS profiler.

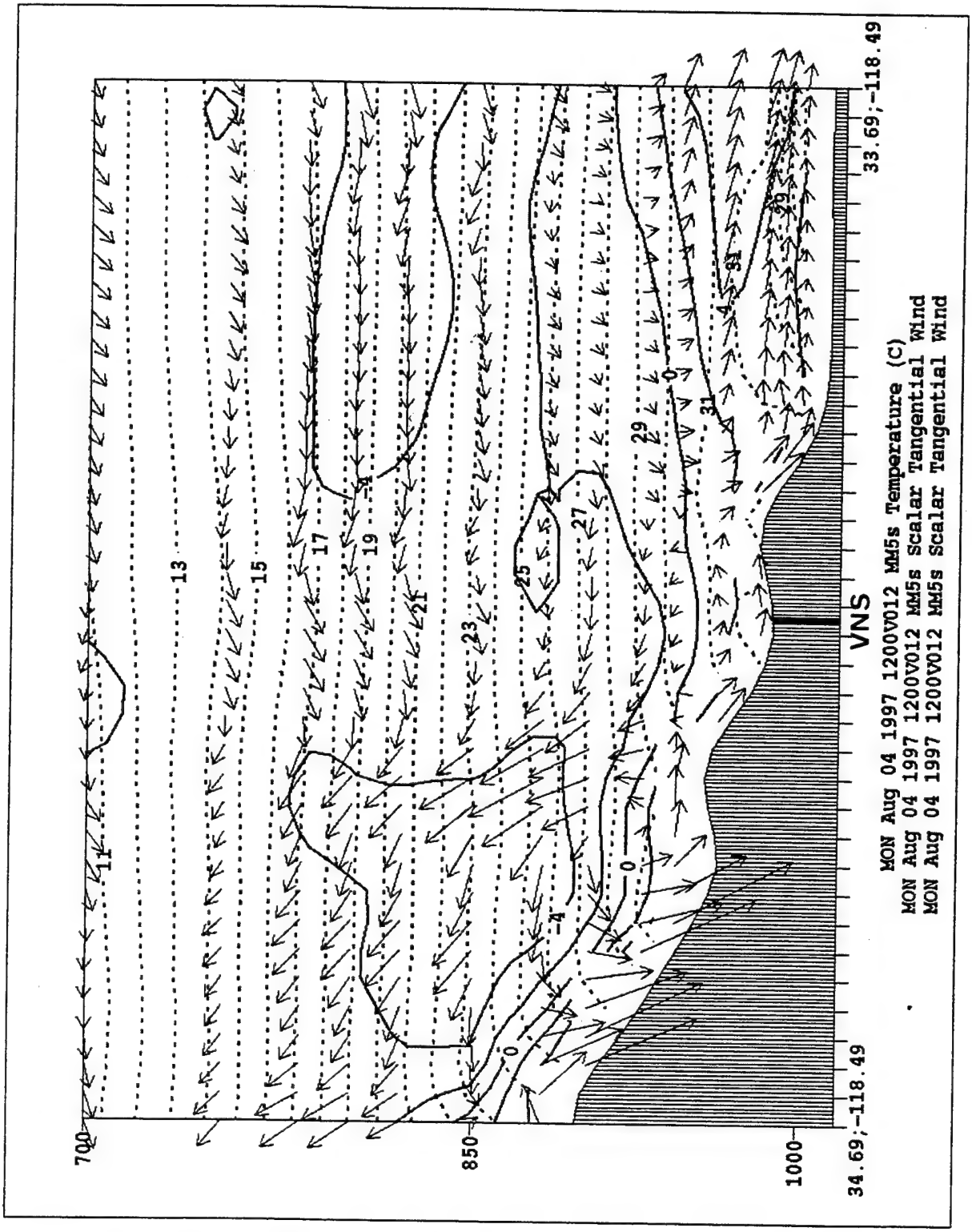

Figure 7-8. 04/12Z MM5 CTRL 3km N-S cross section forecast. Temperature in Celisus (dashed). Direction (arrow) and scalar speeds in m/s. Isotachs (solid) are positive (southward) or negative (northward).

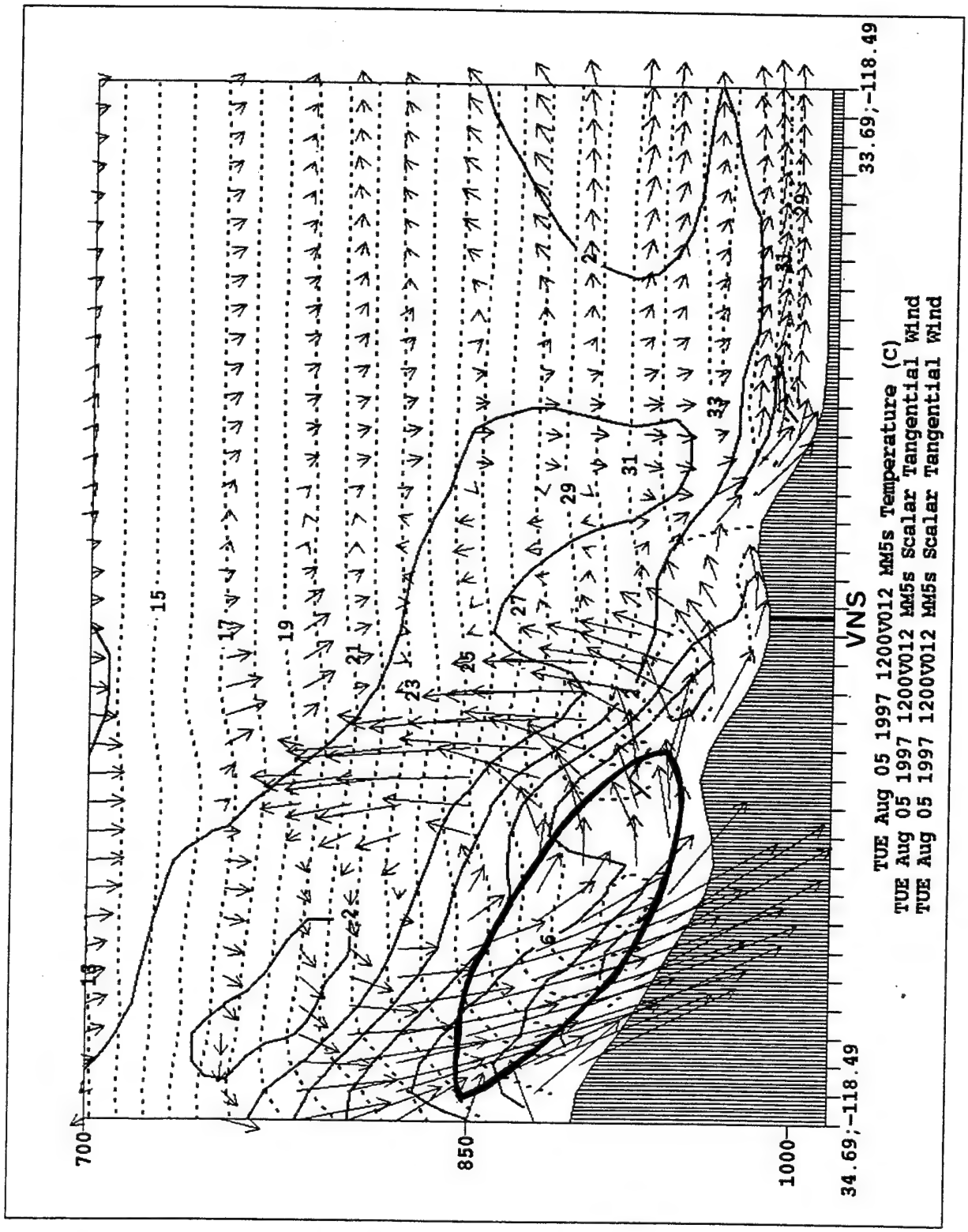

Figure 7-9. 05/12Z MM5 CTRL 3km N-S cross section forecast. Temperature in Celisus (dashed). Direction (arrow) and scalar speeds in m/s. Isotachs (solid) are positive (southward) or negative (northward). LLJ (heavy solid) isotach 12 m/s (out of page).

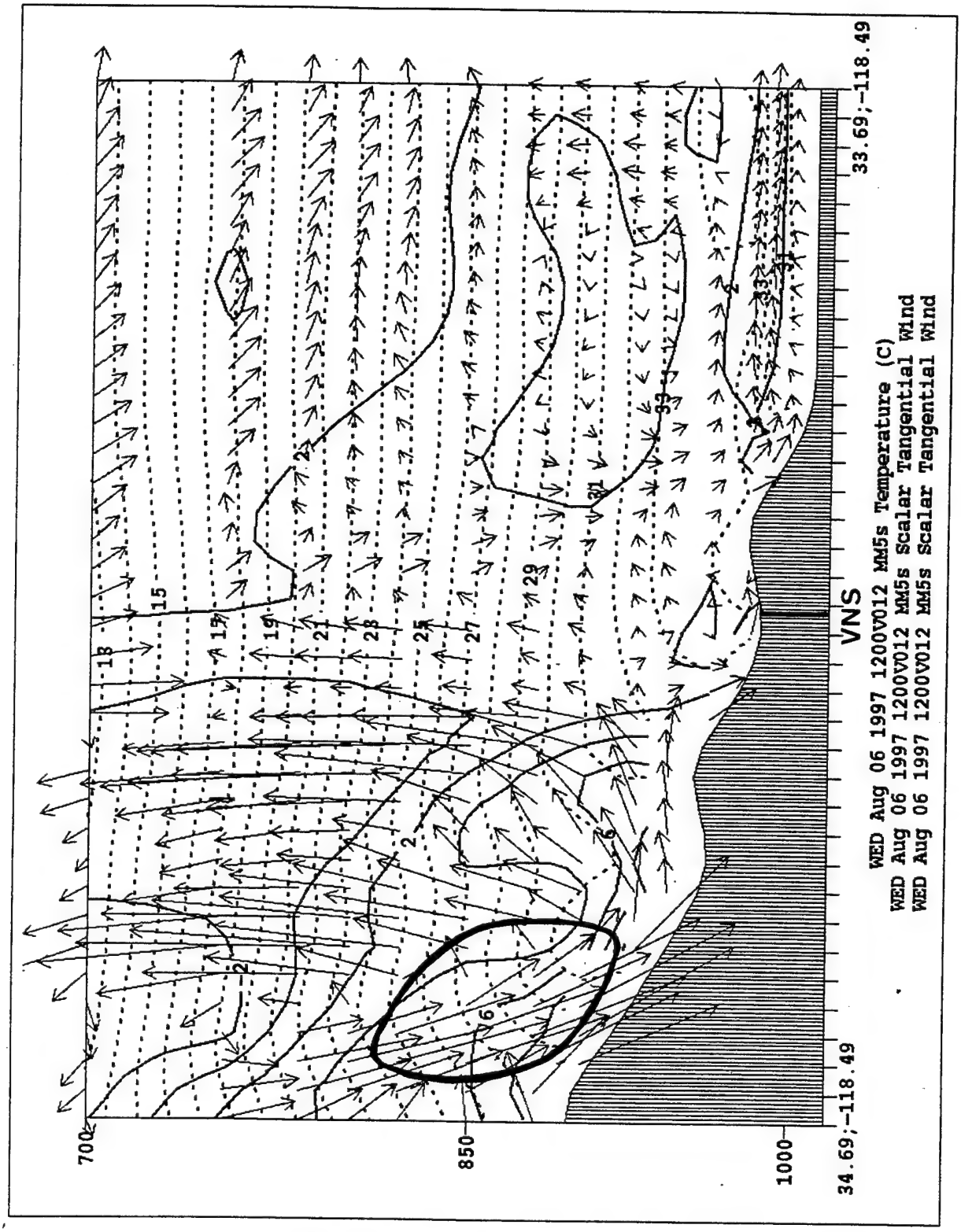

Figure 7-10. 06/12Z MM5 CTRL 3km N-S cross section forecast. Temperature in Celisus (dashed). Direction (arrow) and scalar speeds in m/s. Isotachs (solid) are positive (southward) or negative (northward). LLJ (heavy solid) isotach 10 m/s (out of page).

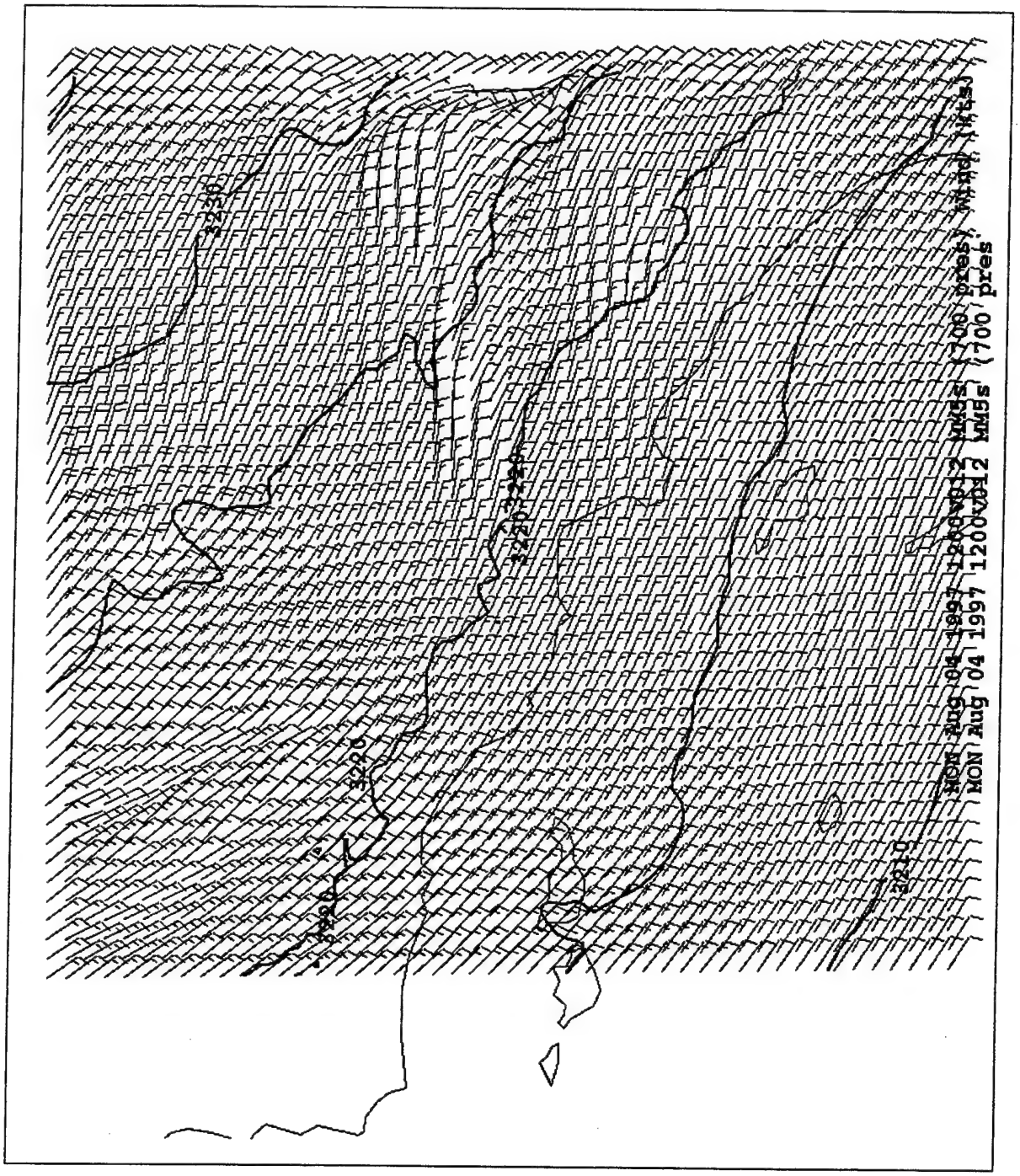

Figure 7-11. 04/12Z MM5 CTRL 3km 12 hour 700mb height(m) and wind(kt) forecasts.

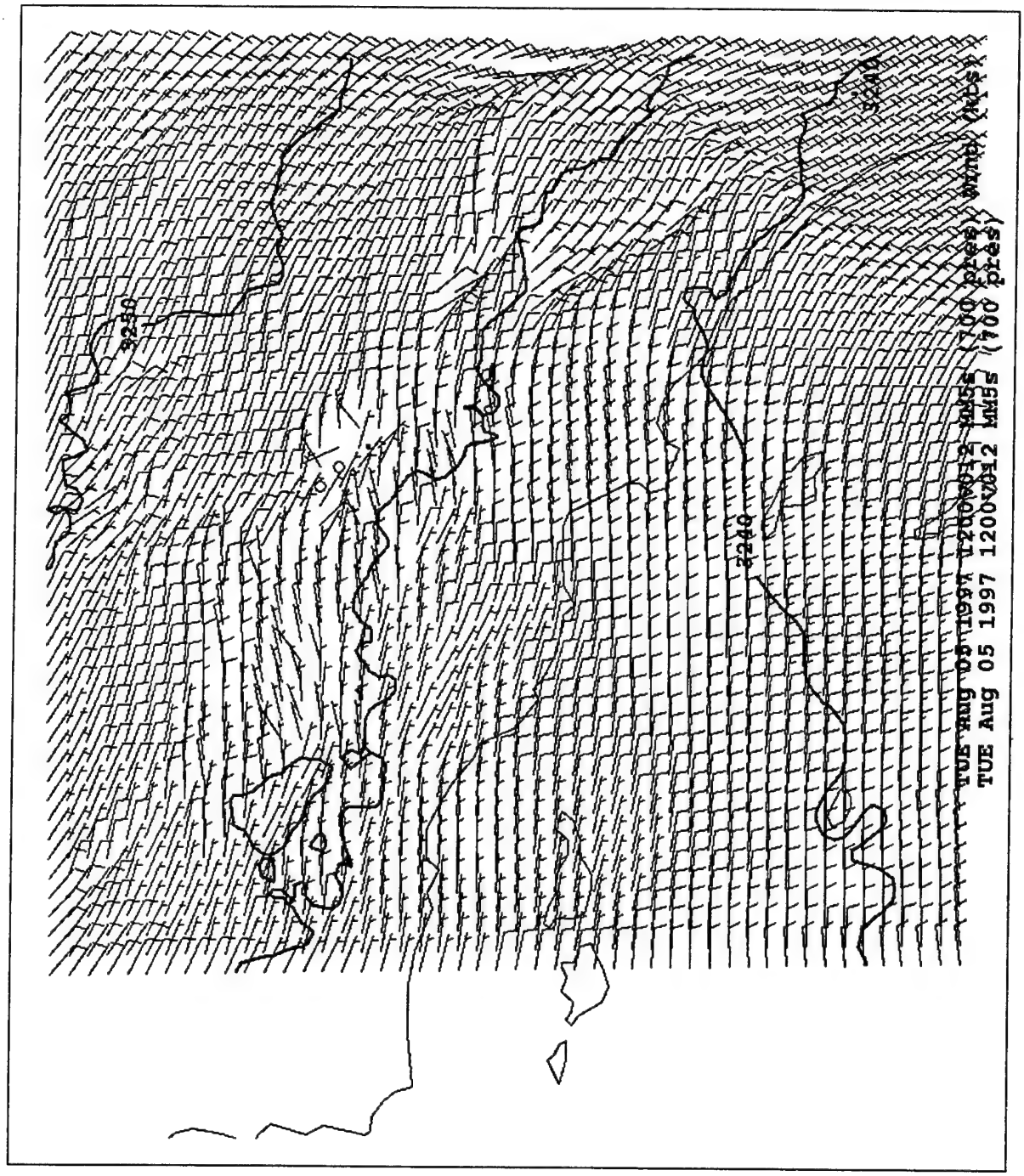

Figure 7-12. 05/12Z MM5 CTRL 3km 12 hour 700mb height(m) and wind(kt) forecasts.

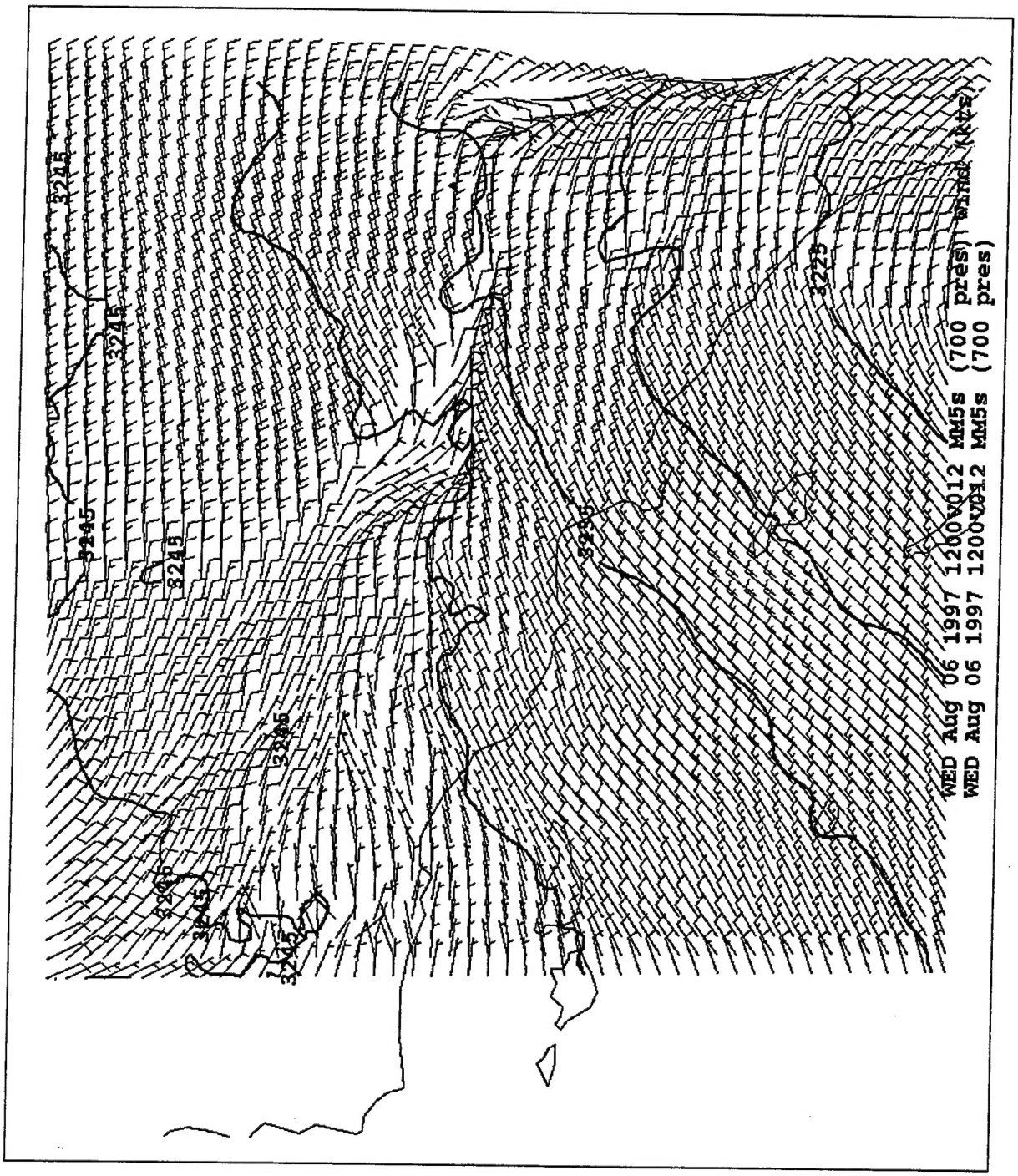

Figure 7-13. 06/12Z MM5 CTRL 3km 12 hour 700mb height(m) and wind(kt) forecasts.

LIST OF REFERENCES

Ahrens, C.D., 1991: *Meteorology Today*, Fourth Edition, West Publishing Company, 577 pp.

Anthes, R.A. and D.P. Baumhefner, 1984: *A Diagram Depicting Forecast Skill and Predictability*. Bulletin of the American Meteorological Society, **65**, 701-703.

Blackadar, A.K., 1979: High Resolution Models of the Planetary Boundary Layer. *Advances in Environmental Science and Engineering*, Volume 1, No. 1, J. Pfafflin and E. Ziegler, Eds., Gordon and Breach, 50-85.

Boucouvala, D., R. Bornstein, D.K. Miller, and J. Wilkinson, 2000: MM5 Simulation of the Meteorological Conditions During a South Coast Ozone Study (SCOS97) Episode. Preprints, *NATO/ITM Conference*, Boulder, Colorado, 15-19 May.

Bruno, D.B., 2000: Climate of Los Angeles, California. NOAA Technical Memorandum NWS WR-261, 173 pp.

Cooperative Program for Operational Meteorology, Education And Training (COMET), 1998. Operated by University of Colorado Atmospheric Research and sponsored by the National Oceanic and Atmospheric Administration.

Gayno, G.A., N.L. Seaman, A.M. Lario, and D.R. Stauffer, 1994: Forecasting Visibility Using a 1.5-Order Closure Boundary Layer Scheme in a 12km Non-Hydrostatic Model. *Tenth American Meteorological Society Conference on Numerical Weather Prediction*, July 18-22.

Kuypers, M.A., *Understanding Mesoscale Error Growth And Predictability*, Master's Thesis, Naval Postgraduate School, Monterey, California, September 2000.

Mohammed, R.M., *Forecasting Mesoscale Winds On Complex Terrain Using a Simple Diagnostic Model*, Master's Thesis, Naval Postgraduate School, Monterey, California, September 2000.

Nuss, W.A., and D.W. Titley, 1994: Use of Multiquadric Interpolation for Meteorological Analysis. *Monthly Weather Review*, **122**, 1611-1631.

Nuss, W.A., 2000: Class notes for MR3262, *Operational Weather Prediction*. Department of Meteorology, Naval Postgraduate School, 86pp.

Pielke, R.A., W.A. Lyons, R.T. McNider, M.D. Moran, R.A. Stocker, R.L. Walko, and M. Uliasz, 1991: Regional and Mesoscale Modeling as Applied to Air Quality Studies. *Air Pollution Modeling and Its Applications VIII*, H van Dop and D.G. Steyn, Eds., Plenum Press, 259-290.

Stauffer, D.R., N.L. Seaman, G.K. Hunter, S. M. Leidner, And A. Lario-Gibbs, 2000: A Field Coherence Technique For Meteorological Field-Program Design for Air Quality Studies. Part I: Description and Interpretation. *Journal of Applied Meteorology*, **39**, 297-316.

Ulrickson, B.L, and C.F. Mass, 1990: Numerical Investigation of Mesoscale Circulations Over the Los Angeles Basin. Part II: Synoptic Influences on Pollutant Transport. *Monthly Weather Review*, **118**, 2161-2184.

Warner, T.T., R.A. Peterson, and R.E. Treadon, 1997: A Tutorial on Lateral Boundary Conditions as a Basic and Serious Limitation to Regional Numerical Weather Prediction. *Bulletin of the American Meteorological Society*, **78**, 2599-2617.

INITIAL DISTRIBUTION LIST

No. Copies

1. Defense Technical Information Center.....2
   8725 John J. Kingman Road, STE 0944
   Ft. Belvoir, Virginia, 22060-6218

2. Dudley Knox Library.....2
   Naval Postgraduate School
   411 Dyer Road
   Monterey, CA 93943-5101

3. Chairman, Code MR/Wx.....1
   Department of Meteorology
   Naval Postgraduate School
   Monterey, CA 93943-5101

4. Chairman, Code OC/Ga.....1
   Department of Oceanography
   Naval Postgraduate School
   Monterey, CA 93943-5101

5. Professor Douglas K. Miller.....1
   Department of Meteorology
   Naval Postgraduate School
   Monterey, CA 93943-5101

6. Professor Robert Bornstein.....1
   Department of Meteorology
   San Jose State University
   San Jose, CA 95192-0001

7. Commander
   Naval Meteorology and Oceanography Command.....1
   1020 Bach Boulevard
   Stennis Space Center, MS 39529-5005

8. LT Christopher J. Sterbis.....4
   8601 North Hickory Drive
   Tucson, AZ 85704